Soil Moisture Active Passive (SMAP)

Algorithm Theoretical Basis Document
Level 2 & 3 Soil Moisture (Passive) Data Products

Revision G
October 12, 2021

Peggy O'Neill, Rajat Bindlish
NASA Goddard Space Flight Center
Greenbelt, MD

Steven Chan, Julian Chaubell, Andreas Colliander, Eni Njoku
Jet Propulsion Laboratory
California Institute of Technology
Pasadena, CA

Tom Jackson
USDA Agricultural Research Service
Beltsville, MD

JPL D-66480

Jet Propulsion Laboratory
California Institute of Technology

The research was carried out at the Jet Propulsion Laboratory, California Institute of Technology, under a contract with the National Aeronautics and Space Administration.

The SMAP Algorithm Theoretical Basis Documents (ATBDs) provide the physical and mathematical descriptions of algorithms used in the generation of SMAP science data products. The ATBDs include descriptions of variance and uncertainty estimates and considerations of calibration and validation, exception control and diagnostics. Internal and external data flows are also described.

The SMAP ATBDs were reviewed by a NASA Headquarters review panel in January 2012 with initial public release later in 2012. The current version of this ATBD is Revision G. The ATBDs may undergo additional revision updates during the mission.

ATBD Revision G dated October 12, 2021 contains the following updates from Revision F dated August 31, 2020:

1. Clarified sentences throughout the document about the baseline algorithm. The SCA-V was the original postlaunch baseline algorithm for the L2/L3_SM_P/P_E products from 2015-2021. As of the October 2021 data release, DCA is the new baseline algorithm (note that soil moisture retrievals from all three algorithms – SCA-H, SCA-V, and DCA – are still provided in the L2/3_SM_P/P_E output products).

2. Updated the output product data field lists in Appendix 1 and 2 to reflect the inclusion of organic content and sand fraction fields and the baseline pointer changes as of the R18 data release in October 2021.

3. Added Appendix 4 on unmixing of surface-corrected T_B in the L1C_TB data used as input to the L2/L3_SM_P/P_E soil moisture retrieval algorithms. This unmixing involves (1) $\boldsymbol{T_B}$ correction over land by removing the emission contribution of nearby water and (2) $\boldsymbol{T_B}$ correction over water by removing the emission contribution of nearby land. Implemented in the R18 data release of October 2021, the impacts of this unmixing are observable mostly around coastal areas and areas surrounding inland open water bodies; the majority (~93%) of global land pixels are generally unaffected by this change.

4. Added Appendix 5 on the addition of the North Polar EASE2 grid for SMAP L2/3_SM_P_E soil moisture products; retrieved soil moisture is still also output on the global EASE2 grid. The polar grid projection offers a more uniform spatial sampling at high latitudes (less distortion than the global grid has at these high latitudes), which will facilitate studies with soil moisture in the boreal and arctic regions.

5. Added algorithm pointer tables for the L2/L3 passive soil moisture product output fields in Appendix 6 as a quick reference for users to associate the correct variable output fields with the correct retrieval algorithm, and to associate the pointer elements to the correct variable. These pointer tables are only applicable to the R18 data release.

General description of changes in the R18 product release for Version 8 of L2/3_SM_P and Version 5 of L2/3_SM_P_E on October 12, 2021:

A point release (R17.1) on April 29, 2021 involved a new Antenna Scan Angle (ASA) correction for the L1B_TB brightness temperature product. The new code examines the initial scan angle in each scan and flags any scan angle that falls out of the normal range as bad (L1B_TB version 5).

For the SMAP Level 2 and 3 passive soil moisture products, the R18 data release of October 2021 includes the following:

- L2/3_SM_P_E soil moisture products are now output on both the global EASE2 and the North Polar EASE2 grids
- Organic content and sand fraction fields have now been added to the output products
- A correction has been applied to unmix surface-corrected T_B in the L1C_TB data used as input to the L2/L3_SM_P/P_E soil moisture retrieval algorithms, mainly affecting areas around coastal areas and surrounding inland open water bodies.
- Based on improved soil moisture retrieval performance in agricultural areas, the DCA algorithm is now the SMAP baseline retrieval algorithm. Default pointers in the output products have been changed accordingly (see Appendix 6 in this ATBD).

As with any satellite retrieval data product, proper data usage is encouraged. The following two simple practices are recommended for using SMAP soil moisture retrievals with maximum scientific benefits:

- Use the **retrieval_qual_flag** field to identify retrievals in the **soil_moisture** field estimated to be of recommended quality. A **retrieval_qual_flag** value of either 0 or 8 indicates high-quality retrievals. Proper use of the **retrieval_qual_flag** field is an effective way to ensure that only retrievals of recommended quality will be used in data analyses.
- For further investigation, use the **surface_flag** field and the associated definition described in the User Guide to determine why the **retrieval_qual_flag** field did not report recommended quality at a given grid cell.

At the time of any new data release, SMAP products are generally re-validated against a variety of validation datasets (primarily *in situ* measured data). The latest assessment reports for SMAP products are posted at NASA's Distributed Active Archive Center (DAAC) at the National Snow and Ice Data Center: https://nsidc.org/data/smap/technical-references. These reports describe changes to the data products in more detail and the impact of these changes on retrieval accuracies.

TABLE OF CONTENTS

SMAP Reference Documents

Requirements:

- SMAP Level 1 Mission Requirements and Success Criteria. (Appendix O to the Earth Systematic Missions Program Plan: Program-Level Requirements on the Soil Moisture Active Passive Project.). NASA Headquarters/Earth Science Division, Washington, DC.
- SMAP Level 2 Science Requirements. SMAP Project, JPL D-45955, Jet Propulsion Laboratory, Pasadena, CA.
- SMAP Level 3 Science Algorithms and Validation Requirements. SMAP Project, JPL D-45993, Jet Propulsion Laboratory, Pasadena, CA.

Plans:

- SMAP Science Data Management and Archive Plan. SMAP Project, JPL D-45973, Jet Propulsion Laboratory, Pasadena, CA.
- SMAP Science Data Calibration and Validation Plan. SMAP Project, JPL D-52544, Jet Propulsion Laboratory, Pasadena, CA.
- SMAP Applications Plan. SMAP Project, JPL D-53082, Jet Propulsion Laboratory, Pasadena, CA.

ATBDs:

- SMAP Algorithm Theoretical Basis Document: L1B and L1C Radar Products. SMAP Project, JPL D-53052, Jet Propulsion Laboratory, Pasadena, CA.
- SMAP Algorithm Theoretical Basis Document: L1B Radiometer Product. Revision D, April, 2021, SMAP Project, GSFC-SMAP-006, NASA Goddard Space Flight Center, Greenbelt, MD.
- SMAP Algorithm Theoretical Basis Document: L1C Radiometer Product. Revision B, October 14, 2015, SMAP Project, JPL D-53053, Jet Propulsion Laboratory, Pasadena, CA.
- SMAP Algorithm Theoretical Basis Document: L2 & L3 Radar Soil Moisture (Active) Products. SMAP Project, JPL D-66479, Jet Propulsion Laboratory, Pasadena, CA.
- SMAP Algorithm Theoretical Basis Document: L2 & L3 Radiometer Soil Moisture (Passive) Products. Revision G, October, 2021, SMAP Project, JPL D-66480, Jet Propulsion Laboratory, Pasadena, CA.
- SMAP Algorithm Theoretical Basis Document: L2 & L3 Radar/Radiometer Soil Moisture (Active/Passive) Products. SMAP Project, JPL D-66481, Jet Propulsion Laboratory, Pasadena, CA.
- SMAP Algorithm Theoretical Basis Document: L3 Radar Freeze/Thaw (Active) Product. SMAP Project, JPL D-66482, Jet Propulsion Laboratory, Pasadena, CA.

- SMAP Algorithm Theoretical Basis Document: L4 Surface and Root-Zone Soil Moisture Product. Revision A, December 9, 2014, SMAP Project, JPL D-66483, Jet Propulsion Laboratory, Pasadena, CA.
- SMAP Algorithm Theoretical Basis Document: L4 Carbon Product. December, 2014, SMAP Project, JPL D-66484, Jet Propulsion Laboratory, Pasadena, CA.
- SMAP Algorithm Theoretical Basis Document: Enhanced L1B_TB_E Radiometer Brightness Temperature Data Product. Revision B, June 6, 2018, SMAP Project, JPL D-56287, Jet Propulsion Laboratory, Pasadena, CA.
- SMAP Algorithm Theoretical Basis Document: L3 Radiometer and Enhanced Radiometer Freeze/Thaw (Passive) Product. Revision C, August 31, 2020 SMAP Project, JPL D-56288, Jet Propulsion Laboratory, Pasadena, CA.

Ancillary Data Reports:

- Ancillary Data Report: Crop Type. SMAP Project, JPL D-53054, Jet Propulsion Laboratory, Pasadena, CA.
- Ancillary Data Report: Digital Elevation Model. SMAP Project, JPL D-53056, Jet Propulsion Laboratory, Pasadena, CA.
- Ancillary Data Report: Land Cover Classification. SMAP Project, JPL D-53057, Jet Propulsion Laboratory, Pasadena, CA.
- Ancillary Data Report: Soil Attributes. Revision B, August 31, 2020, SMAP Project, JPL D-53058, Jet Propulsion Laboratory, Pasadena, CA.
- Ancillary Data Report: Static Water Fraction. SMAP Project, JPL D-53059, Jet Propulsion Laboratory, Pasadena, CA.
- Ancillary Data Report: Urban Area. SMAP Project, JPL D-53060, Jet Propulsion Laboratory, Pasadena, CA.
- Ancillary Data Report: Vegetation Water Content. SMAP Project, JPL D-53061, Jet Propulsion Laboratory, Pasadena, CA.
- Ancillary Data Report: Permanent Ice. SMAP Project, JPL D-53062, Jet Propulsion Laboratory, Pasadena, CA.
- Ancillary Data Report: Precipitation. SMAP Project, JPL D-53063, Jet Propulsion Laboratory, Pasadena, CA.
- Ancillary Data Report: Snow. SMAP Project, GSFC-SMAP-007, NASA Goddard Space Flight Center, Greenbelt, MD.
- Ancillary Data Report: Surface Temperature. SMAP Project, JPL D-53064, Jet Propulsion Laboratory, Pasadena, CA.
- Ancillary Data Report: Vegetation and Roughness Parameters. SMAP Project, JPL D-53065, Jet Propulsion Laboratory, Pasadena, CA.

ACRONYMS AND ABBREVIATIONS

AMSR	Advanced Microwave Scanning Radiometer
ATBD	Algorithm Theoretical Basis Document
CONUS	Continental United States
CMIS	Conical-scanning Microwave Imager Sounder
CV	Calibration / Validation
DAAC	Distributed Active Archive Center
DCA	Dual Channel Algorithm
DEM	Digital Elevation Model
ECMWF	European Center for Medium-Range Weather Forecasting
EOS	Earth Observing System
ESA	European Space Agency
GEOS	Goddard Earth Observing System (model)
GMAO	Goddard Modeling and Assimilation Office
GSFC	Goddard Space Flight Center
IFOV	Instantaneous Field Of View
JAXA	Japan Aerospace Exploration Agency
JPL	Jet Propulsion Laboratory
JPSS	Joint Polar Satellite System
LPRM	Land Parameter Retrieval Model
LSM	Land Surface Model
LTAN	Local Time Ascending Node
LTDN	Local Time Descending Node
MODIS	MODerate-resolution Imaging Spectroradiometer
NCEP	National Centers for Environmental Prediction
NDVI	Normalized Difference Vegetation Index
NPOESS	National Polar-Orbiting Environmental Satellite System
NPP	NPOESS Preparatory Project
NWP	Numerical Weather Prediction
OSSE	Observing System Simulation Experiment
PDF	Probability Density Function
PGE	Product Generation Executable
QC	Quality-Control

RFI	Radio Frequency Interference
RMSD	Root Mean Square Difference
RMSE	Root Mean Square Error
SCA	Single Channel Algorithm
SGP	Southern Great Plains (field campaigns)
SMAPVEX	SMAP Validation EXperiment
SMDPC	Soil Moisture Data Processing Center
SMEX	Soil Moisture EXperiments (field campaigns)
SMOS	Soil Moisture Ocean Salinity (ESA space mission)
T_B	Brightness Temperature
TBC	To Be Confirmed
TBD	To Be Determined
USDA ARS	U.S. Department of Agriculture, Agricultural Research Service
VWC	Vegetation water content (in units of kg/m^2)

1. INTRODUCTION

1.1 Background

The Soil Moisture Active Passive (SMAP) mission is the first of the Earth observation satellites being developed by NASA in response to the National Research Council's first Earth Science Decadal Survey, *Earth Science and Applications from Space: National Imperatives for the Next Decade and Beyond* [1]. The Decadal Survey was released in 2007 after a two-year study commissioned by NASA, NOAA, and USGS to provide them with prioritized recommendations for space-based Earth observation programs. Factors including scientific value, societal benefit, and technical maturity of mission concepts were considered as criteria. In 2008 NASA announced the formation of the SMAP project as a joint effort of NASA's Jet Propulsion Laboratory (JPL) and Goddard Space Flight Center (GSFC), with project management responsibilities at JPL. Launched on January 31, 2015, SMAP is providing high resolution global mapping of soil moisture and freeze/thaw state every 2-3 days on nested 3, 9, and 36-km Earth grids [2]. Its major science objectives are to:

- Understand processes that link the terrestrial water, energy and carbon cycles;
- Estimate global water and energy fluxes at the land surface;
- Quantify net carbon flux in boreal landscapes;
- Enhance weather and climate forecast skill;
- Develop improved flood prediction and drought monitoring capability.

1.2 Measurement Approach

Table 1 is a summary of the SMAP instrument functional requirements derived from its science measurement needs. The goal is to combine the attributes of the radar and radiometer observations (in terms of their spatial resolution and sensitivity to soil moisture, surface roughness, and vegetation) to estimate soil moisture at a resolution of 10 km and freeze-thaw state at a resolution of 1-3 km.

The SMAP instrument incorporates an L-band radar and an L-band radiometer that share a single feedhorn and parabolic mesh reflector. As shown in Figure 1, the reflector is offset from nadir and rotates about the nadir axis at 14.6 rpm (nominal), providing a conically scanning antenna beam with a surface incidence angle of approximately 40°. The provision of constant incidence angle across the swath simplifies the data processing and enables accurate repeat-pass estimation of soil moisture and freeze/thaw change. The reflector has a diameter of 6 m, providing a radiometer 3 dB antenna footprint of 40 km (root-ellipsoidal-area). The real-aperture radar footprint is 30 km, defined by the two-way antenna beamwidth. The real-aperture radar and radiometer data will be collected globally during both ascending and descending passes. The SMAP baseline orbit parameters are:

- Orbit Altitude: 685 km (2-3 day average revisit globally and 8-day exact repeat)
- Inclination: 98 degrees, sun-synchronous
- Local Time of Ascending Node: 6 pm (6 am descending local overpass time)

Table 1. SMAP Mission Requirements

Scientific Measurement Requirements	Instrument Functional Requirements
Soil Moisture: ~± 0.04 cm^3/cm^3 volumetric accuracy (1-sigma) in the top 5 cm for vegetation water content ≤ 5 kg/m^2 Hydrometeorology at ~10 km resolution Hydroclimatology at ~40 km resolution	**L-Band Radiometer (1.41 GHz):** Polarization: V, H, T_3, and T_4 Resolution: 40 km Radiometric Uncertainty*: 1.3 K **L-Band Radar (1.26 and 1.29 GHz):** Polarization: VV, HH, HV (or VH) Resolution: 10 km Relative accuracy*: 0.5 dB (VV and HH) Constant incidence angle** between 35° and 50°
Freeze/Thaw State: Capture freeze/thaw state transitions in integrated vegetation-soil continuum with two-day precision at the spatial scale of landscape variability (~3 km)	**L-Band Radar (1.26 GHz & 1.29 GHz):** Polarization: HH Resolution: 3 km Relative accuracy*: 0.7 dB (1 dB per channel if 2 channels are used) Constant incidence angle** between 35° and 50°
Sample diurnal cycle at consistent time of day (6 am/6 pm Equator crossing); Global, ~3 day (or better) revisit; Boreal, ~2 day (or better) revisit	Swath Width: ~1000 km Minimize Faraday rotation (degradation factor at L-band)
Observation over minimum of three annual cycles	Baseline three-year mission life
* Includes precision and calibration stability ** Defined without regard to local topographic variation	

On July 7, 2015, the High Power Amplifier of the SMAP radar experienced an anomaly which caused the radar to stop transmitting. All subsequent attempts to power up the radar were unsuccessful. The SMAP mission continues to produce high-quality science measurements supporting SMAP's objectives with its radiometer instrument. After the failure of the SMAP radar, the SMAP project used a Backus-Gilbert optimal interpolation scheme which takes advantage of the SMAP radiometer oversampling on orbit to generate an enhanced radiometer-based soil moisture product posted on a 9 km grid (see Sec. 8.2). In addition, a new high-resolution active-passive disaggregation product combining the SMAP L-band radiometer data with Sentinel-1 C-band radar data has been released as a best-effort partial replacement of the SMAP L2/L3_SM_AP product.

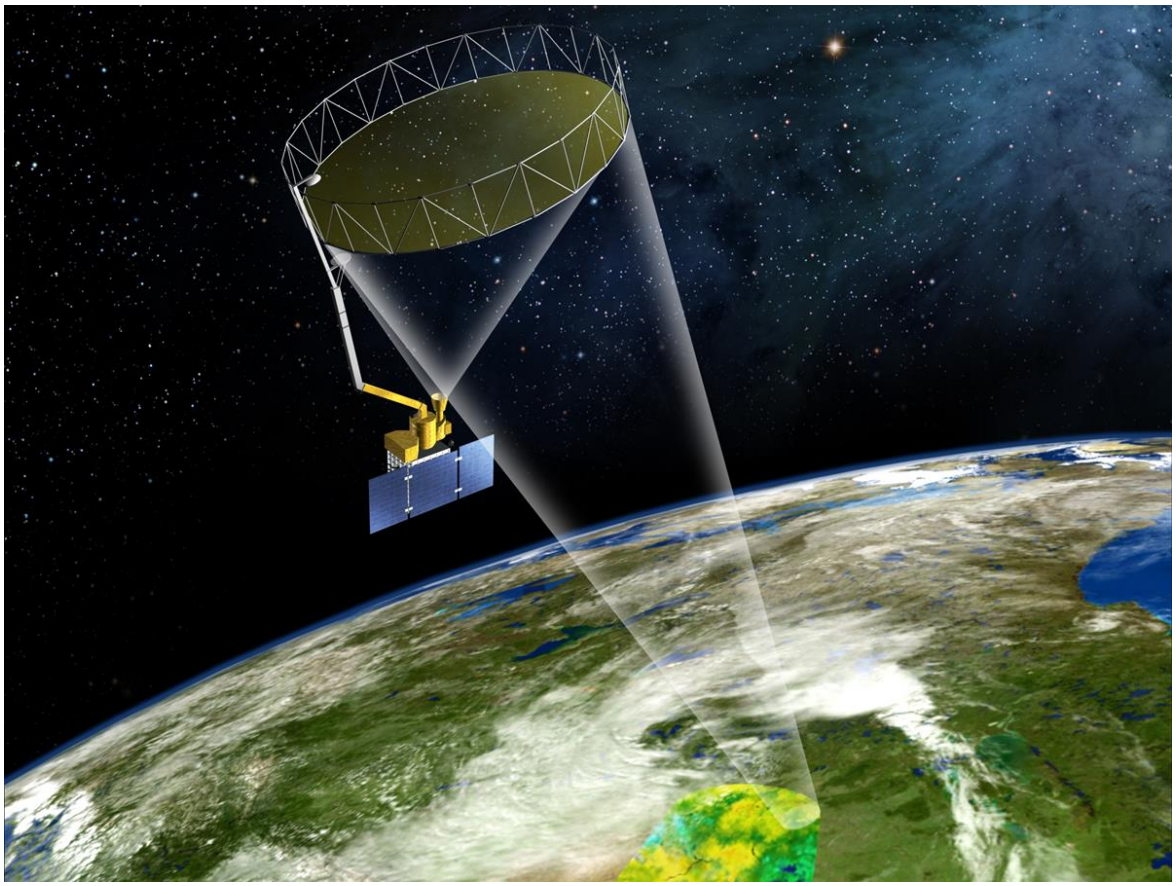

Figure 1. The SMAP mission concept consists of an L-band radar and radiometer sharing a single spinning 6-m mesh antenna in a sun-synchronous dawn / dusk orbit.

The SMAP radiometer measures the four Stokes parameters, V, H, T_3, and T_4 at 1.41 GHz. The T_3-channel measurement can be used to correct for possible Faraday rotation caused by the ionosphere, although such Faraday rotation is minimized by the selection of the 6 am/6 pm sun-synchronous SMAP orbit.

Anthropogenic Radio Frequency Interference (RFI), principally from ground-based surveillance radars, can contaminate both radar and radiometer measurements at L-band. Early measurements and results from ESA's SMOS (Soil Moisture and Ocean Salinity) mission indicate that in some regions RFI is present and detectable. The SMAP radar and radiometer electronics and algorithms have been designed to include features to mitigate the effects of RFI. The SMAP radar utilizes selective filters and an adjustable carrier frequency in order to tune to predetermined RFI-free portions of the spectrum while on orbit. The SMAP radiometer will implement a combination of time and frequency diversity, kurtosis detection, and use of T_4 thresholds to detect and where possible mitigate RFI.

SMAP observations will (1) improve our understanding of linkages between the Earth's water, energy, and carbon cycles, (2) benefit many application areas including numerical weather and climate prediction, flood and drought monitoring, agricultural productivity, human health, and national security, (3) help to address priority questions on climate

change, and (4) potentially provide continuity with brightness temperature and soil moisture measurements from ESA's SMOS (Soil Moisture Ocean Salinity) and NASA's Aquarius missions. The current SMAP data products are listed in Table 2 (as of December, 2016). In the SMAP prelaunch time frame, baseline algorithms were developed for generating (1) Level 1 calibrated, geolocated surface brightness temperature and radar backscatter measurements, (2) Level 2 and Level 3 surface soil moisture products both from radiometer measurements on a 36 km grid and from combined radar/radiometer measurements on a 9 km grid, (3) Level 3 freeze/thaw products from radar measurements on a 3 km grid, and (4) Level 4 surface and root zone soil moisture and Level 4 Net Ecosystem Exchange (NEE) of carbon on a 9 km grid. Level 1 data are the instrument products; Level 2 data are surface soil moisture in half-orbit format; Level 3 data are global daily composites of the Level 2 data; and Level 4 data combine the SMAP satellite observations with modeling to produce value-added products that support key SMAP applications and more directly address the driving science questions.

The details of each SMAP data product will be described in an associated publicly-available Algorithm Theoretical Basis Document (ATBD), which will be updated periodically as warranted. SMAP data products are generated using algorithm software that converts lower level products to higher level products. Each product has a designated baseline algorithm for its generation. One or more algorithm options may be encoded in the software and evaluated along with the baseline algorithm. The ATBDs describe the product algorithms and their implementation, prelaunch testing, and post-launch validation approaches.

1.3 Scope and Rationale

This document is the Algorithm Theoretical Basis Document (ATBD) for the SMAP radiometer-based surface soil moisture products:

1. Level 2 Soil Moisture (L2_SM_P) in half-orbit format.
2. Level 3 Soil Moisture (L3_SM_P) in the form of global daily composites.
3. Level 2 Soil Moisture (L2_SM_P_E) in half-orbit format (as of Dec., 2016).
4. Level 3 Soil Moisture (L3_SM_P_E) in the form of global daily composites (as of Dec., 2016).

The L2/L3_SM_P_E products (Sec. 8.2) use the same soil moisture retrieval algorithms as the standard L2/L3_SM_P products, and so are covered by the algorithm descriptions and procedures described in this ATBD. The complete list of SMAP data products is provided in Table 2. The L2_SM_P and L3_SM_P products represent the surface soil moisture (0-5 cm layer) derived from the SMAP radiometer as output on a fixed 36-km Earth grid. This grid spacing is close to the approximate spatial resolution of 40 km of the SMAP radiometer footprint and permits nesting with the 3-km grid spacing of the SMAP radar-derived products (including L2_SM_SP) and the 9-km grid spacing of the L2_SM_A/P combined active/passive product and the L4_SM and L4_C products. As of December, 2016, L2/3_SM_P includes both AM and PM retrieved soil moisture using the same retrieval algorithms. The L2/ L3_SM_P_E 0-5 cm soil moisture products (both AM and PM) are posted on a 9 km grid.

Table 2. SMAP Data Products*

Product	Description	Gridding (Resolution)	Latency**	
L1A_Radiometer	Radiometer Data in Time-Order	-	12 hrs	Instrument Data
L1A_Radar	Radar Data in Time-Order	-	12 hrs	
L1B_TB	Radiometer T_B in Time-Order	(36x47 km)	12 hrs	
L1B_TB_E	Radiometer T_B Optimally Interpolated on EASE2.0 grid	9 km	12 hrs	
L1B_S0_LoRes	Low Resolution Radar σ_o in Time-Order	(5x30 km)	12 hrs	
L1C_S0_HiRes	High Resolution Radar σ_o in Half-Orbits	1 km (1-3 km)	12 hrs	
L1C_TB	Radiometer T_B in Half-Orbits	36 km	12 hrs	
L1C_TB_E	Radiometer T_B in Half-Orbits, Enhanced	9 km	12 hrs	
L2_SM_A	Soil Moisture (Radar)	3 km	24 hrs	Science Data (Half-Orbit)
L2_SM_P	Soil Moisture (Radiometer)	36 km	24 hrs	
L2_SM_P_E	Soil Moisture (Radiometer, Enhanced))	9 km	24 hrs	
L2_SM_AP	Soil Moisture (Radar + Radiometer)	9 km	24 hrs	
L2_SM_SP	Soil Moisture (Sentinel Radar + Radiometer)	3 km	Best effort	
L3_FT_A	Freeze/Thaw State (Radar)	3 km	50 hrs	Science Data (Daily Composite)
L3_FT_P	Freeze/Thaw State (Radiometer)	36 km	50 hrs	
L3_FT_P_E	Freeze/Thaw State (Radiometer, Enhanced)	9 km	50 hrs	
L3_SM_A	Soil Moisture (Radar)	3 km	50 hrs	
L3_SM_P	Soil Moisture (Radiometer)	36 km	50 hrs	
L3_SM_P_E	Soil Moisture (Radiometer, Enhanced)	9 km	50 hrs	
L3_SM_AP	Soil Moisture (Radar + Radiometer)	9 km	50 hrs	
L4_SM	Soil Moisture (Surface and Root Zone)	9 km	7 days	Science Value-Added
L4_C	Carbon Net Ecosystem Exchange (NEE)	9 km	14 days	

*SMAP radar products were no longer produced operationally after the SMAP radar failed on July 7, 2015. The L2_SM_SP is a new product using Sentinel C-band radar data merged with SMAP radiometer data.

1.4 SMAP Science Objectives and Requirements

As mentioned, the SMAP science objectives are to provide new global data sets that will enable science and applications users to:

- Understand processes that link the terrestrial water, energy and carbon cycles;
- Estimate global water and energy fluxes at the land surface;
- Quantify net carbon flux in boreal landscapes;
- Enhance weather and climate forecast skill;
- Develop improved flood prediction and drought monitoring capability.

To resolve hydrometeorological water and energy flux processes and extend weather and flood forecast skill, a spatial resolution of 10 km and temporal resolution of 3 days are required. To resolve hydroclimatological water and energy flux processes and extend climate and drought forecast skill, a spatial resolution of 40 km and temporal resolution of 3 days are required. To quantify net carbon flux in boreal landscapes, a spatial resolution of 3 km and temporal resolution of 2 days are required. The SMAP mission will also validate a space-based measurement approach that could be used for future systematic hydrosphere state monitoring missions. The SMAP L2/3_SM_P products will meet the needs of the hydroclimatology community, while the L2/L3_SM_P_E products will begin to address the needs of the hydrometeorology community.

The SMAP mission Level 1 and Level 2 requirements state that:

"The baseline science mission shall provide estimates of soil moisture in the top 5 cm of soil with an error of no greater than 0.04 cm^3/cm^3 (one sigma) at 10 km spatial resolution and 3-day average intervals over the global land area excluding regions of snow and ice, frozen ground, mountainous topography, open water, urban areas, and vegetation with water content greater than 5 kg/m^2 (averaged over the spatial resolution scale)."

L2-SR-347: "SMAP shall provide a Level 2 data product (L2_SM_P) at 40 km spatial resolution representing the average soil moisture in the top 5 cm of soil."

Although generated at a coarser 40-km spatial resolution, the L2/3_SM_P radiometer-based data products should still meet the 0.04 cm^3/cm^3 volumetric soil moisture retrieval accuracy specified in the mission Level 1 requirements. The SMAP Science Definition Team specified that data will be binned over annual and 6-month time domain periods (April-September, October-March) globally within the SMAP mask when assessing radiometer performance and mission success in terms of soil moisture retrieval accuracies.

1.5 Document Outline

This document contains the following sections: Section 2 describes the basic physics of passive microwave remote sensing of soil moisture; Section 3 provides a description of the SMAP L2_SM_P and L3_SM_P data products; Section 4 introduces the baseline algorithm, along with other algorithm options; Section 5 addresses the use of the SMAP Algorithm Testbed in assessing algorithm performance and estimating error budgets for each candidate algorithm; Section 6 discusses the use of ancillary data and various flags; Section 7 presents procedures for downselecting to a baseline algorithm and for validating the data products; Section 8 includes brief descriptions of the 6 pm and 9 km products; Section 9 provides a list of references; and Appendices 1 and 2 contain the data fields for the L2_SM_P and L2_SM_P_E output products, respectively. This ATBD will be updated as additional work is completed in the pre- and post-launch periods.

2. PASSIVE REMOTE SENSING OF SOIL MOISTURE

The microwave portion of the electromagnetic spectrum (wavelengths from a few centimeters to a meter) has long held the most promise for estimating surface soil moisture remotely. Passive microwave sensors measure the natural thermal emission emanating from the soil surface. The variation in the intensity of this radiation depends on the dielectric properties and temperature of the target medium, which for the near surface soil layer is a function of the amount of moisture present. Low microwave frequencies (at L band or ~ 1 GHz) offer additional advantages: (1) the atmosphere is almost completely transparent, providing all-weather sensing; (2) transmission of signals from the underlying soil is possible through sparse and moderate vegetation layers (up to at least 5 kg/m^2 of vegetation water content); and (3) measurement is independent of solar illumination which allows for day and night observations.

The microwave soil moisture community has several decades of experience in conducting experiments using ground-based and aircraft microwave sensors [3-6]. These early experiments examined the basic physical relationships between emissivity and soil moisture, determined the optimum frequencies and measurement configurations, and demonstrated the potential accuracies for soil moisture retrievals. From these experiments a number of viable soil moisture retrieval algorithms have evolved, the most promising of which were explored in the Hydros OSSE (Observing System Simulation Experiment) [7] during the risk reduction phase of that project. Hydros was a proposed Earth System Science Pathfinder-class microwave soil moisture mission selected by NASA as a backup mission at the time of the OCO and Aquarius selections in 2002. Funding for Hydros ceased in 2005, but many of its risk reduction activities generated knowledge of direct relevance to SMAP. Additionally, much work was conducted by European and other colleagues prior to the launch of SMOS in 2009 [8-11].

2.1 Physics of the Problem

As mentioned, a microwave radiometer measures the natural thermal emission coming from the surface. At microwave frequencies, the intensity of the observed emission is proportional to the product of the temperature and emissivity of the surface (Rayleigh-Jeans approximation). This product is commonly called the brightness temperature T_B. If the microwave sensor is in orbit above the earth, the observed T_B is a combination of the emitted energy from the soil as attenuated by any overlying vegetation, the emission from the vegetation, the downwelling atmospheric emission and cosmic background emission as reflected by the surface and attenuated by the vegetation, and the upwelling atmospheric emission (Figure 2).

At L band frequencies, the atmosphere is essentially transparent, with the atmospheric transmissivity $\tau_{atm} \approx 1$. The cosmic background Tsky is on the order of 2.7 K. The atmospheric emission is also very small. These small atmospheric contributions will be accounted for in the L1B_TB ATBD, since the primary inputs to the radiometer-derived soil moisture retrieval process described in this L2_SM_P ATBD are atmospherically-corrected surface brightness temperatures as described in Section 3.

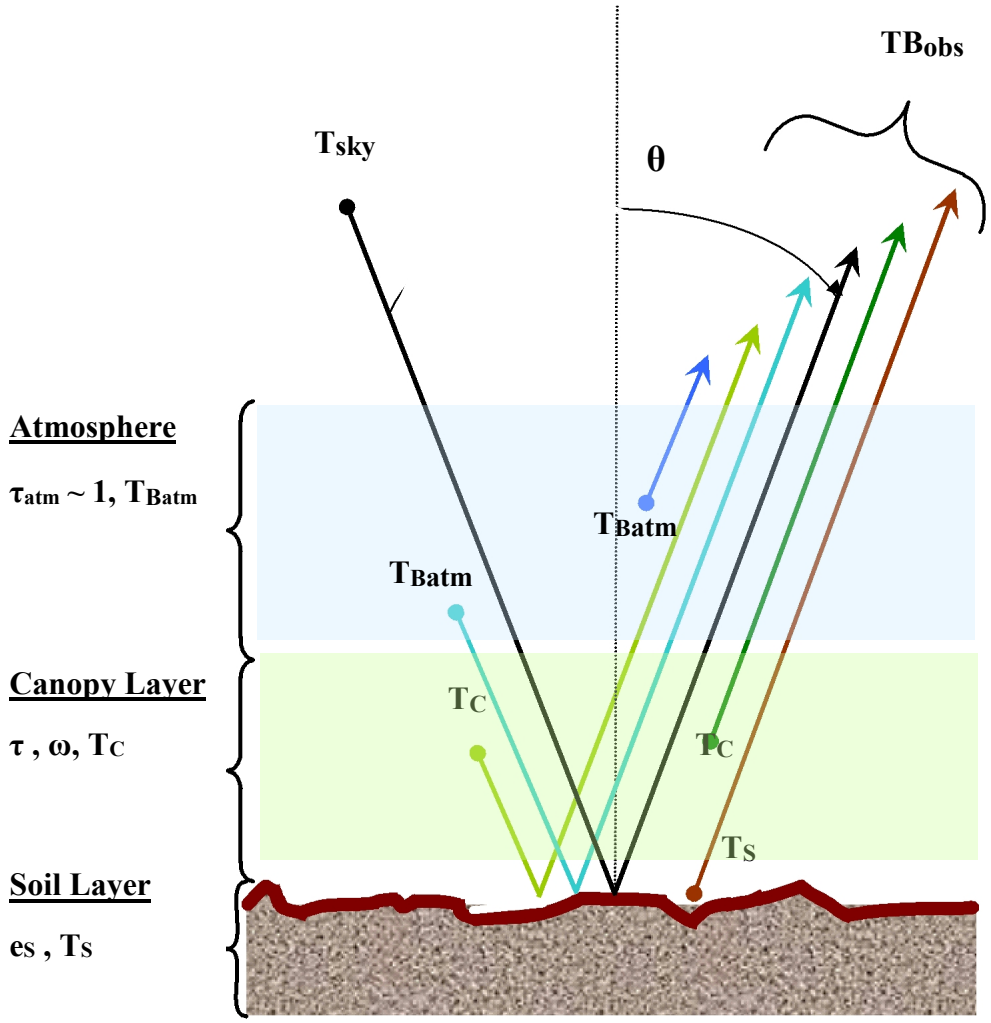

Figure 2. Contributions to the observed brightness temperature T_B from orbit [from SMOS ATBD, ref. 12] .

Retrieval of soil moisture from SMAP surface T_B observations is based on a well-known approximation to the radiative transfer equation, commonly known in the passive microwave soil moisture community as the *tau-omega* model. A layer of vegetation over a soil attenuates the emission of the soil and adds to the total radiative flux with its own emission. Assuming that scattering within the vegetation is negligible at L band frequencies, the vegetation may be treated mainly as an absorbing layer. A model following this approach to describe the brightness temperature of a weakly scattering layer above a semi-infinite medium was developed by [13] and described in [14]. The equation includes emission components from the soil and the overlying vegetation canopy [15]:

$$T_{Bp} = T_s e_p exp(-\tau_p \sec\theta) + T_c(1-\omega_p)[1-exp(-\tau_p \sec\theta)][1+r_p exp(-\tau_p \sec\theta)] \quad (1)$$

where the subscript p refers to polarization (V or H), T_s is the soil effective temperature, T_c is the vegetation temperature, τ_p is the nadir vegetation opacity, ω_p is the vegetation single scattering albedo, and r_p is the rough soil reflectivity. The reflectivity is related to the emissivity (e_p) by $e_p = (1 - r_p)$, and ω_p, r_p and e_p are values at the SMAP look angle of $\theta = 40°$. The transmissivity γ of the overlying canopy layer is $\gamma = \exp(-\tau_p \sec \theta)$. Equation (1) assumes that vegetation multiple scattering and reflection at the vegetation-air interface are negligible. Surface roughness is modeled as $r_{p\ rough} = [Q\ r_{p\ smooth} + (1 - Q)\ r_{q\ smooth}] \exp(-h\ cos^x\ \theta)$ where Q is the polarization mixing factor, h parameterizes the intensity of the roughness effects, the subscript q refers to polarization (V or H), and $x = 0$, 1, or 2. (Current SMAP operational processing has $x = 2$.) Nadir vegetation opacity is related to the total columnar vegetation water content (VWC, in kg/m^2) by $\tau_p = b_p * VWC$ with the coefficient b_p dependent on vegetation type and microwave frequency (and polarization) [15].

If the air, vegetation, and near-surface soil are in thermal equilibrium, as is approximately the case near 6:00 am local time (the time of the SMAP descending pass), then T_c is approximately equal to T_s and the two temperatures can be replaced by a single effective temperature (T_{eff}). Soil moisture can then be estimated from $r_{p\ smooth}$ using the Fresnel and dielectric-soil moisture relationships.

The surface reflectance r_p is defined by the Fresnel equations, which describe the behavior of an electromagnetic wave at a smooth dielectric boundary. At horizontal polarization the electric field of the wave is oriented parallel to the reflecting surface and perpendicular to the direction of propagation. At vertical polarization the electric field of the wave has a component perpendicular to the surface. In the Fresnel equations below, θ is the SMAP incidence angle of 40° and ε is the complex dielectric constant of the soil layer:

$$r_H(\theta) = \left| \frac{\cos\theta - \sqrt{\varepsilon - \sin^2\theta}}{\cos\theta + \sqrt{\varepsilon - \sin^2\theta}} \right|^2 \tag{2}$$

$$r_V(\theta) = \left| \frac{\varepsilon\cos\theta - \sqrt{\varepsilon - \sin^2\theta}}{\varepsilon\cos\theta + \sqrt{\varepsilon - \sin^2\theta}} \right|^2 \tag{3}$$

In terms of dielectric properties, there is a large contrast between liquid water ($\varepsilon_r \sim 80$) and dry soil ($\varepsilon_r \sim 5$). As soil moisture increases, soil dielectric constant increases. This leads to an increase in soil reflectivity or a decrease in soil emissivity ($1 - r_p$). Note that low dielectric constant is not uniquely associated with dry soil. Frozen soil, independent of water content, has a similar dielectric constant to dry soil. Thus, a freeze/thaw flag is needed to resolve this ambiguity. As T_B is proportional to emissivity for a given surface soil temperature, T_B decreases in response to an increase in soil moisture. It is this relationship between soil moisture and soil dielectric constant (and hence microwave emissivity and brightness temperature) that forms the physical basis of passive remote sensing of soil moisture. Given SMAP observations of T_B and information on T_{eff}, h, τ_p, and ω_p from ancillary sources (Section 6) or multichannel algorithm approaches (Section 4), Equation (1) can be solved for the soil reflectivity r_p, and equation (2) or (3) can be

solved for the soil dielectric ε. Soil moisture can then be estimated using one of several dielectric models and ancillary knowledge of soil texture.

2.2 Rationale for L-Band

Within the microwave portion of the electromagnetic spectrum, emission from soil at L-band frequencies can penetrate through greater amounts of vegetation than at higher frequencies. Figure 3 shows microwave transmissivity as a function of increasing biomass at L-band (1.4 GHz), C-band (6 GHz), and X-band (10 GHz) frequencies, based upon modeling. The results clearly show that L-band frequencies have a significant advantage over the C- and X-band frequencies (and higher) provided by current satellite instruments such as AMSR-E and WindSat, and help explain why both SMOS and SMAP are utilizing L band sensors in estimating soil moisture globally over the widest possible vegetation conditions. Another advantage of measuring soil moisture at L-band is that the microwave emission originates from deeper in the soil (typically 5 cm or so), whereas C- and X-band emissions originate mainly from the top 1 cm or less of the soil (Figure 4).

Although the above arguments support the use of low frequencies, there is, however, a lower frequency limit for optimal T_B measurements for soil moisture. At frequencies lower than L-band, radiometric measurements are significantly degraded by manmade and galactic noise. Since there is a protected band at L band at 1.400–1.427 GHz that is allocated exclusively for radiometric use, the SMAP radiometer operates in this band.

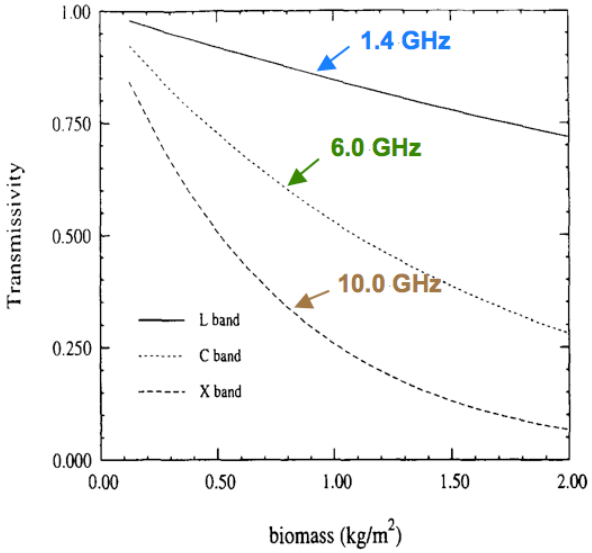

Figure 3. Vegetation transmissivity to soil emission at L-band frequencies (1.4 GHz) is much higher than at C- (6 GHz) or X-band (10 GHz) frequencies [adapted from 22].

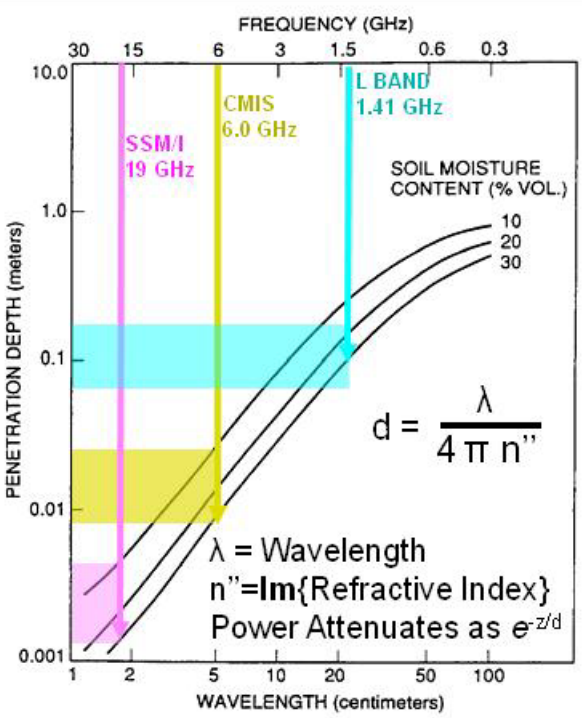

Figure 4. L-band T_B observations are sensitive to emission from deeper in the soil than at higher frequencies [adapted from 23]. Soil moisture curves are given for 10, 20, and 30% (or in absolute units, 100 x cm^3/cm^3).

2.3 Soil Dielectric Models

In the past few decades, a number of soil dielectric models have been developed by the passive microwave remote sensing community. Although they differ in analytical forms, they generally share common dependence on soil moisture, soil texture, and frequency. The details of these models have been described thoroughly in the literature – a good summary can be found in [18, 19]. The SMAP project investigated the use of three different soil dielectric models:

(1) Dobson [20] – a semi-empirical mixing model, the Dobson model retains the physical aspects of the dielectric properties of free water of the soil through the Debye equations while also using certain empirical fitting parameters based on the different soil types studied during the model's development; the model requires frequency, soil moisture, soil temperature, sand fraction, clay fraction, and bulk density as input parameters.

(2) Wang & Schmugge [21] – a central point of this empirical mixing model is the use of a transition point of water content beyond which the dielectric constant increases rapidly with soil moisture; the model predicts and illustrates the substantial impact of bound water (as opposed to free water only) on soil dielectric constant.

(3) Mironov [19] – formally known as the Mineralogy-Based Soil Dielectric Model (MBSDM); using a large soil database, Mironov was able to obtain a set of regression equations to derive many of the spectroscopic parameters needed by a model that he

developed earlier; the resulting model not only applies to a wider range of soil types, but also requires fewer input parameters – with clay percentage as the only soil input parameter.

These three models have been widely used due to their simple parameterizations and applicability at L-band frequencies (1.26-1.41 GHz). As part of SMAP prelaunch and post-launch calibration/validation activities, the performance of these dielectric models in terms of bias and accuracy of the retrieved soil moisture was evaluated and a decision made on which dielectric model to carry forward into the operational production of SMAP data products. The SMAP L2_SM_P processing software has a switch which selects which dielectric model will be used in the soil moisture retrieval. While all three dielectric models are coded in the SMAP software, L2_SM_P currently uses the Mironov model in routine processing. For comparison, ESA's SMOS mission currently uses land cover classification to choose the appropriate dielectric model (Dobson or Mironov). Figure 5 gives an example of the performance of the three dielectric models when used in forward model computations of L band T_B for θ = 40°, assuming smooth bare soils at T_S = 25°C for different soil types.

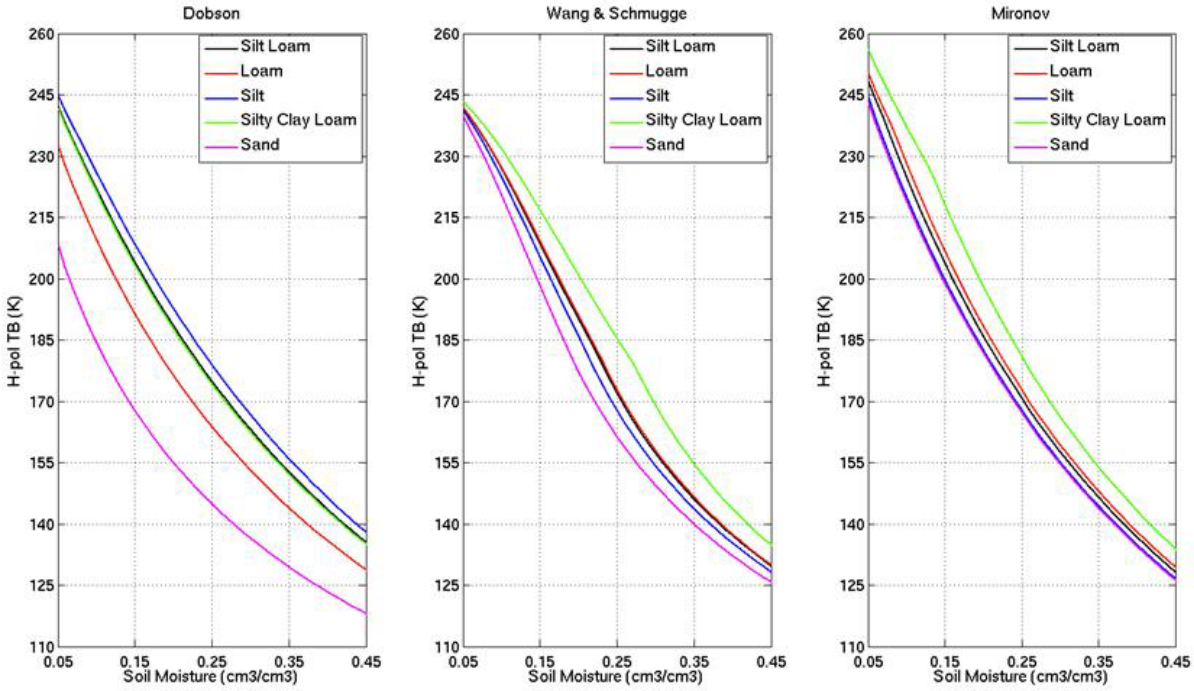

Figure 5. Bare soil T_B as computed by different soil dielectric models. The selected soil types correspond to the top five most dominant soil texture classes, together accounting for over 80% of the global land area.

2.4 Use of the 6:00 AM Descending Node Orbit for the Primary Mission

The decision to place SMAP into a sun-synchronous 6:00 am / 6:00 pm orbit is based on a number of science issues relevant to the L2_SM_P product [24, 25]. Faraday rotation

is a phenomenon in which the polarization vector of an electromagnetic wave rotates as the wave propagates through the ionospheric plasma in the presence of the Earth's static magnetic field. The phenomenon is a concern to SMAP because the polarization rotation increases as the square of wavelength. If uncorrected, the SMAP polarized (H and V) radiometer measurements will contain errors that translate to soil moisture error. Faraday rotation varies greatly during the day, reaching a maximum during the afternoon and a minimum in the pre-dawn hours. By using T_B observations acquired near 6:00 am local solar time as the primary input to the L2_SM_P product, the adverse impacts of Faraday rotation are minimized. Faraday rotation correction to SMAP T_B is described in the L1B_TB ATBD.

At 6:00 am the vertical profiles of soil temperature and soil dielectric properties are likely to be more uniform [13] than at other times of the day (Figure 7). This early morning condition will minimize the difference between canopy and soil temperatures and thermal differences between land cover types within a pixel (Figure 6). These factors help to minimize soil moisture retrieval errors originating from the use of a single effective temperature to represent the near surface soil and canopy temperatures. This same effective temperature can be used as the open water temperature in the water body correction to T_B that will be discussed in Sections 3 and 4.

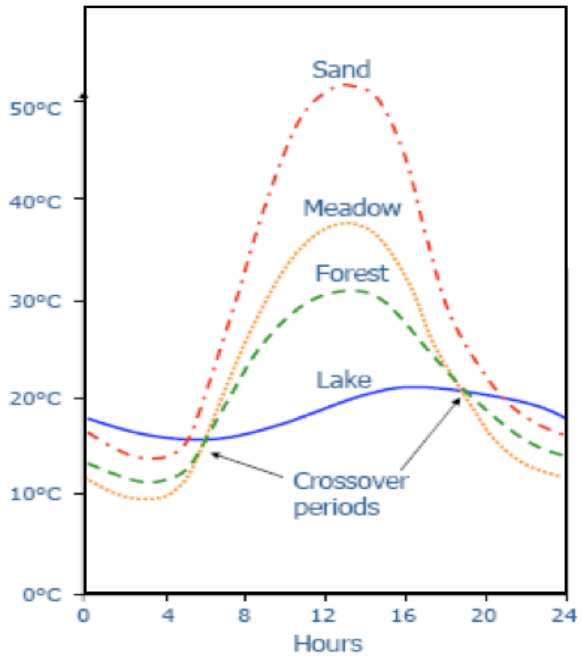

Figure 6. Schematic showing diurnal variation in temperature and thermal crossover times at approximately 6:00 am / 6:00 pm local time for various broad classes of land surface covers [modified from 24].

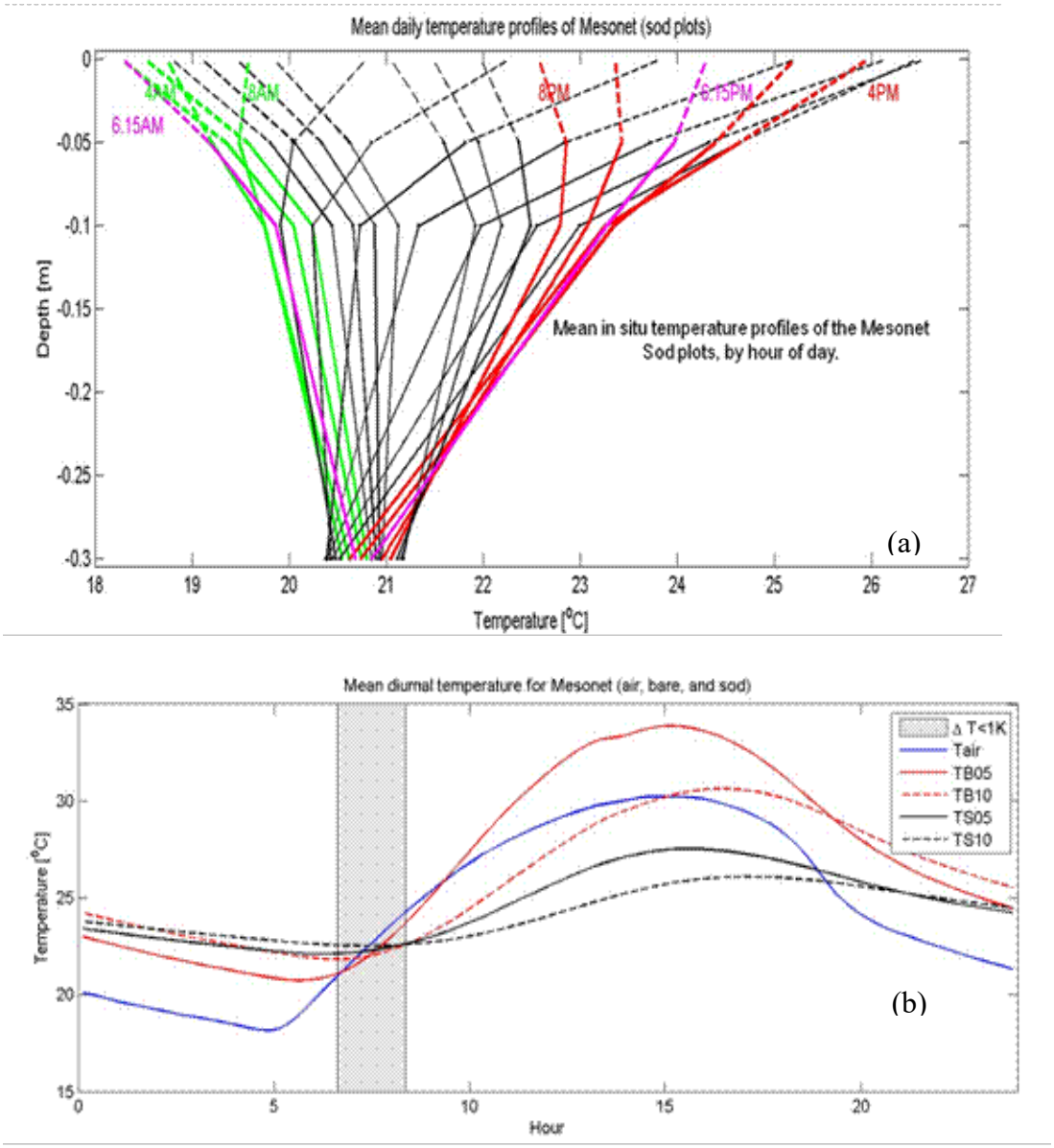

Figure 7. Soil temperature as a function of time based on June 2004 Oklahoma Mesonet data: (a) vertical profiles for a sod covered site and (b) the mean soil temperatures for bare soil (TB05, TB10) and sod (TS05, TS10). The shaded region identifies the period of the day when these effects result in less than 1° C difference among the four temperatures (T. Holmes, personal communication).

Finally, it is desirable to establish a long-term climate data record of L-band brightness temperatures and soil moisture. Such a data record could enable investigations of important trends in emissivity, soil moisture, and other derived variables occurring over annual to decadal periods. Both the SMOS and Aquarius L-band missions will operate in 6 am/6 pm orbits, and SMAP will extend these L-band data records.

As will be discussed in Section 3, the current approach to generation of the baseline L2_SM_P product was originally restricted to input data from the 6:00 am descending passes because of the thermal equilibrium assumption and near-uniform thermal conditions of surface soil layers and overlying vegetation in the early morning hours. Accurate soil moisture retrievals using data from 6:00 pm ascending passes may require use of a land surface model and will be generated as part of the L4_SM product (see ATBD for L4_SM). However, some early results from the SMOS mission suggest that the additional error associated with 6 pm retrievals may not be as large as expected [48]. As described in Section 8.1, the SMAP project starting with L2_SM_P Data Release Version 4 (Dec., 2016) produces a 6 pm retrieved soil moisture product using the same retrieval algorithm as the 6 am soil moisture product and with only very slightly degraded accuracy [61, 63].

3. PRODUCT OVERVIEW

This ATBD covers the two coarse spatial resolution soil moisture products which are based on the SMAP radiometer brightness temperatures: L2_SM_P, which is derived surface soil moisture in half-orbit format at 40 km resolution output on a fixed 36-km Equal-Area Scalable Earth-2 (EASE2) grid, and L3_SM_P, which is a daily global composite of the L2_SM_P surface soil moisture, also at 40 km resolution output on a fixed 36-km EASE2 grid. Utilizing one or more of the soil moisture retrieval algorithms to be discussed in section 4, SMAP brightness temperatures are converted into an estimate of the 0-5 cm surface soil moisture in units of cm^3/cm^3.

3.1 Inputs to Soil Moisture Retrieval

The main input to the L2_SM_P processing algorithm is the SMAP L1C_TB product that contains the time-ordered, geolocated, calibrated L1B_TB brightness temperatures which have been resampled to the fixed 36-km EASE2 grid. In addition to general geolocation and calibration, the L1B_TB data have also been corrected for atmospheric effects, Faraday rotation, and low-level RFI effects prior to regridding. If the RFI encountered is too large to be corrected, the T_B data are flagged accordingly and no soil moisture retrieval is attempted. See the L1B_TB and L1C_TB ATBDs for additional details.

In addition to T_B observations, the L2_SM_P algorithm also requires ancillary datasets for the soil moisture retrieval. These include:

- Surface temperature
- Vegetation opacity (or vegetation water content and vegetation opacity coefficient)
- Vegetation single scattering albedo
- Surface roughness information
- Land cover type classification
- Soil texture (sand, silt, and clay fraction)
- Data flags for identification of land, water, precipitation, RFI, urban areas, mountainous terrain, permanent ice/snow, and dense vegetation

The specific parameters and sources of these and other externally provided ancillary data are listed in Section 6. Other parameters used by the L2_SM_P algorithm are provided internally to the processing chain. These include a freeze/thaw flag, an open water fraction, and a vegetation index; these were originally intended to be provided by the SMAP radar L2_SM_A product (see L2_SM_A ATBD) or other ancillary sources. A radiometer-based freeze/thaw flag is now being generated by the L3_FT_P team, although the L2/3_SM_P and L2/3_SM_P_E products currently use modeled soil temperatures to determine frozen ground.

All input T_B and ancillary datasets used in the retrievals are mapped to the 36-km EASE2 grid prior to entering the L2_SM_P processor. All input data, retrieved soil moisture data, and flags utilize the same grid.

DATA INPUT:
Grid cell location on fixed Earth grid (lat, lon)
Time tag (date and time of day)
Calibrated L1C_TB
Static ancillary data [permanent masks (land / water, urban, etc.), soil type, DEM info, % land cover types]
Dynamic ancillary data :
-- Soil temperature
-- Vegetation water content
-- Vegetation parameters (b, τ, ω)
% open water in pixel [from HiRes radar] -- temperature of open water from Ts at 6 am
Frozen ground flag [from L3_F/T]
Precipitation flag
Snow/ice flag
RFI flag [from L1_TB]
Quality flag [include from L1_TB]

DATA OUTPUT:
Grid cell location on fixed Earth grid (lat, lon)
Time tag (date and time of day)
Calibrated water-corrected L1C_TB
Retrieved soil moisture for 6 am overpass
Dynamic ancillary data :
-- Soil temperature
-- Vegetation water content
-- Vegetation parameters (b, τ, ω)
% open water in pixel -- temperature of open water
Frozen ground flag
Precipitation flag
Snow/ice flag
RFI flag
Quality flag

Figure 8. Conceptual list of input and output information for the L2_SM_P soil moisture product.

3.2 Algorithm Outputs

Figure 8 lists in a conceptual way the variety of input and output data associated with the SMAP L2_SM_P soil moisture product. Many of these parameters will be discussed in Section 4 and Section 6. The primary contents of the output L2_SM_P and L3_SM_P products are the retrieved soil moisture and associated quality control (QC) flags, as well as the values of the ancillary parameters needed to retrieve the output soil moisture for that grid cell. The exact Data Product Description for the L2_SM_P and L3_SM_P products was generated in consultation with SMAP Science Data System (SDS) personnel, and is available to the public through the NSIDC DAAC https://nsidc.org/data/smap/technical-references (see also Appendices 1 and 2).

3.3 Product Granularity

The L2_SM_P product is a half-orbit product. SMAP ascending (6 pm) half-orbits are defined starting at the South Pole and ending at the North Pole, while descending (6 am) half-orbits start at the North Pole and end at the South Pole. Input T_B observations from a given half-orbit are processed to generate output soil moisture retrievals for the same half orbit.

The L3_SM_P product is a daily product generated by compositing one day's worth of L2_SM_P half-orbit granules, separately for ascending and descending half-orbits, onto a global array. T_B observations from descending (6 am) passes are used to retrieve soil moisture for the L2_SM_P and L3_SM_P standard products as mentioned in Section 2.4. Starting with L2_SM_P Data Release Version 4 in December, 2016, 6 pm soil moistures are produced by applying the baseline 6 am retrieval algorithm to T_B data from the 6 pm ascending passes. The 6 pm soil moisture data will be done on a best effort basis and will not be included in assessments of whether the L2_SM_P product meets the mission Level 1 requirements. However, the 6 pm retrievals will also be compared against observations of soil moisture to assess their accuracy. Currently, the data volume estimate for the L2_SM_P product is 15 MB/day and the data volume estimate for the L3_SM_P product is 41 MB/day; these values are based on products from the 6 am descending pass only.

3.4 SMAP Product Suite

The L2_SM_P and L3_SM_P products are part of the suite of SMAP products shown previously in Table 2. The SMAP L1-L3 products will be generated by the SMAP Science Data Processing System (SDS) at JPL, while the SMAP L4 products will be produced by the Global Modeling and Assimilation Office (GMAO) at NASA GSFC. All SMAP data products approved for release will be archived and made available to the public through a NASA-designated Earth Science Distributed Active Archive Center. NASA HQ has designated that the National Snow and Ice Data Center (NSIDC) in Boulder, CO will be the primary SMAP DAAC, although SMAP HiRes radar data will be archived separately at the Alaska Satellite Facility (ASF) in Fairbanks, AK.

3.5 EASE Grid

The grid selected for the SMAP geophysical (L2-L4) products is the updated Equal-Area Scalable Earth-2 (EASE2) grid [26]. This grid was originally conceived at the NSIDC and has been used to archive several satellite instrument data sets including SMMR, SSM/I, and AMSR-E [27]. Using this same grid system for SMAP provides user convenience, facilitates continuity of historical data grid formats, and enables re-use of heritage gridding and extraction software tools developed for EASE grid.

The EASE grid has a flexible formulation. By adjusting one scaling parameter it is possible to generate a family of multi-resolution EASE grids that "nest" within one another. The nesting can be made "perfect" in that smaller grid cells can be tessellated to form larger grid cells, as shown in Figure. 9a. This feature provides SMAP data products with a convenient common projection for both high-resolution radar observations and low-

resolution radiometer observations. Figure 9b illustrates the different resolutions for the 3-, 9-, and 36-km EASE grids.

A nominal EASE grid dimension of 36 km has been selected for the L2/3_SM_P products. This is close to the 40-km resolution of the radiometer footprint and scales conveniently with the 3 km and 9 km grid dimensions that have been selected for the radar-only (L2/3_SM_A) and combined radar/radiometer (L2/3_SM_A/P) soil moisture products, respectively. A global 36-km EASE grid can be constructed having an integer number of rows and columns (408 and 963), with northernmost/southernmost latitudes of ±86.6225°, using a scaling parameter[1] that is almost exactly 36 km. Starting with data release R18 in October 2021, the soil moisture product is also provided on the North Polar EASE2 grid projection in addition to the Global EASE2 grid projection (see Appendix 5 for details).

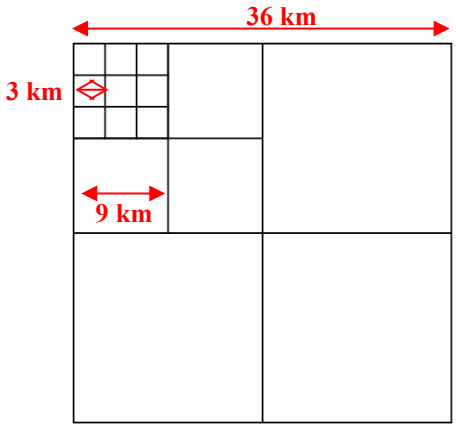

Figure 9a. Perfect nesting in EASE grid – smaller grid cells can be tessellated to form larger grid cells.

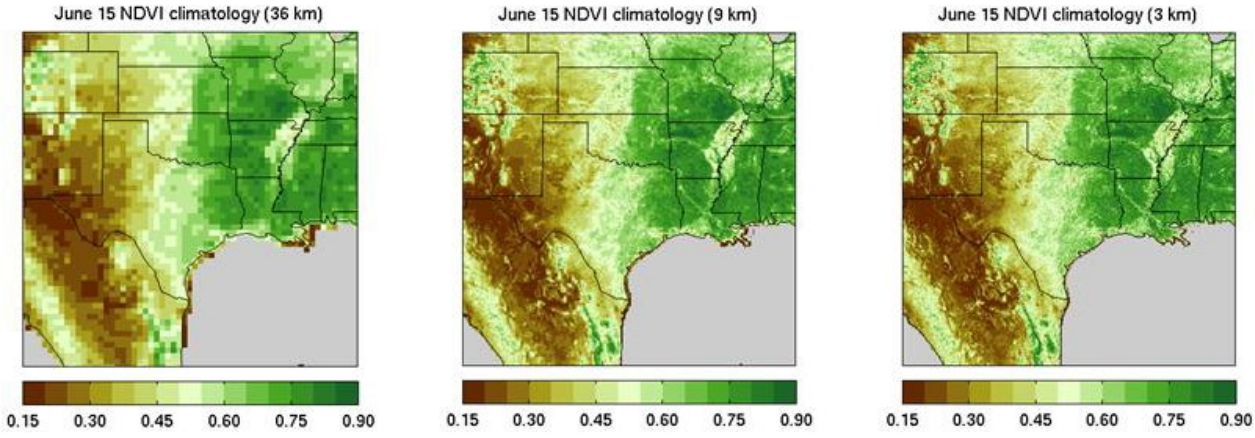

Figure 9b. Example of ancillary NDVI climatology data displayed on the SMAP 36-km, 9-km, and 3-km EASE grids.

[1] The precise value of the scaling parameter is 36.00040003 km at ±30° latitudes.

3.6 Soil Moisture Retrieval Process

Figure 10 illustrates the conceptual process used in retrieving soil moisture from SMAP radiometer brightness temperature measurements. In order for soil moisture to be retrieved accurately, a variety of global static and dynamic ancillary data are required (Section 6). Static ancillary data are data which do not change during the mission, while dynamic ancillary data require periodic updates in time frames ranging from seasonally to daily. Static data include parameters such as permanent masks (land/water/forest/urban/ mountain), the grid cell average elevation and slope derived from a DEM, permanent open water fraction, and soils information (primarily sand and clay fraction). The dynamic ancillary data include land cover, precipitation, vegetation parameters, and effective soil temperatures. Although surface roughness can vary temporally, especially seasonal changes in agricultural areas, the current SMAP operational code treats surface roughness as a static variable. The SMAP Project is investigating the value, impact, and operational complexity of having surface roughness vary with time. Measurements from the SMAP radar were planned to be one source of information on open water fraction and frozen ground, in addition to water information obtained from a MODIS-derived surface water data base and temperature information from the GMAO model used in L4_SM. Ancillary data

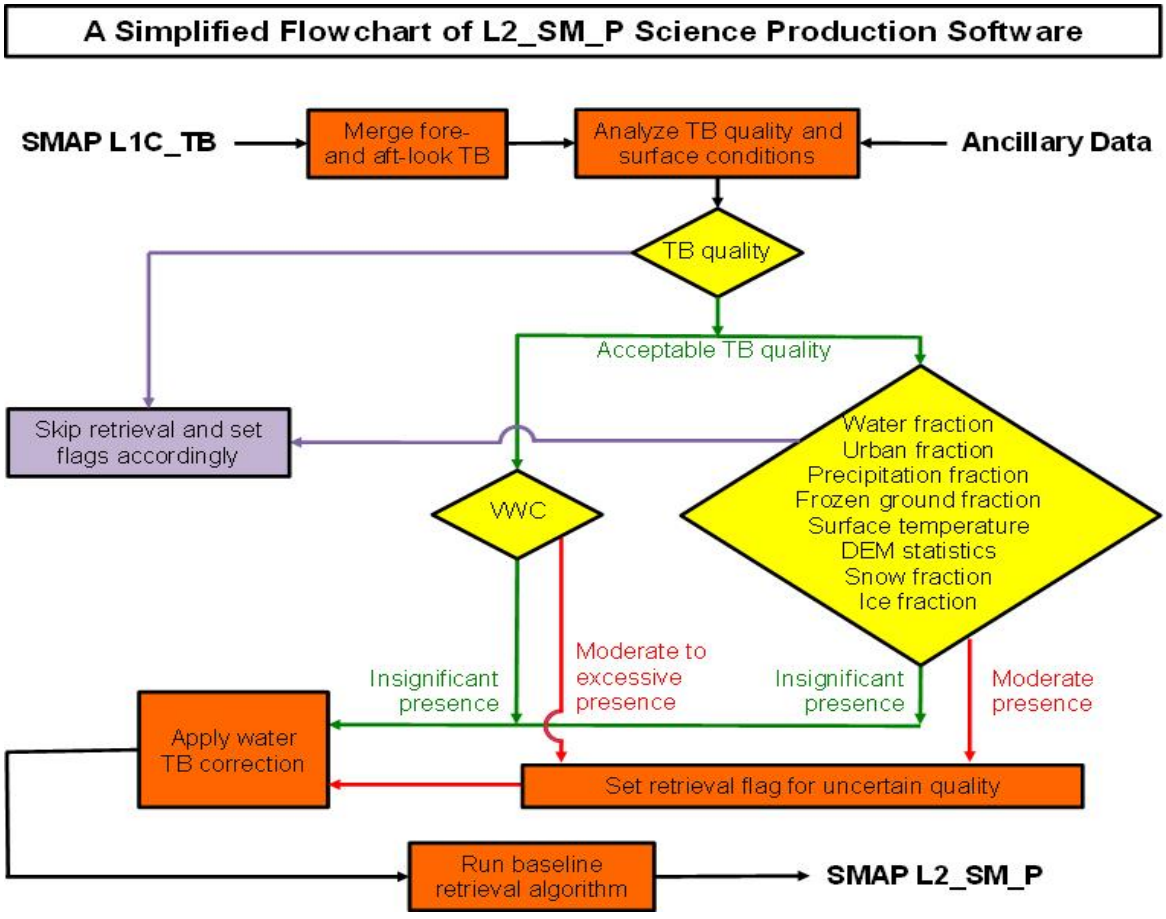

Figure 10. Conceptual flow of L2_SM_P process from input of T_B to output of retrieved soil moisture.

will also be employed to set flags which help to determine either specific aspects of the processing (such as corrections for open water to be discussed in Section 4) or the quality of the retrievals (e.g. precipitation flag). Basically, these flags would provide information as to whether the ground is frozen, snow-covered, or flooded, or whether it is expected to be actively precipitating at the time of the satellite overpass. Other flags will indicate whether masks for steeply sloped topography, or for urban, heavily forested, or permanent snow/ice areas are in effect. All input data to the L2_SM_P processor are pre-mapped to the 36-km EASE2 grid.

Consistent with the SMAP Level 2 mission requirements [28], the L2_SM_P product is a half-orbit product — T_B observations from a given half orbit go through the retrieval algorithm to produce retrieved soil moisture for the same half orbit. An example of the L2_SM_P soil moisture from part of a single half orbit over the United States as simulated on the SMAP Algorithm Testbed (Section 5) is shown in Figure 11. This example is based on a single-channel algorithm operating on H-polarized T_B observations simulated using geophysical data from a land surface model.

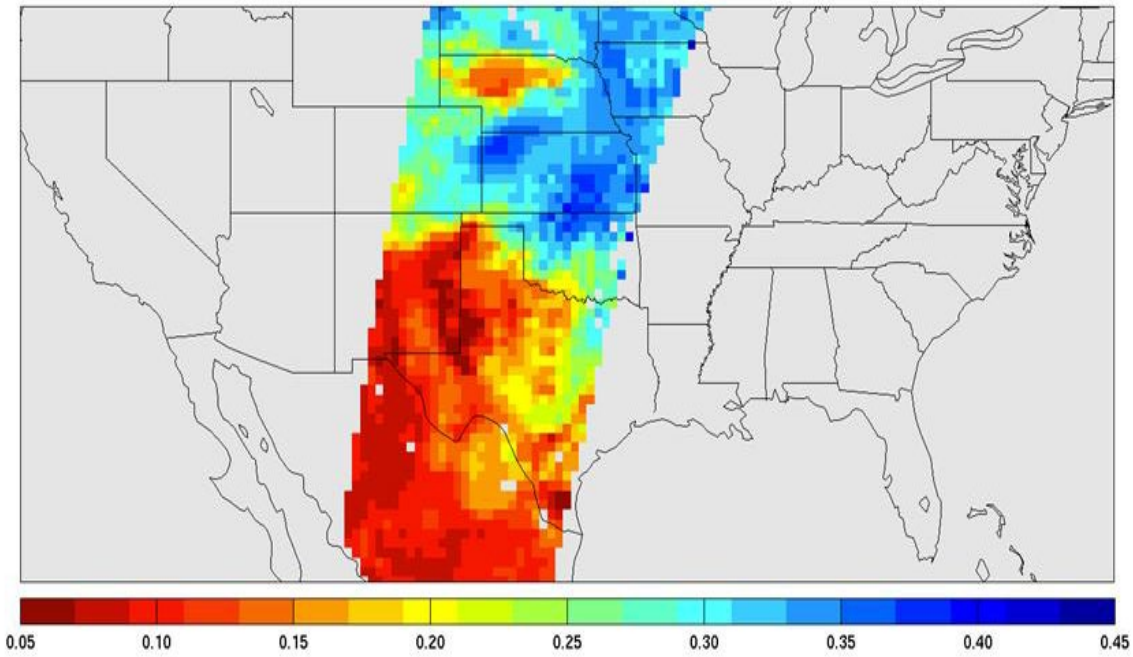

Figure 11. Example of SMAP retrieved soil moisture in cm^3/cm^3. The half-orbit swath pattern is simulated using the orbital sampling module on the SMAP Algorithm Development Testbed.

3.7 Level 3 Radiometer-Based Soil Moisture Product (L3_SM_P)

The L3_SM_P product is a daily global product. To generate the product, individual L2_SM_P half-orbit granules acquired over one day are composited to produce a daily multi-orbit global map of retrieved soil moisture.

The L2_SM_P swaths overlap poleward of approximately ±65° latitude. Where overlap occurs, three options are considered for compositing multiple data points at a given grid cell:

1. Use the most recent (or "last-in") data point
2. Take the average of all data points within the grid cell
3. Choose the data point observed closest to 6:00 am local solar time

The current approach for the L3_SM_P product is to use the nearest 6:00 am local solar time (LST) criterion to perform Level 3 compositing (a similar procedure is used for 6 pm starting in Data Release Version 4). According to this criterion, for a given grid cell, an L2 data point acquired closest to 6:00 am local solar time will make its way to the final Level 3 granule; other 'late-coming' L2 data points falling into the same grid cell will be ignored. For a given granule whose time stamp (yyyy-mm-ddThh:mm:ss) is expressed in UTC, only the hh:mm:ss part is converted into local solar time. For example,

UTC Time Stamp	**Longitude**	**Local Solar Time**
2011-05-01T23:19:59	60E	23:19:59 + (60/15) hrs = 03:19:59

The local solar time 03:19:59 is then compared with 06:00:00 in Level 3 processing for 2011-05-01 to determine if the swath is acquired closest to 6:00 am local solar time. If so, that data point (and only that data point) will go to the final Level 3 granule. Under this convention, an L3 composite for 2011-05-01 has all Level 2 granules acquired within 24 hours of 2011-05-01 UTC and Level 2 granules appearing at 2011-05-02 6:00 am local solar time at the equator. Note that this is also the conventional way to produce Level 3 products in similar missions and is convenient to users interested in global applications. Figure 12 shows an example of the L3_SM_P soil moisture output for one day's worth of simulated SMAP descending orbits globally (Fig. 12a) and over just the continental U.S. (CONUS) (Fig. 12b).

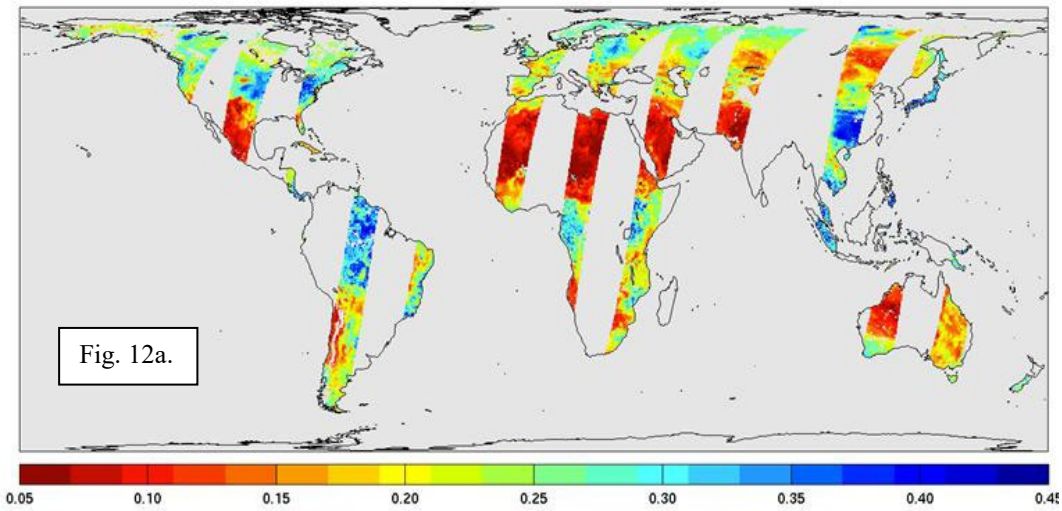

Fig. 12a.

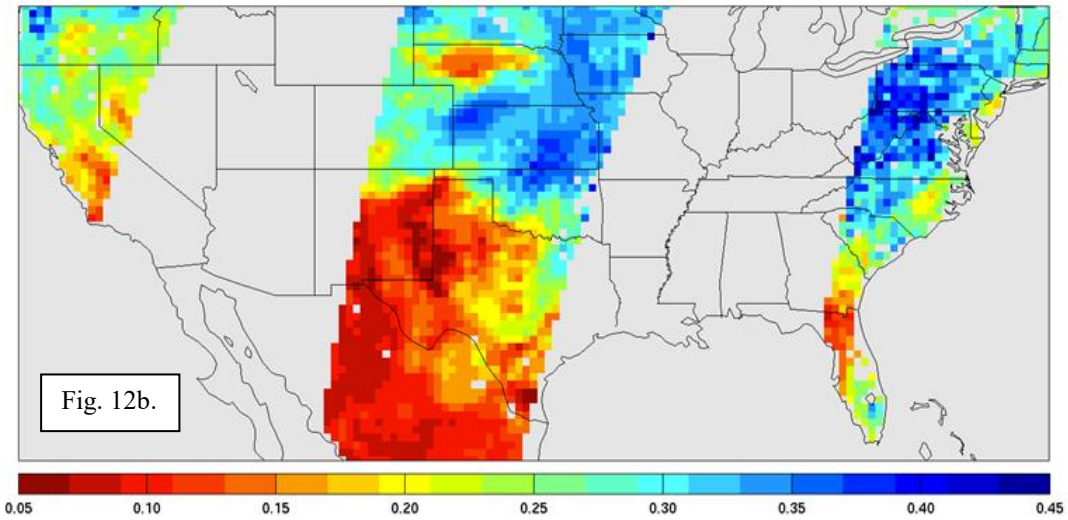

Figure 12. Simulation of L3_SM_P retrieved soil moisture in cm^3/cm^3. This example is based on the single channel algorithm operating on H-polarized T_B observations simulated using geophysical data from a land surface model.

4. RETRIEVAL ALGORITHMS

Decades of research by the passive microwave soil moisture community has resulted in a number of viable soil moisture retrieval algorithms that can be used with SMAP T_B data. ESA's SMOS mission currently flies an aperture synthesis L-band radiometer which produces T_B data at multiple incidence angles over the same ground location. The baseline SMOS retrieval algorithm is based on the *tau-omega* model described in Section 2.1 but utilizes the SMOS multiple incidence angle capability to retrieve soil moisture. SMAP retrievals will also be based on the *tau-omega* model but will use the constant incidence angle T_B data produced by the SMAP conically-scanning radiometer. Other needed parameters in the retrieval will be obtained as ancillary data.

SMAP algorithms are evaluated for their soil moisture retrieval performance during the pre- and post-launch time frames. The algorithms will be compared using theoretical simulations and observational data. Upon periodic assessment and review by the SMAP science team, a retrieval algorithm option with better performance than the baseline algorithm may replace the earlier baseline and become the new baseline.

For the SMAP L2_SM_P and L2_SM_P_E products, three soil moisture retrieval algorithms are currently being implemented operationally:

- Single Channel Algorithm at V polarization (SCA-V)
- Single Channel Algorithm at H polarization (SCA-H)
- Dual Channel Algorithm (DCA)

A previous optional algorithm (Modified Dual Channel Algorithm – MDCA) has been renamed back to the original DCA as of the R17 data release in August, 2020.

Evaluations are done using SMAP measurements and simulations, testing with observational data from the PALS airborne and ComRAD ground-based instruments (SMAP simulators), other field campaign data and *in situ* cal/val (CV) site data, as well as by applying candidate SMAP algorithms to SMOS and Aquarius satellite T_B data. All candidate algorithms are described in this section. Prior to implementing the actual soil moisture retrieval, a preliminary step in the processing is to perform a water body correction to the brightness temperature data for cases where a significant percentage of the grid cell contains open water.

4.1 Water TB Correction

At the 40-km footprint resolution scale of the SMAP radiometer, a significant percentage of footprints within the SMAP land mask will contain some amount of open fresh water due to the presence of lakes, rivers, wetlands, and transient flooding. It is assumed that all ocean pixels will be masked out using the SMAP ocean/land mask. For soil moisture retrieval purposes, the presence of open water within the radiometer footprint (IFOV) is undesirable since it dramatically lowers the brightness temperature and results in anomalously high retrieved soil moisture for that grid cell if soil moisture is retrieved without knowledge of the presence of open water. This results in a bias which degrades the overall soil moisture retrieval accuracy. It is therefore important to correct the SMAP Level 1 T_B observations for the presence of water, to the extent feasible, prior to using them as inputs to the L2_SM_P soil moisture retrieval. Fortunately, this bias can be corrected, especially when it occurs at dawn near inland water/land boundaries where the temperature of water can be reasonably approximated as the temperature of land (as shown in Fig. 6).

Prior to implementing a soil moisture retrieval, a preliminary step in SMAP processing is to perform a water body correction to the brightness temperature data for cases where a significant percentage of the grid cell contains open water. New to the End-of-Prime-Mission release in June, 2018 for Version 2 of the L2_SM_P_E and Version 5 of the L2_SM_P soil moisture products, water correction is performed at the footprint level using the SMAP radiometer antenna gain pattern [69]. This correction procedure is performed in the Version 4 SMAP L1B Radiometer Half-Orbit Time-Ordered Brightness Temperatures (L1B_TB) product. Both the horizontally and vertically polarized L1B brightness temperatures over land are corrected for the presence of water within the antenna field of view (FOV). The resulting L1B brightness temperatures are then interpolated on the 9 km EASE Grid 2.0 projections using the Backus-Gilbert optimal interpolation method for the L1C_TB_E product and on the 36 km EASE Grid 2.0 projections using the inverse-distance squared interpolation method for the L1C_TB product. Note that both L1C products have water-corrected and uncorrected TB fields stored separately in their output fields.

Over land, the resulting brightness temperatures become warmer upon the removal of the contribution of water to the original uncorrected observations. As stated in the product

page of the Version 4 SMAP L1B_TB product, water correction is performed as long as the antenna-gain-weighted water fraction within the antenna FOV is less than or equal to 0.9 and when the antenna boresight falls on a land location as indicated by a static high-resolution land/water mask. Further details of this procedure can be found in the User Guide, L1B_TB ATBD, or Assessment Report of the Version 4 SMAP L1B_TB product. The water-corrected brightness temperatures are further checked against valid data bounds (TB_{max} and TB_{min}) prior to being used in L2 soil moisture retrieval, where TB_{max} is set to be 340 K and TB_{min} is derived from the Klein-Swift water dielectric model, assuming zero salinity and water temperature predicted by the ancillary GMAO GEOS-5 surface temperature data.

It is important to recognize that there is a threshold for the areal fraction of water within the antenna IFOV above which the correction may generate enough errors that the SMAP's target retrieval accuracy of 0.04 cm^3/cm^3 may not be met. Figure 12 shows how water fraction and land/water classification error affect the retrieval accuracy. Given the uncertainties of T_B observations as well as other model, ancillary, and environmental parameters, a relatively tight margin (0.005 cm^3/cm^3) of retrieval accuracy is plotted as a function of water fraction and classification error for three vegetation water contents (VWC) levels: 0.0, 2.5, and 5.0 kg/m^2. The figure shows that, for a given water fraction, water TB mixed with bare-soil TB is more easily correctable than with densely vegetated TB. In the worst-case scenario (the green curve in Figure 13), a water fraction of 4% with a classification error no greater than 5% is needed to meet a retrieval accuracy of 0.005 cm^3/cm^3 at VWC = 5 kg/m^2.

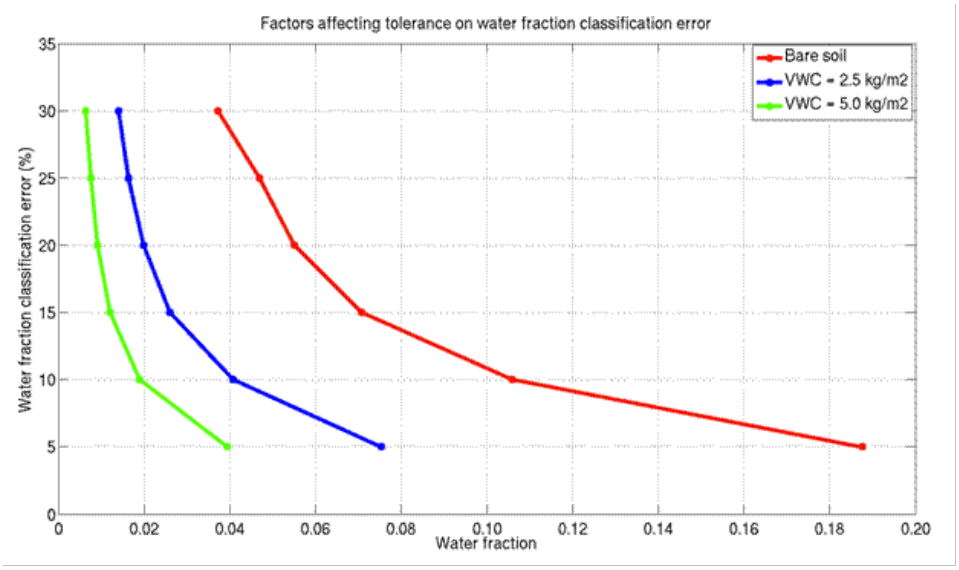

Figure 13. For a given soil moisture retrieval RMSE (0.005 cm^3/cm^3 in this case), more accurate estimation of the water fraction is needed for T_B observations that contain a larger water fraction and/or a larger vegetation water content.

4.2 Single Channel Algorithm

From a broad perspective, there are five steps involved in extracting soil moisture using passive microwave remote sensing. These steps are normalizing brightness temperature to emissivity, removing the effects of vegetation, accounting for the effects of soil surface roughness, relating the emissivity measurement to soil dielectric properties, and finally relating the dielectric properties to soil moisture.

In the single channel algorithm (SCA) [4], horizontally polarized T_B are traditionally used due to their sensitivity to soil moisture, but the same algorithm can also be applied to V polarization T_B. The use of H pol T_B with the SCA was the prelaunch SMAP baseline algorithm; SCA-V was the original baseline for the postlaunch release of L2_SM_P data. In the SCA approach, brightness temperatures are converted to emissivity using a surrogate for the physical temperature of the emitting layer. The derived emissivity is corrected for vegetation and surface roughness to obtain the soil emissivity. The Fresnel equation is then used to determine the dielectric constant. Finally, a dielectric mixing model is used to obtain the soil moisture. Additional details on these steps follow.

At the L band frequency used by SMAP, the brightness temperature of the land surface is proportional to its emissivity (e) multiplied by its physical temperature (T). It is typically assumed that the temperatures of the soil and the vegetation are the same at the SMAP overpass time of 6 am. The microwave emissivity at the top of the soil surface or vegetation canopy is given by (the polarization subscript p is suppressed in the following equations):

$$e = \frac{T_B}{T} \tag{6}$$

If the physical temperature is estimated independently, emissivity can be determined. In the SMAP formulation, ancillary surface temperature in the form of a Numerical Weather Predication model product is utilized to estimate T (see SMAP Ancillary Data Report: Surface Temperature, JPL D-53064).

The emissivity retrieved above is that of the soil as modified by any overlying vegetation and surface roughness. In the presence of vegetation, the observed emissivity is a composite of the soil and vegetation. To retrieve soil water content, it is necessary to isolate the soil surface emissivity (e^{surf}). Following Jackson and Schmugge [15], the emissivity

$$e = [1-\omega][1-\gamma][1+\left(1-e^{surf}\right)\gamma] + e^{surf}\gamma \tag{7}$$

Both the single scattering albedo (ω) and the one-way transmissivity of the canopy (γ) are dependent upon the vegetation structure, polarization and frequency. The transmissivity is a function of the optical depth (τ) of the vegetation canopy:

$$\gamma = \exp[-\tau \sec\theta] \tag{8}$$

At L-band the single scattering albedo tends to be very small, and sometimes is assumed to be zero in order to reduce dimensionality for computational purposes. For SMAP, the capability for a nonzero ω will be retained. Substituting equation 8 into equation 7 and rearranging yields

$$e^{surf} = \frac{e-1+\gamma^2+\omega-\omega\gamma^2}{\gamma^2+\omega\gamma-\omega\gamma^2} \tag{9}$$

The vegetation optical depth is also dependent upon the vegetation water content (*VWC*). In studies reported in [15], it was found that the following functional relationship between the optical depth and vegetation water content could be applied:

$$\tau = b * VWC \tag{10}$$

where *b* is a proportionality value which depends on both the vegetation structure and the microwave frequency. Since *b* is related to the structure of the overlying vegetation, it is likely that *b* will also vary with microwave polarization for at least certain types of vegetation. The variation of the *b* parameter with polarization is currently being studied by the SMAP team – it is expected that analysis of SMOS data and other field data will resolve when a polarization dependence is evident and is therefore needed to improve soil moisture retrieval accuracy for that type of vegetation.

For SMAP implementation of the SCA, the polarization mixing factor *Q* was set equal to zero, while the values of *h*, *b*, and ω will be provided by means of a land cover-based look up table (an example is in Table 3 – note that the most current set of SMAP parameters used in routine processing will be available for download from NSIDC post-launch as the L2_SM_P team works to calibrate the model parameters throughout the cal/val phase of the mission). The vegetation water content can be estimated using several ancillary data sources (Section 6.3). For SMAP, the baseline approach utilizes a set of land cover-based equations to estimate VWC from values of the Normalized Difference Vegetation Index (NDVI) (an index derived from visible-near infrared reflectance data from the EOS MODIS instruments now and the JPSS VIIRS instrument in the SMAP time frame) (see Equation 18). The τ-ω parameters are derived from information in the refereed literature, from past experiences and analyses conducted by the SMAP team, and from informal discussions with subject matter experts [11, 12, 15, and others]. These values will be updated, and polarization-dependent values added, as new information becomes available.

The emissivity that results from the vegetation correction is that of the soil surface, including any effects of surface roughness. These effects must be removed in order to determine the smooth surface soil emissivity (e^{soil}) which is required for the Fresnel equation inversion. One approach to removing this effect is a model described in [16] that yields the bare smooth soil emissivity:

$$e^{soil} = 1 - [1 - e^{surf}] \exp[-h \cos^2 \theta] \tag{11}$$

The $cos^2\theta$ term is sometimes changed to $cos\ \theta$ or dropped completely to avoid overcorrecting for roughness – the specific exponent to use will be determined during the SMAP CV phase. SMAP currently uses $cos^2\theta$. The parameter h is dependent on the polarization, frequency, and geometric properties of the soil surface and is related to the surface height standard deviation s. h values for different land cover types will be included in the SMAP τ-ω parameter look up table.

Emissivity is related to the dielectric properties (ε) of the soil and the viewing or incidence angle (θ). For ease of computational inversion, it can be assumed that the real component (ε_r) of the dielectric constant provides a good approximation of the complex dielectric constant; however, the complex form is also retained in the SMAP L2_SM_P processor. The Fresnel equations link the dielectric constant to emissivity. For horizontal (H) polarization (eq. 2 rewritten for emissivity):

$$e_H(\theta) = 1 - \left| \frac{\cos\theta - \sqrt{\varepsilon_r - \sin^2\theta}}{\cos\theta + \sqrt{\varepsilon_r - \sin^2\theta}} \right|^2 \tag{12}$$

and for vertical (V) polarization the relationship is (eq. 3 rewritten for emissivity):

$$e_V(\theta) = 1 - \left| \frac{\varepsilon_r \cos\theta - \sqrt{\varepsilon_r - \sin^2\theta}}{\varepsilon_r \cos\theta + \sqrt{\varepsilon_r - \sin^2\theta}} \right|^2 \tag{13}$$

The dielectric constant of soil is a composite of the values of its components – air, soil, and water – which have greatly different values. A dielectric mixing model is used to relate the estimated dielectric constant to the amount of soil moisture. As described in Section 2.2, there are three dielectric mixing models under consideration that seem to perform differently in different soil moisture ranges (Wang and Schmugge [21], Dobson et al. [20], and Mironov [19]). The SMOS team is evaluating the relative merits of these dielectric models and their impact on overall soil moisture retrieval accuracy, and is currently using mainly the Mironov model. The SMAP project plans to closely monitor and review the SMOS results in making the selection of a dielectric model for SMAP. The SMAP processor has options for all three of the dielectric models, with the Mironov model also the current SMAP baseline.

Table 3. Example of Look Up Table of Algorithm Parameters by IGBP Class (note: may not be the SMAP current set)

ID	MODIS IGBP land classification	*s*	*h*	*b*	ω	*Stem factor*
0	Water Bodies	--	0	0	0	--
1	Evergreen Needleleaf Forests	1.60	0.160	0.100	0.070	15.96
2	Evergreen Broadleaf Forests	1.60	0.160	0.100	0.070	19.15
3	Deciduous Needleleaf Forests	1.60	0.160	0.120	0.070	7.98
4	Deciduous Broadleaf Forests	1.60	0.160	0.120	0.070	12.77
5	Mixed Forests	1.60	0.160	0.110	0.070	12.77
6	Closed Shrublands	1.00	0.110	0.110	0.050	3.00
7	Open Shrublands	1.10	0.110	0.110	0.050	1.50
8	Woody Savannas	1.00	0.125	0.110	0.050	4.00
9	Savannas	1.00	0.156	0.110	0.080	3.00
10	Grasslands	1.56	0.156	0.130	0.050	1.50
11	Permanent Wetlands	1.00	0	0	0	4.00
12	Croplands - Average	1.08	0.108	0.110	0.050	3.50
	- Wheat	0.83	0.083	TBD	TBD	TBD
	- Mixed (Wheat, Barley, Oats)	1.08	0.108	TBD	TBD	TBD
	- Corn	0.94	0.094	TBD	TBD	TBD
	- Soybean	1.48	0.148	TBD	TBD	TBD
13	Urban and Built-up Lands	--	0	0.100	0.030	6.49
14	Crop-land/Natural Vegetation Mosaics	1.30	0.130	0.110	0.065	3.25
15	Snow and Ice	--	0	0	0	0
16	Barren	1.50	0.150	0	0	0

An example of retrieved soil moisture using the SCA and site-specific correction parameters is shown in Figure 14:

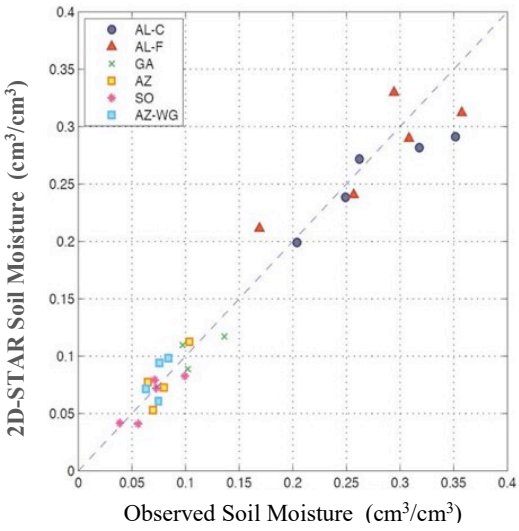

Site	RMSE (cm^3/cm^3)	Corr
Alabama	0.033	0.89
Georgia	0.013	0.62
Arizona	0.012	0.85
Sonora	0.011	0.88
All	0.022	0.98

Figure 14. Soil moisture retrieval error based on L-band H-polarized T_B airborne observations. The vegetation parameter *b* and roughness parameter *h* are optimized using ground measurements of soil moisture from the SMEX03 and SMEX04 field campaigns [[30]; also D. Ryu, personal communication]. The canopy and soil temperatures are assumed to be equal (i.e., $T_c = T_s = T_{eff}$) under the hydraulic equilibrium assumption.

4.2.1 Nonlinear VWC Correction

In terms of soil moisture retrieval performance, the Hydros OSSE [7] revealed that the SCA could produce biased retrievals based on linear VWC correction aggregated from high-resolution vegetation data. However, two relatively simple approaches were developed to create an effective VWC that helps to reduce the bias and overall RMSE in retrieved soil moisture [31, 32]. For example, from [32], the observed $T_B{}^{obs}$ integrated over the IFOV can be written as (assuming uniform soil moisture, soil temperature, surface roughness, and antenna gain):

$$\begin{aligned} T_B{}^{obs} &= \frac{1}{N}\sum_{i=1}^{N} T_{Bi} \\ &= \frac{1}{N}\sum_{i=1}^{N} T_{si}[1 - R_{oi}(m_{vi})e^{-h_i}e^{-2\tau_i}] \\ &= T_s\left[1 - R_o(m_v)e^{-h}\frac{1}{N}\sum_{i=1}^{N} e^{-2\tau_i}\right] \\ &= T_s\,[1 - R_o(m_v)e^{-h}e^{-2\tau^*}] \end{aligned}$$

$$e^{-2\tau^*} = \frac{1}{N}\sum_{i=1}^{N} e^{-2\tau_i} \;,\; \text{or } \tau^* = -\frac{1}{2}\ln\left[\frac{1}{N}\sum_{i=1}^{N} e^{-2\tau_i}\right] \quad \text{(nonlinear VWC correction)} \quad (14)$$

These methods have been successfully applied to the SCA (Figure 15).

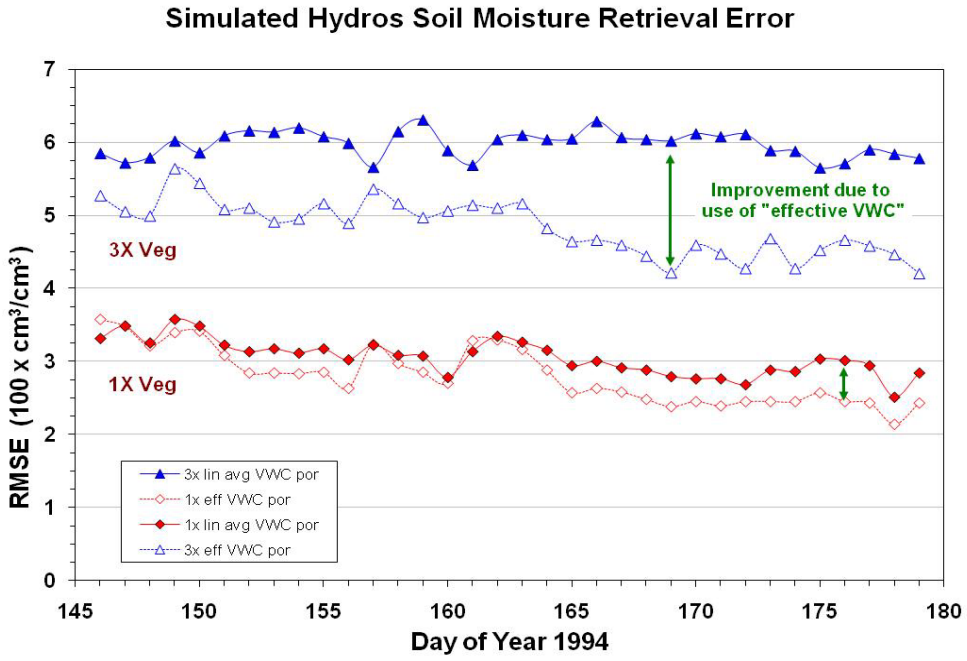

Figure 15. Improvement in simulated Hydros soil moisture retrieval error using a simple effective VWC correction with the SCA algorithm for existing vegetation (1X) and for artificially increased simulated vegetation amounts (3X) [31].

4.3 Dual Channel Algorithm

The Dual Channel Algorithm (DCA) uses both H-polarized and V-polarized T_B observations to simultaneously retrieve soil moisture and vegetation optical depth [33] by minimizing the cost function *F*

$$F(sm,\tau) = \left(TB_V^{obs} - TB_V^{modeled}\right)^2 + \left(TB_H^{obs} - TB_H^{modeled}\right)^2 + \lambda^2(\tau - \tau^*)^2,$$

where $TB_V^{modeled}$ and $TB_H^{modeled}$ are the brightness temperature modeled by the *tau-omega* model addressed in Section 2.1, equation 1. Similar to the SCA, some estimates of model parameters (e.g., surface temperature, surface roughness, and vegetation single scattering albedo) must be provided using ancillary datasets in the inversion process. In contrast with the SCA, the polarization mixing factor is assumed to be linearly related to the roughness parameter *h* as in $Q = 0.1771\ h$ [65]. *h* is provided to the algorithm through a pre-computed static ancillary file with global values of *h* over the 3 km EASE-2 grid (see Section 6 for details). In addition to these differences, DCA uses different values than SCA for the vegetation single scattering albedo. The new values of omega were selected based on several independent sources. Table 4 displays the values of albedo proposed by different independent teams (SMAP L2, SMAP L4, SMOS-IC [67] and the Multi-Temporal Dual Channel Algorithm (MTDCA) [66]) and the resulting values used by the current DCA implementation (last column).

The regularization term $\lambda^2(\tau - \tau^*)^2$ was applied to reduce the temporal and spatial noise caused by the nature of the cost function. τ^* is the initial guess for the unknown vegetation optical depth derived from MODIS NDVI vegetation water content climatology. The parameter λ is the regularization parameter weight which was assumed to be $\lambda = 20$. The λ value was selected trying to balance the noise reduction and at the same time to give the optimization process enough freedom to converge to values sufficiently distant from τ^*. Figure 16 shows an example of the cost function for different values of λ. The black point represents the initial guess and the red points are the solution when the observed brightness temperatures are perturbed with noise. While for $\lambda = 0$, the solutions jump along the blue valley (very noisy), the solutions for $\lambda = 40$ (center) get clustered very close to the τ^* initial guess value, a situation that is not desired due to the nature of the NDVI tau. Therefore, as a compromise, λ was set equal to 20. Figure 17 displays histograms of the standard deviation of the Nyquist frequency for the global daily climatology of DCA tau before and after regularization; the clear shift of the peak to the left of the histograms shows the reduction of the temporal noise in the retrievals of the vegetation optical depth. The selection of the parameter λ based on the standard deviation of the Nyquist frequency of DCA τ (without regularization, $\lambda = 0$) time series at a particular grid point and the initial guess τ^* based on DCA climatology will be the subject of future work.

Note that an assumption implicit in this algorithm is that the optical depth is identical for both polarizations.

Table 4. Vegetation single scattering albedo ω provided by four independent scientific teams. The DCA omega values were adopted after evaluation of the proposed omega values from the four independent teams [SMAP L2, SMAP L4, Multi-Temporal Dual Channel Algorithm (MTDCA from MIT) and SMOS-IC].

ID	MODIS IGBP land classification	SMAP SCA	SMAP L4	MTDCA	SMOS-IC	SMAP DCA
0	Water Bodies	0.000	--	0.00	0.00	0.00
1	Evergreen Needleleaf Forests	0.050	0.11	0.07	0.06	0.07
2	Evergreen Broadleaf Forests	0.050	0.07	0.08	0.06	0.07
3	Deciduous Needleleaf Forests	0.050	0.11	0.06	0.06	0.07
4	Deciduous Broadleaf Forests	0.050	0.09	0.07	0.06	0.07
5	Mixed Forests	0.050	0.10	0.07	0.06	0.07
6	Closed Shrublands	0.050	0.09	0.08	0.10	0.08
7	Open Shrublands	0.050	0.09	0.06	0.08	0.07
8	Woody Savannas	0.050	0.12	0.08	0.06	0.08
9	Savannas	0.080	0.13	0.07	0.10	0.10
10	Grasslands	0.050	0.06	0.06	0.10	0.07
11	Permanent Wetlands	0.000	0.13	0.16	0.10	0.10
12	Croplands - Average	0.050	0.10	0.10	0.12	0.06
13	Urban and Built-up Lands	0.030	0.10	0.08	0.10	0.08
14	Crop-land/Natural Vegetation Mosaics	0.065	0.14	0.09	0.12	0.10
15	Snow and Ice	0.000	0.09	0.11	0.10	0.00
16	Barren	0.000	0.07	0.02	0.12	0.00

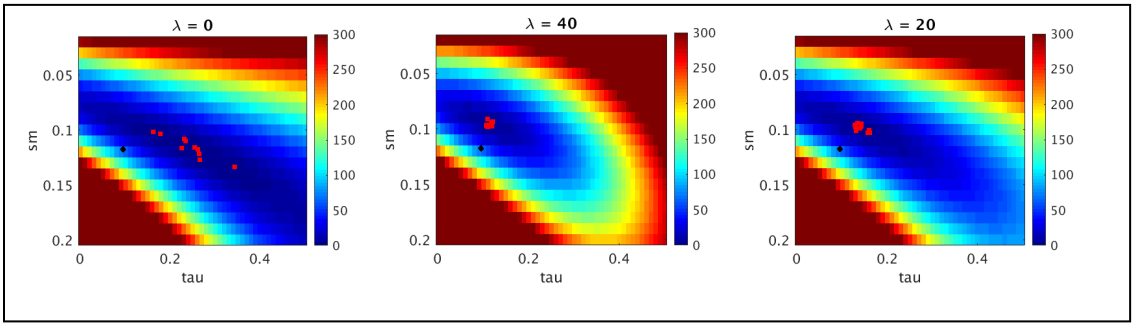

Figure 16. Image of the cost function F for different values of lambda. From left to right: $\lambda = 0$, $\lambda = 40$ and $\lambda = 20$. The black dot represents the initial value and the red dots are the solution for different realizations of the perturbed brightness temperatures.

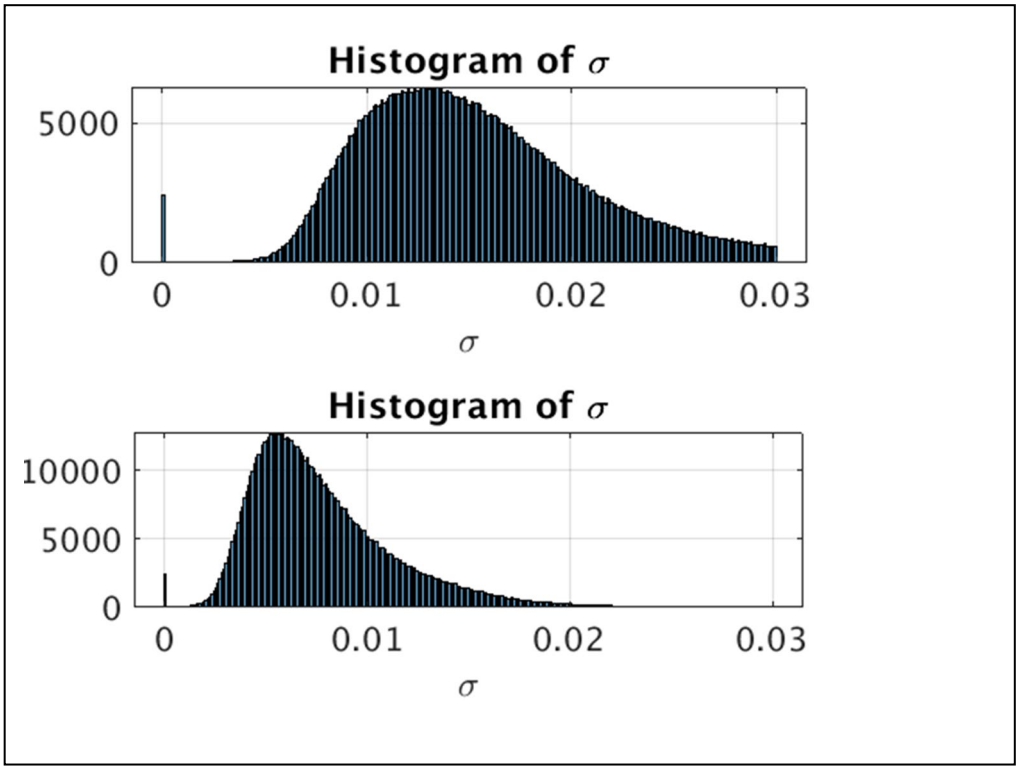

Figure 17. Histograms of σ , standard deviation of the Nyquist frequency of DCA τ before (top) and after (bottom) regularization.

4.4 Land Parameter Retrieval Model

The Microwave Polarization Ratio Algorithm (MPRA) is discontinued as of the R16.3 data release. MPRA, based on the Land Parameter Retrieval Model [35], is an index-based retrieval model that uses dual polarization channels at a single microwave frequency (typically C or X-band) to derive soil moisture and vegetation optical depth. As implemented on multi-frequency satellites such as AMSR-E, it also uses the Ka-band V-polarized channel to retrieve physical temperature of the surface. Only a few studies [36] have examined the applicability of this model at L-band frequencies, although analysis of SMOS data with LPRM is currently underway [R. de Jeu, personal communication, 2011]. Because there are no Ka-band V-polarized T_B observations available from the SMAP instruments, surface temperature will be obtained using ancillary data sets as with the other L2_SM_P algorithms.

In the MPRA, the radiative transfer model operates on two assumptions: (1) the soil and canopy temperatures are considered equal (T), and (2) the vegetation transmissivity (γ) and the single-scattering albedo (ω) are the same for both H and V polarizations. If e_s is the soil emissivity, the T_B can be expressed by the *tau-omega* model (Eq. 1) with $T_C = T_S = T$:

$$T_B = e_s\gamma T + (1-\omega)(1-\gamma)T + \gamma(1-e_s)(1-\omega)(1-\gamma)T \quad (15)$$

The single scattering albedo ω represents the loss of energy in the canopy and is assumed by MPRA to be constant globally, in contrast to the other L2_SM_P algorithms where a nonzero ω is assumed to be a function of land cover type and is input as an ancillary parameter (from look up table). In a previous study [36] using L-band T_B from an aircraft experiment in Australia, the global ω was set equal to 0; however, for the ongoing SMOS analyses, $\omega = 0.05$ is being used as the global value [R. de Jeu, personal communications, 2011].

The Microwave Polarization Difference Index (MPDI) and the observed emissivity (e_H and e_V) are used in MPRA to derive the vegetation optical depth [38], which in turn is used to calculate the transmissivity (γ). The MPDI and vegetation optical depth are calculated as follows:

$$MPDI = \frac{T_{BV} - T_{BH}}{T_{BV} + T_{BH}} \quad (16)$$

$$\tau = \cos(\theta)\, ln\left[ad + \sqrt{(ad)^2 + a + 1}\right] \quad (17)$$

where a and d are $a = 0.5\ [(e_V - e_H) / \text{MPDI} - e_V - e_H]$ and $d = 0.5\ \omega / (1 - \omega)$.

The observed emissivity can also be modeled as a function of soil moisture and temperature in three steps. First, the dielectric constant is calculated as a function of soil moisture, temperature, and soil type following the parameterization of Wang and Schmugge [21]. Second, the smooth surface emissivity is calculated by applying the Fresnel equations. Third, this emissivity is corrected for roughness effects according to Choudhury *et al*. [16]. The roughness parameterization requires an estimate of the parameter h, which is dependent on the polarization, frequency and geometric properties of the soil surface. In previous applications of this approach using C- and X- band, it was found acceptable to set this roughness parameter to a constant; with SMAP, a land cover-based roughness will likely be used for consistency with the other algorithms. With this set of equations, soil moisture is retrieved in an optimization routine that minimizes the error between the modeled and observed H-polarized brightness temperatures. The vegetation optical depth at this optimized soil moisture value is an additional retrieval result.

4.5 Extended Dual Channel Algorithm (E-DCA)

The E-DCA is a variant of DCA and it is discontinued as of the R16.3 data release. Like DCA, E-DCA uses both the vertically and horizontally polarized T_B observations to solve for soil moisture and vegetation optical depth. In E-DCA, however, the cost function (Φ^2) is formulated in a way different from that of DCA. Instead of minimizing the sum of squares of the differences between the observed and estimated T_Bs as in DCA (Equation 1 above), the E-DCA attempts to minimize the sum of squares of the difference between the observed and estimated normalized polarization differences (expressed in natural

logarithm) and the difference between the observed and estimated T_Bs (also expressed in natural logarithm) as follows:

$$\min \Phi^2_{\mathrm{E-DCA}} = \left[\log\left(\frac{T^{obs}_{B,v} - T^{obs}_{B,h}}{T^{obs}_{B,v} + T^{obs}_{B,h}}\right) - \log\left(\frac{T^{est}_{B,v} - T^{est}_{B,h}}{T^{est}_{B,v} + T^{est}_{B,h}}\right)\right]^2 + \left[\log\left(T^{obs}_{B,h}\right) - \log\left(T^{est}_{B,h}\right)\right]^2 \quad (18)$$

In each iteration step, soil moisture and vegetation opacity are adjusted simultaneously until the cost function attains a minimum in a least square sense. It is clear that when both Φ^2_{DCA} and $\Phi^2_{\mathrm{E-DCA}}$ attain their theoretical minimum value (i.e. zero) in the absence of uncertainties of modeling, observations, and ancillary data, $T^{obs}_{B,v} = T^{est}_{B,v}$ and $T^{obs}_{B,h} = T^{est}_{B,h}$, implying that DCA and E-DCA converge to the same solutions. The advantage of E-DCA over DCA, however, is apparent when in reality there is finite uncertainty (e.g., a dry bias associated with the ancillary soil temperature data) -- this uncertainty will be cancelled from the numerator and denominator in the calculation of the normalized polarization difference in $\Phi^2_{\mathrm{E-DCA}}$, leaving such uncertainty affecting only one component of the cost function instead of two components as in Φ^2_{DCA}. This reduction in the impact of soil temperature uncertainty on soil moisture retrieval should make E-DCA more tolerant of soil temperature uncertainty, resulting in fewer instances of retrieval failure than DCA. At present, there are a few caveats associated with E-DCA: (1) its exact performance is being evaluated in the ongoing Cal/Val activities and is not included in the assessment reports to date, and (2) the choice of the horizontally polarized T_B in the $\Phi^2_{\mathrm{E-DCA}}$ formulation is subject to further assessment as analyses of new observations and Cal/Val data become available.

4.6 Algorithm Error Performance

One measure of algorithm performance is determining the accuracy of the retrieved soil moisture in a root square sense. Different algorithms respond differently to uncertainty in a given model / ancillary parameter. One initial pre-launch test performed by the SMAP team involved retrieving soil moisture from one year of global simulated SMAP brightness temperatures, varying one parameter in turn while keeping the other parameters constant with no error (the SMAP Algorithm Testbed will be described in Section 5). Table 5 lists the error in retrieved volumetric soil moisture (in cm^3/cm^3) for each of four SMAP L2_SM_P candidate algorithms over the full range of soil and vegetation water content (VWC) conditions encountered in the global simulation. The first column lists the parameter and its assigned error. Across this full range of conditions, with error only in one parameter at a time, all of the algorithms appear to perform to acceptable levels in retrieving soil moisture.

A more stringent simulation is to assign some error to all parameters simultaneously and then assess the accuracy in retrieved soil moisture. Figure 18 shows the results obtained when the indicated errors were applied to the indicated parameters and soil moisture was retrieved for one year and compared to the "true" soil moisture. All

algorithms meet the SMAP mission requirements of retrieving soil moisture to an accuracy of 0.04 cm^3/cm^3 for areas within the SMAP mask where VWC is ≤ 5 kg/m^2 when averaged across all VWC bins. For this simulation, parameters such as *b* and *h* were assumed to be the same for both H and V polarization. This assumption will be re-examined as new information is obtained (through analysis of SMAP, SMOS and other field data) regarding quantification of any polarization dependence of any of the algorithm parameters. [Note that the metrics in Table 5 and Figure 18 reflect the prelaunch implementation of the different algorithms and do not reflect the performances of the algorithms as implemented in subsequent postlaunch data releases; current algorithm performance can be obtained from the latest assessment report posted at NSIDC: https://nsidc.org/data/smap/technical-references].

Additional studies using a new more realistic global simulation (GloSim3) confirmed the initial results of algorithm performance. Although the baseline SCA algorithm performed somewhat better in these simulations, all algorithms have been coded in the L2_SM_P processor and will be analyzed during the official SMAP CV period. The algorithm which produces the best overall soil moisture retrievals will then be designated as the current SMAP baseline retrieval algorithm. New algorithms providing improved performance will be implemented as warranted throughout the mission.

4.7 Algorithm Downselection

Downselection of the baseline SMAP algorithm for the L2_SM_P product will be based on a combination of demonstrated higher accuracy in retrieved soil moisture, lower bias, better overall performance across land cover classes globally, and operational considerations. Performance results were assessed pre-launch using: (1) simulated data from GloSim3, (2) analyses of past and new field campaign data, especially SMAPVEX-12 and ComRAD (APEX12), and (3) application of SMAP algorithms to SMOS T_B data at the SMAP incidence angle of 40°. Post-launch, performance assessments were made based on comparisons to *in situ* CV site data and other CV approaches (section 7) during the official SMAP calibration / validation period. However, algorithm performance will continually be assessed throughout the SMAP mission, and one of the other algorithms could be substituted for the baseline algorithm should a problem be detected later. This approach insures that the best possible algorithm will be used in order to deliver the best possible product to the public and NASA archives. The SCA-V was the original postlaunch baseline algorithm for the L2/L3_SM_P and L2/L3_SM_P_E products from 2015-2021. As of the October 2021 data release, DCA is the new baseline algorithm (soil moisture retrievals from all three algorithms – SCA-H, SCA-V, and DCA – are still provided in the L2/3_SM_P/P_E output products). Output fields for the SMAP passive soil moisture products can be found in Appendix 1 and 2.

Table 5. Simulated Retrieval Error by Parameter for each Algorithm

	Baseline	Option 1	Option 2	Option 3
Model/Ancillary Uncertainty	SCA (H) RMSE (cm^3/cm^3)	SCA (V) RMSE (cm^3/cm^3)	DCA RMSE (cm^3/cm^3)	MPRA RMSE (cm^3/cm^3)
Gridding + Aggregation	0.00612	0.00581	0.00591	0.00582
5% h	0.00645	0.00595	0.00595	0.00583
5% omega	0.00629	0.00605	0.00619	0.00611
5% sand fraction	0.00729	0.00699	0.00702	0.00697
5% clay fraction	0.00615	0.00585	0.00594	0.00585
2K T5	0.00871	0.01000	0.01120	0.01200
5% VWC	0.00656	0.00608	–	–
10% VWC	0.00717	0.00647	–	–
5% water fraction	0.00612	0.00582	0.00591	0.00582
10% water fraction	0.00612	0.00582	0.00591	0.00583
20% water fraction	0.00614	0.00584	0.00593	0.00583
1.3 K TB	0.00681	0.00674	0.00828	0.00951
RSS	0.0203	0.0201	0.0205	0.0214

Based on GloSim.

L2_SM_P Error Analysis								
	h	omega	sandfrc	clayfrc	T5	VWC	watrfrc	TB
RMSE	5%	5%	5%	5%	2 K	5%	10%	1.3 K

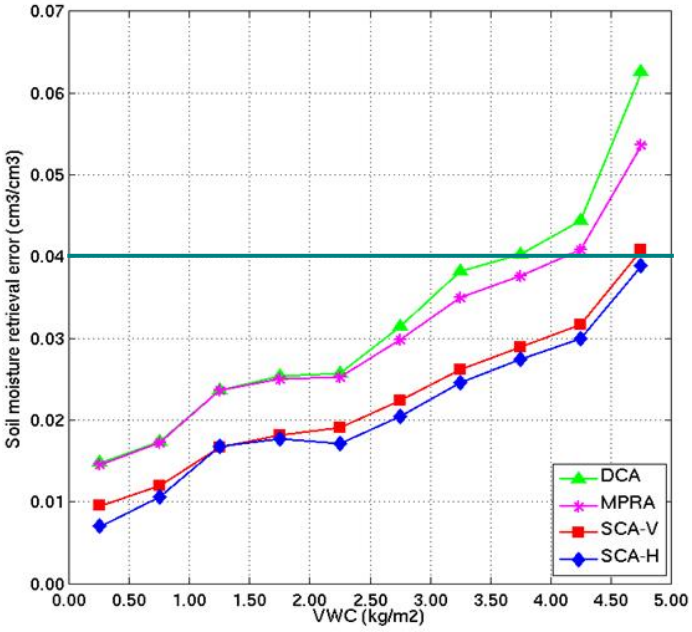

RMSE averaged across all VWC bins			
SCA-H	SCA-V	DCA	MPRA
0.0213	0.0227	0.0323	0.0305

Figure 18. Simulated error performance of all L2_SM_P candidate retrieval algorithms. One year of simulated global SMAP main-beam H- and V-polarized L1C_TB (GloSim3) were used to retrieve soil moisture using perturbed model and ancillary parameters. Static water T_B correction was applied after T_B gridding.

4.7.1 Preliminary Results of Using SMOS Data to Simulate SMAP

Microwave observations from the SMOS mission have been reprocessed to simulate SMAP observations prelaunch at a constant incidence angle of 40° (details of the SMOS reprocessing will be explained in Section 7.1.1). This procedure provides a brightness temperature data set that closely matches the observations that will be provided by the SMAP radiometer. SMOS brightness temperatures provide a global real-world, rather than simulated, input for evaluating the different SMAP radiometer-only soil moisture algorithm alternatives. The use of real-world global observations will also help in the development and selection of different land surface parameters (roughness and vegetation) and ancillary observations needed for the L2_SM_P soil moisture algorithms. The ancillary data sets required are dependent on the choice of the soil moisture algorithm. For example, for its needed vegetation information, the single channel algorithm (SCA) might use (a) SMOS-estimated vegetation optical depth, (b) MODIS-based vegetation climatology data, or (c) actual MODIS observations.

Initial results using the SCA-H with a SMOS-based simulated SMAP T_B data set and MODIS-based vegetation (NDVI) climatology data are presented here. For this preliminary analysis, the roughness parameter (h), vegetation parameter (b), and the single scattering albedo (ω) were assumed constant for all land cover classes (h = 0.1, b = 0.08, ω = 0.05). In subsequent analyses, these parameters will be further refined for different land cover classes as information becomes available and the τ-ω parameter look up table is updated. ECMWF estimates of soil temperature for the top layer (as provided as part of SMOS ancillary data) were used to correct for surface temperature effects and to derive microwave emissivity. ECMWF data were also used for precipitation forecasts and to note the presence of snow and frozen ground.

Figure 19 shows the average soil moisture estimated using the SCA algorithm with the SMOS-simulated SMAP TB data for the ascending orbits (overpass time of 6 AM) for two time periods: (a) June 1-10 and (b) July 1-10, 2011. A MODIS-based NDVI and supporting relationships between NDVI and optical depth were used to correct for vegetation effects. The soil moisture spatial patterns are consistent with geographical features. The estimated soil moisture is very low for desert and arid regions (Africa, Middle East, Central Asia, and Central Australia). High values of soil moisture were observed for forested areas in northern latitudes (Canada and Russia). High soil moisture is also observed over portions of South America.

In June 2011, the northern latitudes of Canada and Siberia had either snow on the ground or the top soil layer was frozen based on the ECMWF forecasts. These areas were flagged during the soil moisture retrieval process. The surface temperature increased in these areas above the freezing mark for the second test period in July 2011. During July, a large part of South-East Asia, Northern South America and Central America is flagged because ECMWF forecasts indicated precipitation at the time of the SMOS overpasses.

Soil moisture retrieved using the SCA-H with SMOS-simulated SMAP T_B for January 2010 – May 2013 was compared to data from *in situ* soil moisture networks in USDA ARS watersheds that have previously been extensively used in satellite-based soil moisture

validation (Jackson et al., 2010, 2011). Figure 20 shows the comparison between observed and estimated soil moisture over the Little River (LR), Little Washita (LW), Walnut Gulch (WG), and Reynolds Creek (RC) watersheds for SMOS ascending orbits (overpass time of 6 AM). Table 6 shows the statistical performance of the SCA-H algorithm over these watersheds. The overall range of soil moisture conditions for the period of record was fairly wide. The SCA retrievals over LR have a low bias and RMSE. For LW, most of the error is because of a dry bias in the soil moisture estimates (-0.028 cm^3/cm^3). The SCA-H soil moisture retrievals for the WG watershed have a good agreement with the *in situ* data with near zero bias. In order to eliminate the effect of snow on SMOS/SMAP retrievals over the RC watershed, only data from July-September were used in the analysis. The SCA results over RC have an underestimation bias that results in a high RMSE. The correlation between the *in situ* observations and estimated soil moisture is good for all the watersheds. As noted earlier, constant values of the roughness parameter, vegetation parameter, and single scattering albedo were used in this analysis, possibly contributing to the observed soil moisture bias.

A second preliminary analysis regridded SMOS 40° T_B data onto the SMAP 36-km EASE2 grid and used SMAP-gridded ancillary data with the SCA to retrieve soil moisture. These retrievals were also compared to *in situ* soil moisture data from the USDA watersheds without site-specific calibration for *h, b,* and ω (RMSE = 0.037 cm^3/cm^3, R=0.71) and with site-specific calibration (RMSE = 0.021 cm^3/cm^3, R=0.78). These results are encouraging for the potential of SMAP to meet its required soil moisture accuracy for the L2_SM_P product.

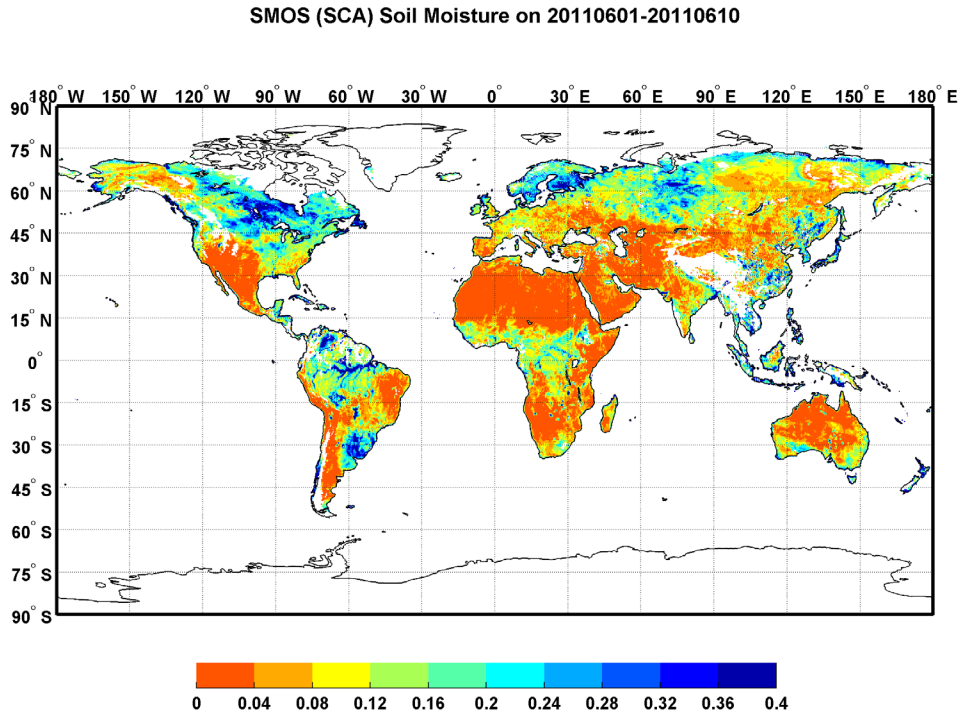

Figure 19a. Average estimated soil moisture using the single channel algorithm (SCA) for SMOS ascending orbits for the period of June 1-10, 2011.

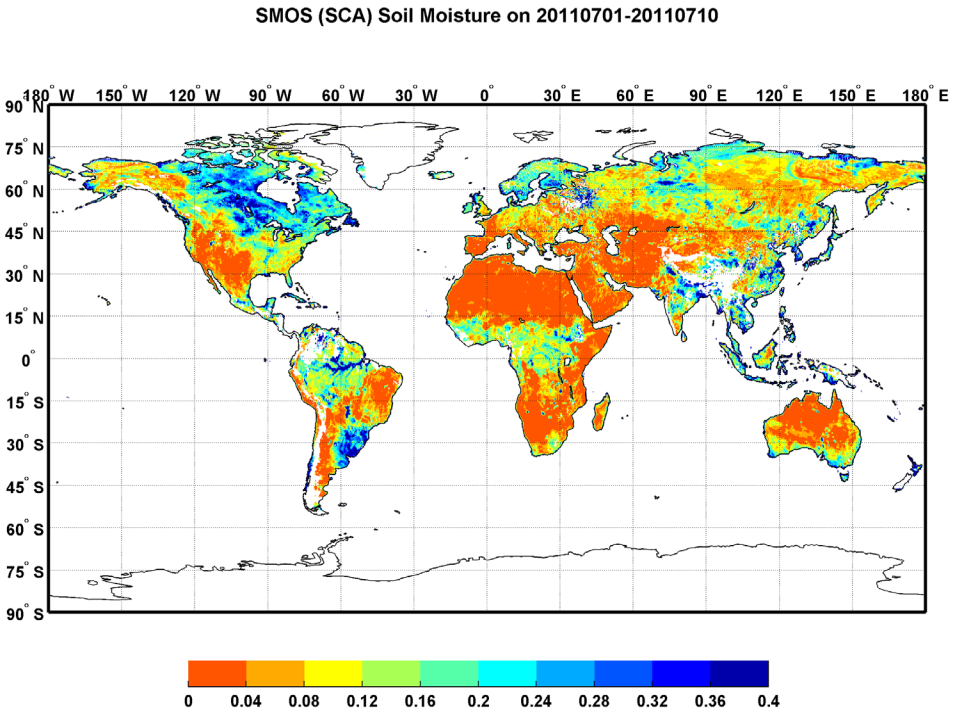

Figure 19b. Average estimated soil moisture using the single channel algorithm (SCA) for SMOS ascending orbits for the period of July 1-10, 2011.

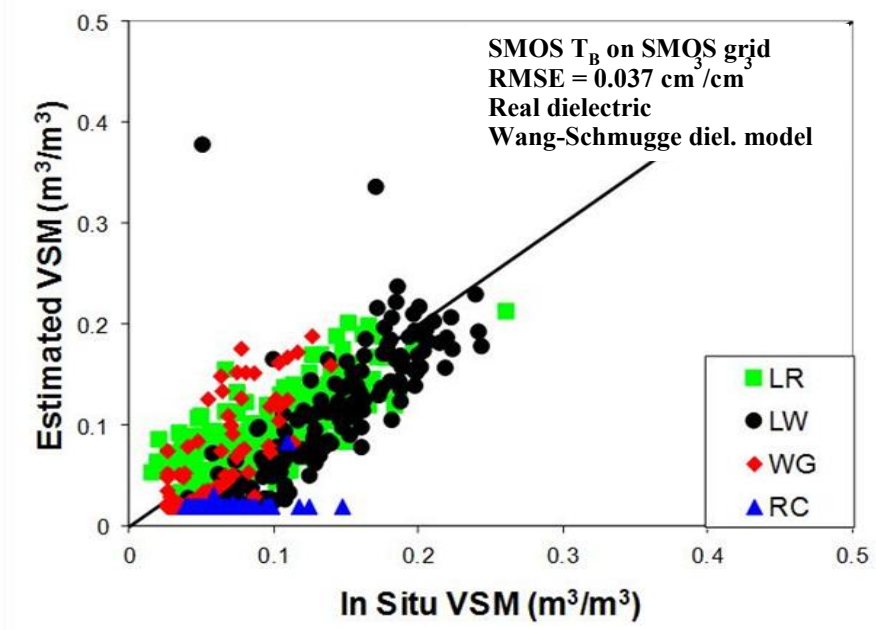

Figure 20. Comparison of estimated soil moisture using SMOS-simulated SMAP T_B with *in situ* observations over USDA ARS watershed sites for ascending orbits (6 AM overpass time) for January 2010-May 2013. One of the two outliers is due to the likely presence of wet snow not predicted by ECMWF; the other outlier is due to an unpredicted active rain event.

Table 6. Statistical summary of the SMOS/SMAP/SCA retrieval algorithm over the USDA watersheds for ascending orbits (6 am overpass time), January 2010 - May 2013.

Watershed	Count	RMSE	R	Bias
Little River, GA	247	0.028	0.767	-0.003
Little Washita, OK	245	0.047	0.841	-0.028
Walnut Gulch, AZ	231	0.025	0.789	-0.008
Reynolds Creek, AZ	74	0.050	0.219	-0.045
Overall	**797**	**0.037**	**0.745**	**-0.016**

RMSE (Root Mean Square Error) and Bias are in cm^3/cm^3 (or m^3/m^3). R = correlation coefficient, N = number of samples. Overall results are essentially the same when binned over 6-month summer and winter seasons (summer RMSE = 0.038, winter RMSE = 0.034).

5. SMAP ALGORITHM DEVELOPMENT TESTBED

The SMAP project has developed and is currently using the Algorithm Development Testbed, a software infrastructure designed to simulate the passive and active microwave observations acquired by SMAP. The Testbed attempts to address the following objectives:

1. To obtain a more rigorous assessment of the soil moisture measurement capability for SMAP relative to that reported in the previous Hydros Risk Mitigation Study,
2. To evaluate how the soil moisture and freeze/thaw measurement capability for SMAP is impacted by different science, instrument, and/or mission trades,
3. To evaluate the relative merits of different microwave models, retrieval algorithms, and ancillary data for meeting the SMAP soil moisture and freeze/thaw science objectives, based on a common set of input and processing conditions, and
4. To provide an end-to-end system that can be used to test the integrated suite of SMAP science product algorithms as a prototype for the SMAP Science Data Processing System (SDPS).

Of relevance to this ATBD, the Testbed can be used to evaluate the performance of different retrieval algorithms and to establish the corresponding error budgets based on a common set of geophysical and instrument conditions. Within the Testbed environment, the following three approaches are adopted: (1) numerical analyses based on land surface model (LSM) outputs, (2) numerical analyses based on Monte Carlo simulations, and (3) algorithm validation based on observations from field campaigns that feature L-band active and passive observations (e.g. SGP99, SMEX, CLASIC, and SMAPVEX). These components and the interrelationships among them are summarized in Figure 21.

With LSM outputs, the Testbed can generate simulated brightness temperature and radar backscatter observations according to SMAP's orbital and instrument sampling pattern. One full year of LSM outputs over global and the continental United States (CONUS) domains are available for simulations. These simulations have been used for initial assessments of algorithm performance as described in the last section. A global

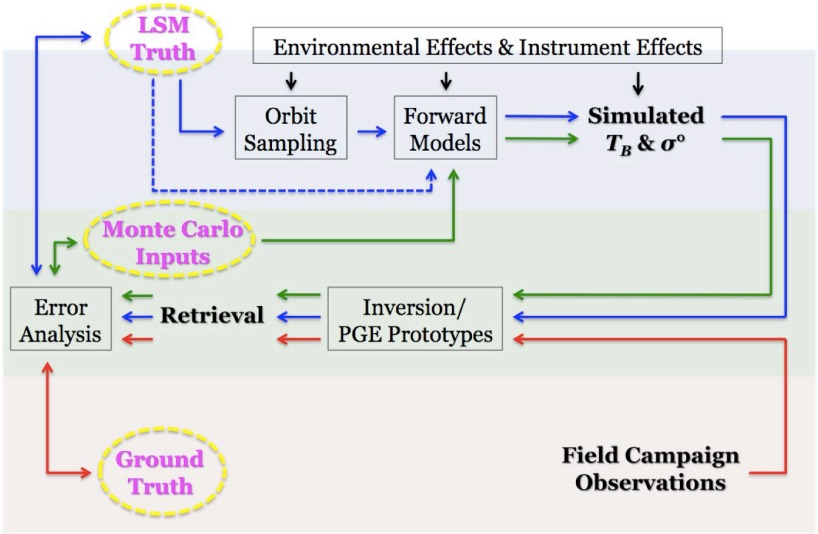

Figure 21. The various simulation modules and input data sources for the SMAP Algorithm Development Testbed.

map of retrieved soil moisture RMSE from one of these simulations is shown in Figure 22. As evident in the figure, retrieval error varies depending on the amount of vegetation, among other factors. Antenna sidelobe contamination along coastlines and river/lake boundaries also leads to high retrieval errors. Overall, the retrieved soil moisture RMSE stays below 0.04 cm^3/cm^3 over areas with low to moderate amounts of vegetation.

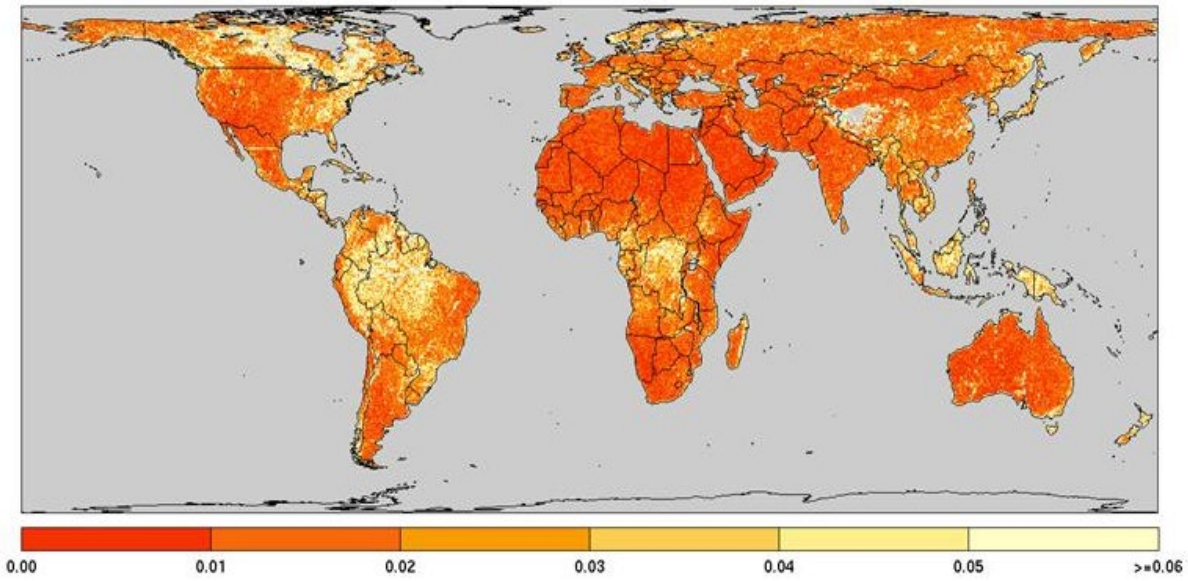

Figure 22a. Global soil moisture retrieval error based on simulations using LSM outputs and a L2_SM_P baseline algorithm.

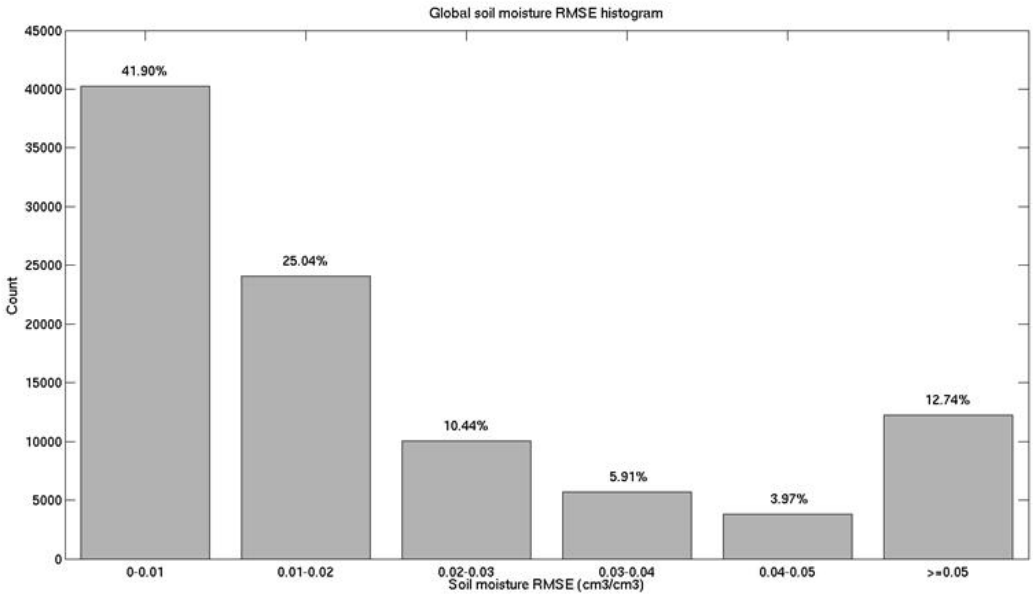

Figure 22b. Histogram of global soil moisture retrieval error based on simulation shown in (a). Approximately 83% of the area in the SMAP land mask has a soil moisture retrieval error ≤ 0.04 cm^3/cm^3.

New improved global simulations (GloSim2 and 3) are essentially complete. They enhance the realism of SMAP forward simulations by adding:

- Consistent global input forcings based on GMAO global nature run data,
- Finer grid resolutions (9-km dynamic fields and 1-km static fields),
- Finer temporal resolution (hourly),
- Improved ancillary datasets (e.g., soil texture, VWC, water fraction, etc),
- Enhanced radar forward modeling (more data cubes),
- More realistic error modeling (consistent spatial scaling of random and non-random perturbations), and
- Data format closer to the SMAP Data Product Specifications.

6. ANCILLARY DATA SETS

6.1 Identification of Needed Parameters

Ancillary data sets are defined as external data sets that are required as inputs to SMAP retrieval algorithms in the generation of the standard L2/3 products. Ancillary data needed by the SMAP mission fall into two categories -- static ancillary data are data that do not change during the mission while dynamic ancillary data require periodic updates in time frames ranging from seasonally to daily. Static data include parameters such as permanent masks (land / water / forest / urban / mountain), the grid cell average elevation and slope derived from a DEM, permanent open water fraction, and soils information (primarily sand and clay fraction). All of the static ancillary data are resampled to the same 3, 9, and 36-km SMAP EASE grids as the output products and will be available to any algorithm or end user who needs them. The dynamic ancillary data include land cover, surface roughness, precipitation, vegetation parameters, and effective soil temperatures. Although most ancillary data are by definition external to SMAP, originally the SMAP radar was planned to provide key pieces of information to the L2_SM_P algorithms including the open water fraction and the frozen ground flag (see L2_SM_A, L3_FT_A, and L3_FT_P ATBDs). While the exact types of ancillary datasets needed are specific to a given retrieval algorithm, all standard L2/3 products require some ancillary datasets to meet the specified retrieval accuracies.

Table 7 lists the fourteen ancillary data parameters identified as required by one or more of the SMAP product algorithms along with the primary source of information for that parameter (in all cases, there are alternative options for these parameters from climatological data sets, forecast models, or data sets acquired in past or current missions). The choice of which ancillary data set to use for a particular SMAP product is based on a number of factors, including its availability and ease of use, its inherent error and resulting impact on the overall soil moisture or freeze/thaw retrieval accuracy, and its compatibility with similar choices made by the SMOS mission. Latency, spatial resolution, temporal resolution, and global coverage are also important. The choice of a primary source for each of the fourteen ancillary data parameters is fully documented in individual SMAP Ancillary Data Reports which are available to the user community (these data reports are included in the list of SMAP Reference Documents at the front of this ATBD – see also http://smap.jpl.nasa.gov/science/dataproducts/ATBD/).

6.2 Soil Temperature Uncertainty

Errors in ancillary data are factored into the error budgets for each of the SMAP candidate soil moisture retrieval algorithms during SMAP simulations (Section 4.5). A major issue prelaunch is to quantify the expected errors of these ancillary data parameters, especially the error in the effective soil temperature parameter, since it requires the most frequent (daily) updates and is used by all L2_SM_P algorithms. The time resolution of the soil temperature (T_{soil}) is also important – currently, the major global forecast centers (including NCEP, ECMWF, and GMAO) produce T_{soil} forecast products at a time resolution relevant to SMAP (minimum time resolution of 3 hours). For L2/3_SM_P

processing, a local 6:00 am T_{soil} will be generated by interpolating in time between the closest available 3-hourly T_{soil} snapshots. A preliminary assessment of the accuracy of ECMWF forecast temperatures was made for an area in the central U.S. encompassing the state of Oklahoma and compared against ground truth temperatures from the Oklahoma Mesonet for every day in 2003 (Figure 23), with an RMSE between forecast and measured surface temperatures of approximately 2.4°C [31].

Table 7. Anticipated Primary Sources of Ancillary Parameters

1	**Soil Temperature**	**GSFC GMAO GEOS-FP [consistency ↔ L2-L4]**
2	**Surface Air Temperature**	**GSFC GMAO GEOS-FP**
3	**Vegetation Water Content (VWC)**	**MODIS NDVI [T. Jackson/R. Hunt approach]**
4	**Soil Attributes (sand & clay fraction)**	**Combination of HWSD (global), regional data sets (STATSGO-US, ASRIS-Australia, NSD-Canada), FAO [replaced in R17 2020 data release by SoilGrid250m available at https://openlandmap.org]**
5	**Urban Area**	**GRUMP data set – Columbia University**
6	**Open Water Fraction**	**a priori static water fraction from MODIS MOD44W to be used in conjunction with open water fraction from SMAP HiRes radar**
7	**Crop Type**	**combination of USDA Cropland Data Layer, AAFC-Canada, Ecoclimap-Europe**
8	**Land Cover Class**	**MODIS IGBP; crop class will be further subdivided into four general crop types**
9	**Precipitation**	**GSFC GMAO GEOS-FP**
10	**Snow**	**Snow & Ice Mapping System (IMS) - NOAA**
11	**Mountainous Area [DEM]**	**GMTED-2010**
12	**Permanent Ice**	**MODIS IGBP**
13	***b*, ω, and τ Vegetation Parameters**	**land cover-driven lookup table (different ω for SCA & DCA)**
14	***h* Roughness Parameter (table)**	**land cover-driven lookup table for SCA**
15	***h* Roughness Parameter (file)**	**pre-computed static file over 3 km EASE-2 grid for use with DCA (see sections 4.6 and 6.5)**

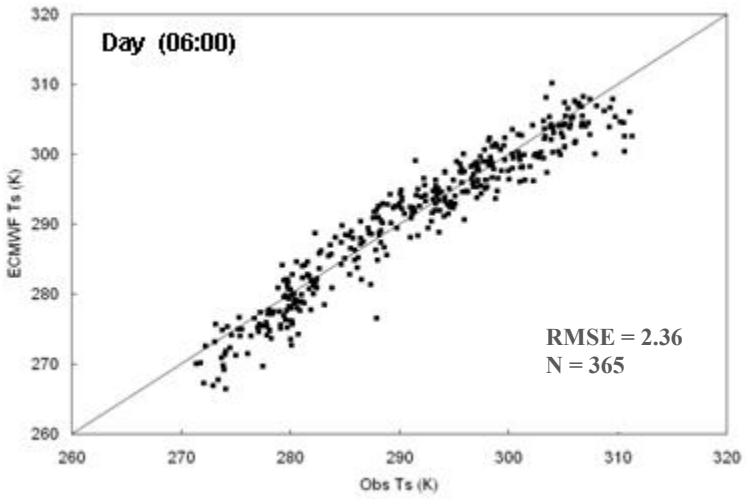

Figure 23. ECMWF forecast surface temperatures and Oklahoma MESONET (2 mm) surface temperatures at the overpass time of 06:00 AM local time for 2003 [31].

More recently, T. Holmes et al. [39] compared the accuracy of 0-5 cm soil temperature derived from the three NWP centers (MERRA is a GMAO data set) against *in situ* soil temperature data from the Oklahoma Mesonet for years 2004 and 2009 [39]. Figure 24 illustrates that at an overpass time of ~ 6 am, all synchronized NWP-derived surface temperature products have errors below 2 K, which is the amount of error budget allocation that is nominally carried for the surface temperature ancillary data parameter.

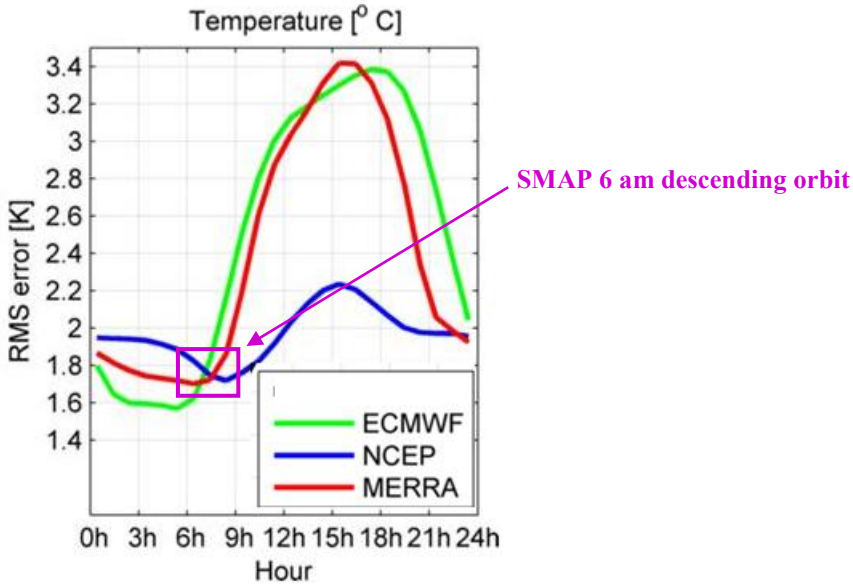

Figure 24. Accuracy of NWP forecast surface soil temperature compared against in situ temperatures for the Oklahoma Mesonet for 2004 and 2009.

6.2.1 Effective Soil Temperature

Postlaunch, dynamic surface temperature forecast information is routinely ingested by SMAP from the GMAO GEOS-FP model and processed as an ancillary data input as part of the operational processing of the SMAP passive soil moisture product. The effective surface temperature (T_{eff}) is a critical parameter in passive soil moisture retrieval but is not to be confused with an actual physical temperature measured at a single depth. The original baseline computation of T_{eff} consisted of using the average of the GMAO surface temperature and soil temperature at 10 cm. Preliminary analyses showed that a more sophisticated model for computing T_{eff} was required due to non-uniform soil temperature profiles, especially in arid areas, which led to soil moisture retrieval issues. In order to address this problem, several options for T_{eff} were considered and evaluated using SMAP T_B observations along with GMAO soil temperatures for the soil profile.

New to the End-of-Prime-Mission data release in 2018 was an improved depth correction scheme for the effective soil temperature, with the parameterization in this scheme reexamined for the R17 release in 2020. At L-band frequency, the contributing soil depth of microwave emission may be different from the pre-defined discrete soil depths at which the soil temperatures are available from a land surface model. The resulting discrepancy will lead to dry bias of retrieved soil moisture (i.e., retrieval lower than *in situ* soil moisture) if the model-based effective soil temperature is colder than the soil temperature "seen" by the radiometer. Conversely, wet bias of retrieved soil moisture will occur if the model-based effective soil temperature is warmer than the soil temperature "seen" by the radiometer. Since the contributing soil depth of microwave emission varies with soil moisture, the corresponding depth correction scheme for the effective soil temperature must account for soil moisture variability for brightness temperature observations acquired between AM (descending overpasses) and PM (ascending passes). To achieve this objective, the following modified formulation of the Choudhury model [58] has been found to result in good agreement between the *in situ* soil moisture data and the retrieved L2_SM_P and L2_SM_P_E soil moisture:

$$T_{eff} = K \times [\, T_{soil2} + C\,(T_{soil1} - T_{soil2})\,]$$

where C = 0.246 for AM soil moisture retrieval and 1.000 for PM soil moisture retrieval, and K = 1.007. K is a factor included to address an observed bias between ancillary modeled soil temperature and measured *in situ* temperature at core validation sites and sparse network stations. T_{soil1} refers to the average soil temperature for the first soil layer (5-15 cm) and T_{soil2} refers to the average soil temperature for the second soil layer (15-35 cm) of the GMAO GEOS-FP land surface model. Additional information on T_{eff} can be found in Appendix 3.

6.3 Vegetation Water Content

As described in previous sections, a number of retrieval algorithms under investigation rely on vegetation water content (VWC) as an input ancillary parameter. Accurate

temporal estimates of VWC, especially at high spatial resolution on a global basis, are very important to achieving accurate soil moisture retrieval using SMAP algorithms. Since VWC is not a parameter that can be measured directly by existing remote sensing techniques, it must be indirectly inferred from other measurable parameters with which it has high correlation. One such parameter is the Normalized Difference Vegetation Index (NDVI).

As described in the SMAP Ancillary Data Report for Global Vegetation Water Content [40], the SMAP team has been collaborating in the development of a more robust and reliable method for estimating VWC from NDVI, taking land cover variability into consideration. This new approach leverages the existing NDVI-based methodology to estimate the foliage water content (leafy part of the vegetation canopy), while using a combination of past field observations and Leaf Area Index (LAI) modeled by NDVI to account for the stem water content (stem and branch part of the vegetation canopy). The result is an estimate of VWC with water content contributions from the foliage and stem components, adjusted for the land cover types in the MODIS IGBP classification scheme.

While the foliage component is expressed in terms of NDVI, the stem component is expressed in terms of Leaf Area Index (LAI), along with annual maximum and minimum NDVI. As LAI exhibits distinct dynamics for different land cover types, this approach makes it possible to use NDVI and land cover classification data sets to construct a global VWC database at high spatial resolution. For croplands and grasslands the current NDVI is used for $NDVI_{ref}$; for all other vegetation types, the annual maximum NDVI is used for $NDVI_{ref}$:

$$VWC = (1.9134 \times NDVI^2 - 0.3215 \times NDVI) + StemFactor \times (NDVI_{ref} - 0.1) / (1 - 0.1) \quad (19)$$

where the stem factor is the product of the average height of a land cover class and the ratio of sapwood area to leaf area. Sapwood area to leaf area ratio [55] is based on the physical requirements for water transport from the soil through the xylem and into the leaves in order to replace water lost by transpiration. When the stem factor is multiplied by leaf area index (derived from canopy water content), the result is the approximate volume of water in the actively-conducting stem xylem per unit ground area (see the last column of Table 3). An example of the VWC distribution using the above formulation over the US for July is shown in Figure 25.

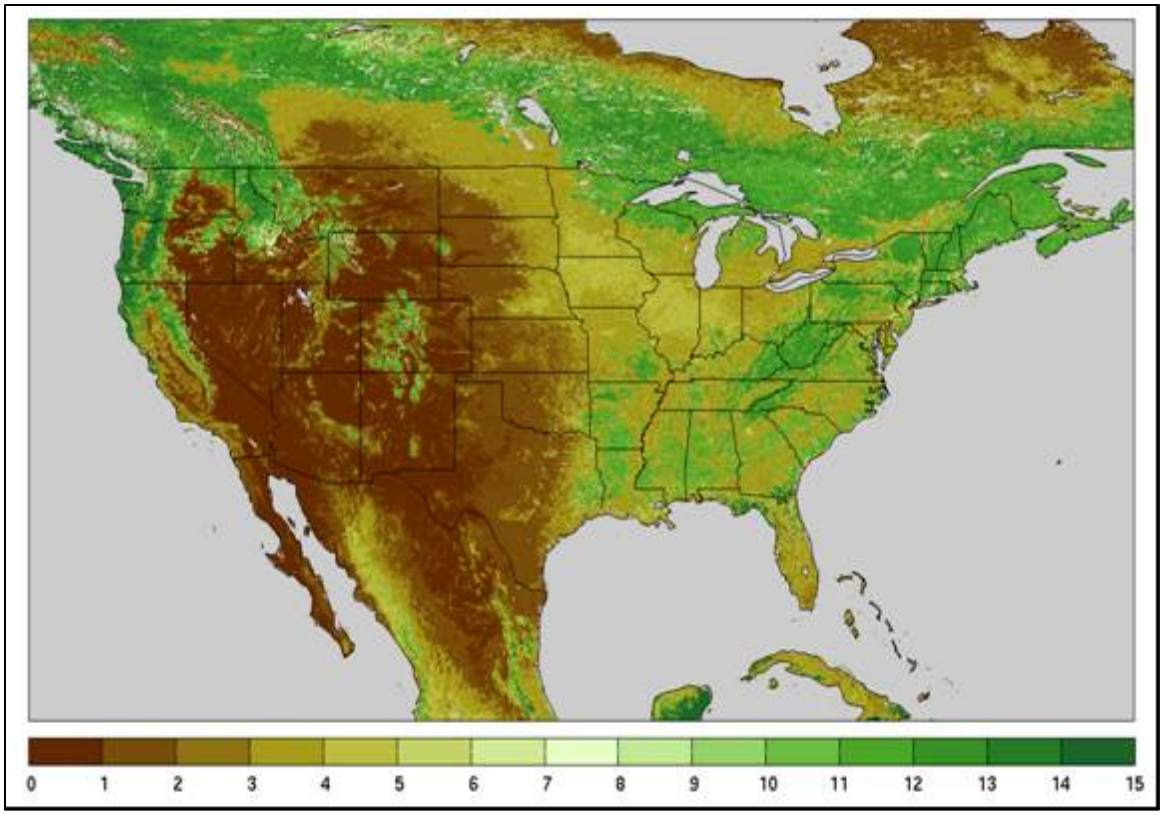

Figure 25. VWC over the continental U.S. for the month of July on a 1-km EASE grid as constructed from a 10-year MODIS NDVI climatology and land cover products.

This new methodology for determining VWC was used in creating a new global 10-year MODIS NDVI climatology at 1 km spatial resolution for use by SMAP [41]. The new climatology was derived from MODIS data from 2000-2010, and is binned over 10-day periods throughout the year; prior to the SMAP launch, this climatology will be updated for the period 2000-2013. In the absence of concurrent NDVI data during the SMAP mission, the historical NDVI for any day of the year for any location can be determined and then used in the VWC calculation described in Equation 17; the annual maximum NDVI is also readily obtained. Figure 26 illustrates the new NDVI climatology for the USDA watershed at Walnut Creek, IA (interpolated where snow is present). Calculation of VWC also serves to set the dense vegetation flag, which is triggered when the calculated VWC > 5 kg/m^2 for the given grid cell.

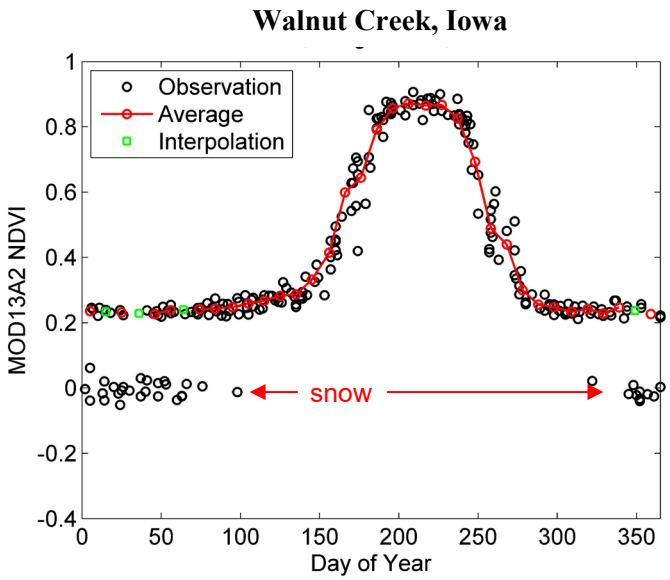

Figure 26. Annual climatology of NDVI for Walnut Creek, IA derived from 2000-2010 MODIS data.

6.4 Soil Texture

Soil moisture retrieval algorithms require information about soil texture, specifically sand and clay fraction. Prior to the SMAP R17 data release in 2020, a global dataset was assembled from an optimized combination of the FAO (Food & Agriculture Organization), HWSD (Harmonized World Soil Database), STATSGO (State Soil Geographic—US), NSDC (National Soil Database Canada), and ASRIS (Australian Soil Resources Information System) soil databases. This composite dataset used the best available sources in 2012 for a given region [54]. A negative consequence of this decision was the potential for discontinuities at international boundaries, such as between the United States and Canada.

Over the period after the SMAP launch in 2015, there were many advances made in the field of soil sciences, data acquisition (*in situ* and remote sensing), statistical techniques, computing hardware, and free software. These advances led to the creation of high resolution soil attribute databases, such as the global SoilGrid250m [70], a new 250-m resolution soil attribute dataset available at https://openlandmap.org. Dai et al. [71] evaluated the quality and accuracy of the SoilGrid250m data against other available global resources (such as HWSD), and reported that the SoilGrid250m database has the most accurate estimate of soil properties when compared against the *in situ* soil profile data from the World Soil Information Service (WoSIS). However, the comparison is not completely independent because some of the sites used for the compilation of these products are also used in computing the statistics.

The SMAP mission took notice of the high-resolution soil database (SoilGrid250m) because of the soil moisture product resolution enhancement activities for the L2_SM_P_E (gridded 9 km) and the L2_SM_SP (3 km and 1 km) products. It is better to have ancillary information and data more compatible with these spatial resolutions. The SMAP SAS

processing needs clay fraction data to compute the dielectric constant of the soil that is needed to invert brightness temperature into soil moisture. Before ingesting the SoilGrid250m data in the SMAP SAS processing, an analysis was conducted by the project to evaluate the SoilGrid250m database. There are significant differences between the new (SoilGrid250m via OpenLandMap) (Figure 27) and old (composite soil data) soil texture databases in the amount of soil clay fraction in many parts of the world. These differences in clay fraction will produce some small changes in volumetric soil moisture retrievals, with the magnitude of soil moisture retrieval differences between the older version and the newer version dependent on the % differences in the clay fraction. Studies conducted within the SMAP project show that clay fraction has a second-order impact on soil moisture retrieval using the tau-omega model. A positive increase in soil moisture is observed with increasing clay fraction, and vice versa. More details of the analysis are mentioned in the Soil Attribute Ancillary Report, Revision B (JPL D-53058), which can be found on the SMAP web site at JPL http://smap.jpl.nasa.gov/science/dataproducts/ATBD/ and on the NSIDC SMAP Technical References page https://nsidc.org/data/smap/technical-references.

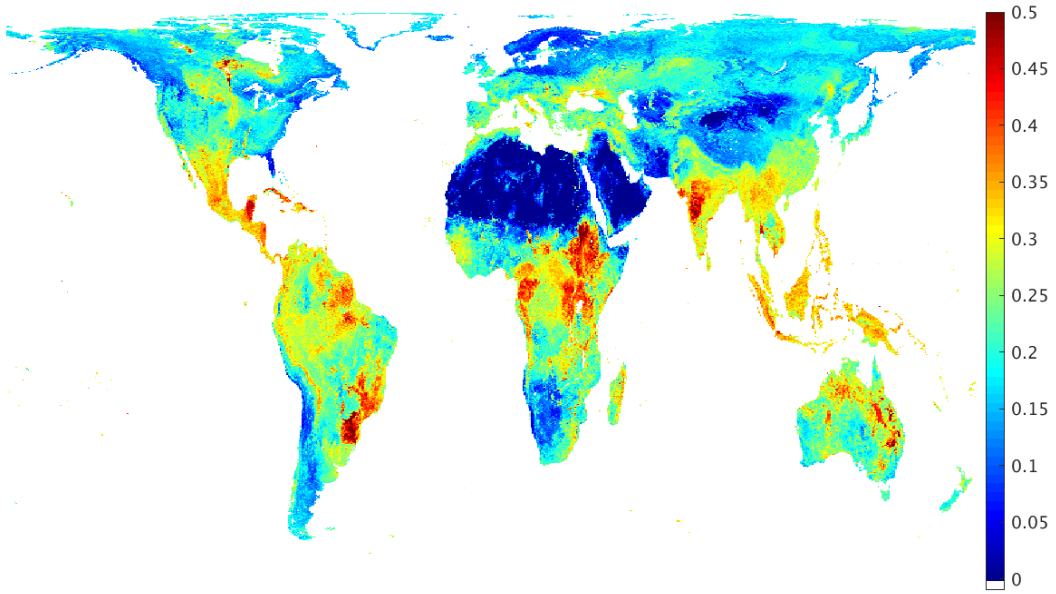

Figure 27. Global clay fraction from SoilGrid250m soil texture database (available at https://openlandmap.org).

6.5 Roughness Coefficient Ancillary File for DCA

The roughness coefficient ancillary file provides to DCA the roughness parameter *h* needed to perform the retrieval of soil moisture and vegetation optical depth (see Figure 28). To generate the static ancillary file, the modified dual channel algorithm was used to retrieve soil moisture and roughness coefficient *h'* (instead of soil moisture and vegetation opacity) using five years of SMAP 9 km gridded passive data (04/01/2015-03/31/2020). The DCA algorithm (with $\lambda = 0$) was fed with the vegetation single scattering albedo ω from Table 3 and the vegetation optical depth from NDVI. This process enabled the generation of a time series of *h'* for each grid cell *(i,j)* over the 9 km EASE-2 grid. The

time series of *h'* at the *(i, j)* grid cell is identified by *h'(i,j,k)* and time index k, and similarly *τ(i,j,k)* is the time series of the associated vegetation optical depth from NDVI. Defining

$$\tau_{min}(i,j) = min\{\, \tau(i,j,k), \text{ for all } k\} \quad \text{and} \quad \tau_{max}(i,j) = max\, \{\tau(i,j,k), \text{ for all } k\},$$

the values of h are computed over the EASE-2 grid as

$$h(i,j) = ave\{h'(i,j,k): \tau(i,j,k) <= \tau_{min}(i,j) + .05(\tau_{max}(i,j) - \tau_{min}(i,j))\}$$

in this way minimizing the local effect of vegetation. Figure 28 displays the resulting global map of *h*. The file was then disaggregated to a 3 km EASE-2 grid to accommodate handling by the SMAP ancillary file reader.

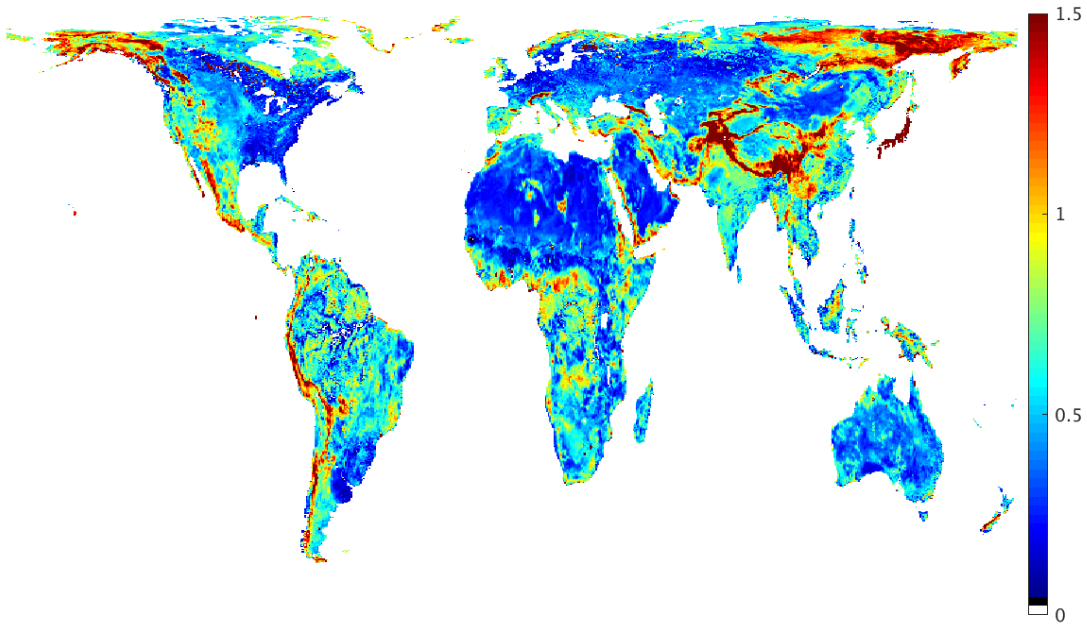

Figure 28. Global map of the roughness parameter h ancillary file used in the implementation of the DCA.

6.6 Data Flags

Ancillary data will sometimes also be employed to help to determine either specific aspects of the processing (such as corrections for transient water) or the quality of the retrievals (e.g. precipitation flag). Basically, these flags will provide information as to whether the ground is frozen, snow-covered, or flooded, or whether it is actively precipitating at the time of the satellite overpass. Other flags will indicate whether masks for steeply sloped topography, or for urban, heavily forested, or permanent snow/ice areas are in effect. All flag threshold values are currently under review and may be modified during postlaunch calibration/validation activities.

6.6.1 Open Water Flag

The open water fraction will be produced by *a prioi* information on permanent open fresh water from the MOD44W database. It is always reported as part of the L2_SM_P output product (see Appendix 1). This information serves as a flag to affect soil moisture retrieval processing in the following way:

- If water fraction is 0.00–0.05, then flag for recommended quality and retrieve soil moisture
- If water fraction is 0.05–0.50, then flag for uncertain quality and attempt to retrieve soil moisture
- If water fraction is 0.50–1.00, then flag but do not retrieve soil moisture

6.6.2 RFI Flag

The presence of radio frequency interference can markedly impact SMAP T_B, and in turn can adversely affect soil moisture retrieval accuracy or prevent a retrieval from being attempted. RFI is detected and corrected for in the L1B_TB (SPL1BTB) product, which sets an RFI flag which is eventually passed to the L2_SM_P processor (see L1B_TB ATBD). The RFI flag affects soil moisture retrieval processing in the following way:

- If RFI is not detected (bit 2=0 in SPL1BTB's tb_qual_flag), then flag for recommended quality and retrieve soil moisture
- If RFI is detected and can be corrected successfully (bit 3=0 in SPL1BTB's tb_qual_flag), then flag for recommended quality and retrieve soil moisture
- If RFI is detected but can only be corrected partially (bit 14=1 in SPL1BTB's tb_qual_flag), then flag for uncertain quality and attempt to retrieve soil moisture
- If RFI is detected and cannot be corrected (bit 3=1 in in SPL1BTB's tb_qual_flag), then flag but do not retrieve soil moisture.

Note that the RFI information is not embedded in SPL2SMP's surface condition flag. It is mentioned here because it, along with the status of other surface conditions, helps to determine the quality of soil moisture retrieval.

6.6.3 Snow Flag

Although the SMAP L band radiometer can theoretically see through dry snow with its low dielectric to the soil underneath a snowpack, the snow flag is currently envisioned as an area snow fraction based on the NOAA IMS database. The snow flag affects soil moisture retrieval processing in the following way:

- If snow fraction is 0.00–0.05, then flag for recommended quality and retrieve soil moisture
- If snow fraction is 0.05–0.50, then flag for uncertain quality and attempt to retrieve soil moisture
- If snow fraction is 0.50–1.00, then flag but do not retrieve soil moisture

Permanent snow/ice fraction as indicated in the SMAP ancillary land cover map is also treated similarly to snow fraction with the same lower and upper permanent snow/ice thresholds.

6.6.4 Frozen Soil Flag

At the start of the SMAP mission, the intention was to set the SMAP frozen soil flag during internal SDS processing based on either the radar ground flag (see L3_FT_A ATBD) or on the GMAO-based T_{eff}. After the failure of the SMAP radar on July 7, 2015, a procedure was developed to replace the radar-based frozen soil flag with one generated from the SMAP radiometer data using normalized polarization ratios (see L3_FT_P ATBD). However, due to uncertainties in reference freeze/thaw conditions, subgrid scale heterogeneity, and polarization changes due to changing vegetation and soil moisture conditions during the growing season at low-to-mid latitudes, the L3_FT_P frozen flag can result in false F/T indications. For these reasons, currently (at the time of the R17 data release in 2020) the frozen soil area fraction is still based on the temperature information from the GMAO GEOS-FP model used by the SMAP operational processor (byte value of 0 or 8 in the Retrieval Quality Flag). Since the frozen soil flag is generated at high spatial resolution compared to the 36-km grid cell spacing of the L2_SM_P products, a frozen fraction is generated which affects soil moisture retrieval processing in the following way:

- If frozen soil fraction is 0.00–0.05, then flag for recommended quality and retrieve soil moisture
- If frozen soil fraction is 0.05–0.50, then flag for uncertain quality and attempt to retrieve soil moisture
- If frozen soil fraction is 0.50–1.00, then flag but do not retrieve soil moisture

6.6.5 Precipitation Flag

The SMAP precipitation flag is currently set based on forecasts of precipitation from the GEOS-FP model. The use of observational data from the Global Precipitation Mission (GPM) will be evaluated as the mission progresses. The precipitation flag gives the rain rate in mm/hr (or $kg/m^2/s$), indicating the presence or absence of precipitation in the 36-km grid cell at the time of the SMAP overpass. The presence of liquid in precipitation incident on the ground at the time of the SMAP overpass can adversely bias the retrieved soil moisture due to its large impact on SMAP T_B (precipitation in the atmosphere is part of the atmospheric correction done in SPL1BTB processing). Unlike with other flags, soil moisture retrieval will always be attempted even if precipitation is flagged. However, this flag serves as a warning to the user to view the retrieved soil moisture with some skepticism if precipitation is present.

- If precipitation rate is 0.0–1.0 mm/hr, then flag for recommended quality and retrieve soil moisture
- If precipitation rate is 1.0–25.4 mm/hr, then flag for uncertain quality and attempt to retrieve soil moisture
- If precipitation rate is > 25.4 mm/hr, then flag but do not retrieve soil moisture.

6.6.6 Urban Area Flag

Since the brightness temperature of manmade, impervious, and urban areas cannot be estimated theoretically, the presence of urban areas in the 36-km L2_SM_P grid cell cannot be corrected for during soil moisture retrieval. Thus, the presence of even a small amount of urban area in the radiometer footprint is likely to adversely bias the retrieved soil moisture. The SMAP urban flag will be set based on Columbia University's GRUMP data set [42]. The urban fraction affects soil moisture retrieval processing in the following way:

- If urban fraction is 0.00–0.25, then flag for recommended quality and retrieve soil moisture
- If urban fraction is 0.25–1.00, then flag for uncertain quality and attempt to retrieve soil moisture

6.6.7 Mountainous Area Flag

Large and highly variable slopes present in the radiometer footprint will adversely affect the retrieved soil moisture. The SMAP mountainous area flag will be derived from a statistical threshold based on the slope standard deviation (SD) within each 36-km grid cell. Most likely, soil moisture retrieval will still be attempted in most areas flagged as mountainous.

- If slope standard deviation is 0-3°, then flag for recommended quality and retrieve soil moisture
- If slope standard deviation is 3-6°, then flag for uncertain quality and attempt to retrieve soil moisture
- If slope standard deviation is > 6°, then flag but do not retrieve soil moisture

6.6.8 Proximity to Water Body Flag

For any given instantaneous measurement, the SMAP radiometer receives a portion of its energy from outside its 3 dB footprint. This becomes an issue if a large water body is just outside the boundaries of a 36-km EASE Grid 2.0 cell but still contributes to the observed signal, since the microwave brightness temperature of standing water is significantly cooler than that of land and would adversely bias the soil moisture retrieved inside the 36-km cell. The proximity to nearby water body flag affects soil moisture retrieval processing in the following way:

- If distance to nearby water body > one 36-km grid cell, then flag for recommended quality and retrieve soil moisture
- If distance to nearby water body < one 36-km grid cell, then flag for uncertain quality and attempt to retrieve soil moisture

6.6.9 Dense Vegetation Flag

The presence of dense vegetation in the grid cell negatively affects the accuracy of retrieved soil moisture. However, at the request of the science community, a soil moisture retrieval will always be attempted regardless of the amount of vegetation present. The dense vegetation flag affects soil moisture retrieval processing in the following way:

- If vegetation water content is 0-5 kg/m^2, then flag for recommended quality and retrieve soil moisture
- If vegetation water content is 5-30 kg/m^2, then flag for uncertain quality and attempt to retrieve soil moisture
- If vegetation water content is > 30 kg/m^2, then flag but do not retrieve soil moisture

6.7 Latency

The SMAP mission requirements impose latency requirements on all SMAP products. L2_SM_P data products have a latency requirement of 24 hours and the L3_SM_P products have a latency of 48-50 hours (to allow for the accumulation of 24 hours of half orbits and their subsequent processing). In operational processing, the SDS is thus responsible for generating the L2_SM_P products within the stated periods from the moment of satellite data acquisition to delivery to the SMAP NSIDC DAAC for distribution to the public.

To meet these requirements, the external ancillary datasets that will be used in L2/3_SM_P processing must be available within the stated periods. The major NWP forecast centers have indicated that most of the needed ancillary data parameters which are highly dynamic and time critical (e.g., surface temperature) will be available to the SMAP SDS for routine product generation within 6 hours of the forecast.

7. CALIBRATION AND VALIDATION

7.1 Algorithm Selection

As discussed in section 4.6, the selection of the algorithm to be used operationally to produce the standard SMAP L2_SM_P and enhanced L2_SM_P_E surface soil moisture products will be made just prior to the first SMAP bulk reprocessing and continually assessed throughout the mission. Performance evaluations pre- and postlaunch will include:

- comparisons of soil moisture estimates using SMOS T_B data processed to the SMAP configuration with *in situ* soil moisture data sets and SMOS algorithm retrievals,
- comparisons of soil moisture estimates based on tower and aircraft field campaign data with ground-based observations,
- sensitivity and uncertainty analyses based upon GloSim3
- comparisons of SMAP retrievals with *in situ* data from CV sites.

L2_SM_P products will satisfy the mission requirement that the retrieved soil moisture will have an ubRMSE (unbiased RMSE) of no more than 0.04 cm^3/cm^3 over areas where the vegetation water content ≤ 5 kg/m^2; this target accuracy was confirmed as achievable in a previous study (Figure 29) for the *Hydros* mission using three candidate algorithms [7]. The *Hydros* study showed that when retrievals were aggregated at the basin level (575,000 km^2), all three algorithms met the target accuracy of 0.04 cm^3/cm^3 volumetric soil moisture, although for individual pixels with high vegetation water content and/or high surface heterogeneity, the soil moisture retrieval accuracy degraded [note: the *Hydros* reflectivity ratio algorithm is not a candidate SMAP algorithm]. These general results also apply to SMAP. Accuracy assessments can be found for the SMAP L2_SM_P and L2_SM_P_E mission products in the assessment reports available from NSIDC [59-61, 63, 68]. Note that the accuracy of L2_SM_P_E retrievals is assessed starting in reference [61] and subsequent assessment reports.

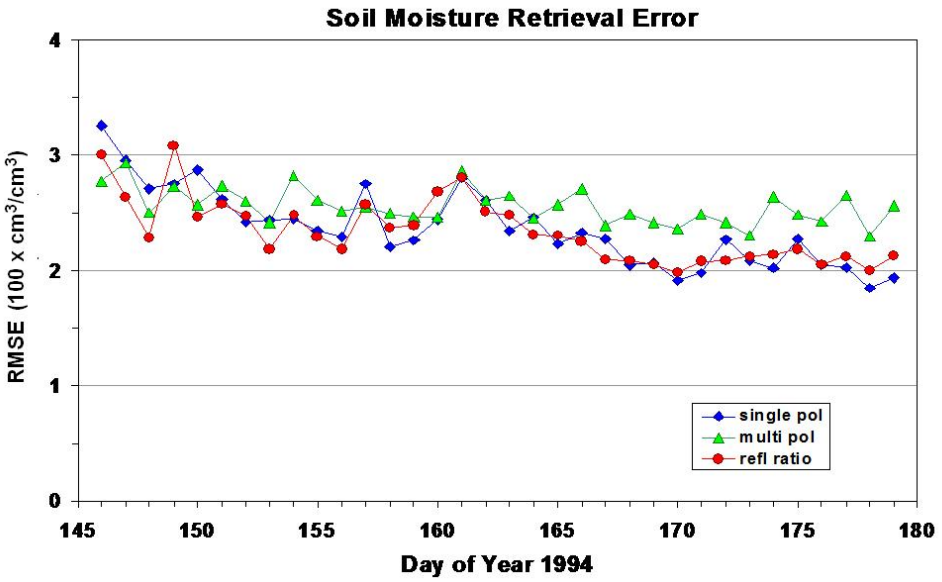

Figure 29. Performance comparison among three candidate retrieval algorithms for the *Hydros* mission based on an OSSE over the Arkansas-Red River basin [7].

7.1.1 SMOS and Aquarius Data Products

The SMAP L2_SM_P team is in a unique position to assess the relative merits of alternative algorithms because data from two currently operating satellites, SMOS and Aquarius, can be used as surrogates for SMAP. SMOS is currently providing L-band brightness temperature as well as a retrieved soil moisture product (since November 2009) [43]. Aquarius began providing brightness temperature data in August, 2011 (launched June 2011) [44] and has also released a soil moisture product [57]. The brightness temperatures from each of these missions require reprocessing in order to simulate the constant 40° incidence angle observations that SMAP will provide. Unfortunately, the SAC-D/Aquarius mission failed in June, 2015, a few months after SMAP launched.

Initially, the plan was to use the SMOS global gridded L1C browse brightness temperature product as a SMAP surrogate with minimal reprocessing. This SMOS product consists of swath-based dual/full polarization observations resampled to an Earth-fixed grid with a standard incidence angle of 42.5° at the nominal spatial resolution of SMAP. This product provides antenna reference brightness temperatures, but the required parameters for performing the rotation to true surface polarized T_B (including Faraday angle) are not available in the browse product. Upon further consideration of the differences (e.g., grid, incidence angle, etc.) between the two missions and an evaluation of the radiometric quality of the browse product, it was decided that it would be necessary to reprocess the SMOS data using the standard L1C product. Only the unaliased FOV portions of the SMOS orbit are used in the processing. The procedures adopted will result in a higher quality brightness temperature data set at a constant incidence angle of 40° matched to the SMAP grid. Although this product will have a reduced swath width as a consequence of the reprocessing, the loss of some swath width is not critical to the algorithm performance assessment objectives of this analysis.

The following files are acquired for each swath in order to conduct the subsequent analyses: SMOS L2 soil moisture DAP (Data Analysis Product), SMOS L2 soil moisture UDP (User Analysis Product), ECMWF forecast files, and SMOS tau vegetation parameter files for forest and non-forest areas (τ). The first stage of SMOS analysis is generating the constant 40° incidence angle brightness temperature data from the SMOS L1C T_B product. This involves the following steps:

- Removing the extended FOV portions of the SMOS orbit
- Filtering to remove anomalous T_B observations and RFI check
- Interpolation to fill in full/dual-pol T_B observations for each snapshot (needed for the next step)
- Transforming from antenna to Earth reference frame (Computing X-Y to H-V T_B)
- RFI check ($0<T_B<320$, $T_{BH}<T_{BV}$)
- For each grid point, brightness temperatures at all available incidence angles are used to develop a prediction equation for T_B as a function of angle, and values at 40 degrees are then predicted.

The next stage of analysis is the retrieval of soil moisture with alternative SMAP algorithms using the SMOS products in their original grid system. All ancillary data are derived from SMOS files. These retrievals will be compared to the SMOS soil moisture products, ground-based soil moisture, and possible model-based products.

Finally, the new 40° SMOS product will be transferred to the SMAP grid. The alternative SMAP algorithms will then be applied with the SMAP ancillary data sets. As described above, evaluation will utilize ground-based observations from well-studied validations sites, the SMOS soil moisture product (re-gridded), and model-based products. Ground-based data sets will include all site data provided by SMAP cal/val partners that meet the product scale and minimum requirements. The validation site analysis will compute standard statistical parameters (RMSE, bias, correlation) for each algorithm at

each validation site over at least one annual cycle. Each site will be evaluated individually and then treated as a group to provide a ranking of the algorithms. This process was evaluated in a rehearsal campaign.

In addition to the analysis above that focuses on a number of well-characterized sites, evaluations that incorporate a global synoptic perspective will be conducted. The entire global SMOS soil moisture data set will be compared to the products provided by the candidate SMAP soil moisture algorithms. The performance of each algorithm, relative to SMOS, will be evaluated on an overall basis as well as for categories that include land cover types, NDVI levels, and continents. Statistics will include RMSD, ubRMSD, bias, and correlation. This analysis assumes that the SMOS soil moisture product is accurate and reliable. While it is expected that the SMOS team is doing its best to achieve this goal, it is possible that there may be regions and land covers where the SMOS results are less reliable. It is also possible that some data quality issues may remain, especially the issue of SMOS aliasing, which are likely to be more significant in the algorithms that utilize more than a single polarization. Methods to possibly mitigate this aliasing are currently being investigated.

Aquarius brightness temperature and radar data became available beginning in August, 2011. Aquarius provided L-band data for three beam positions with incidence angles of 28.7, 37.8, and 45.6 degrees. Although methods for normalizing incidence angle will be explored, initially only the middle beam position data will be utilized. The radiometric calibration and quality of the Aquarius data is high, based upon the necessity for high radiometric quality data in order to achieve the mission objectives of measuring sea surface salinity (which has a small dynamic range of T_B). Since its initial data release, there have been two reprocessings by Aquarius as well as SMOS changes that have resulted in Aquarius and SMOS brightness temperatures being closer to each other over the same target. A drawback to the Aquarius data is its spatial resolution, which is several times coarser than SMAP. This coarse resolution (>100 km) might reduce the range of estimated soil moisture and increase the impact of surface heterogeneity. In addition, almost all of the global ground-based soil moisture validation sites have been developed to support products with a spatial resolution of 25-50 km. The coarser scale of Aquarius relative to the ground-based data will have to be carefully considered in the algorithm assessments. The Aquarius program supports the generation of a soil moisture product [57]. Analyses indicate that the SMOS and Aquarius products are similar on a global basis.

7.1.2 Tower and Aircraft Field Experiment Data Sets

Because of the natural heterogeneity of landscapes and the inherent coarse scale of satellite radiometers, it can prove challenging to identify the causes of algorithm errors when using satellite-based sensors. Tower and aircraft-based sensors have higher resolutions that allow the control of variability introduced by land cover and soils. Therefore, these instrument platforms can provide additional and valuable insights that are relevant to the algorithm selection decision [56].

Several recent field experiments have provided L-band dual polarization datasets that are used to evaluate algorithm performance under real-world conditions. These datasets have been compiled and archived for SMAP investigations. These datasets include aircraft observations of SMEX02, CLASIC, SMAPVEX08, CanEx-SM10, SMAPVEX12, SMAPVEX15-16, and tower-based observations from ComRAD and other instruments. When closely examined, these experiments only cover a limited set of conditions as a result of either design or meteorological circumstances. Therefore, it would be highly desirable for the algorithm selection process to acquire additional data sets. Tower (ComRAD APEX12) and aircraft (SMAPVEX12 SMAPVEX15-16) experiments were successfully conducted in the SMAP prelaunch and postlaunch time frames; data are currently being analyzed.

In addition, several other field experiments outside of North America may prove valuable to the algorithm selection process. The airborne soil moisture field campaigns are listed in Table 8.

Table 8. Airborne Soil Moisture Field Campaigns

Campaign	Location	Description
Washita'92	Oklahoma	The first campaign to attempt to collect a time series of spatially distributed hydrologic data, focusing on soil moisture and evaporative fluxes, using both conventional and remotely sensed methods. A NASA C-130 supported the ESTAR L band microwave radiometer and a DC-8 carried Airsar. One of the most successful and scientifically valuable campaigns ever conducted as a result of meteorological conditions and aircraft/instrument performance.
Washita'94	Oklahoma	The primary objective of this experiment was to provide combined ground and aircraft remotely sensed data sets in conjunction with the Space Shuttle Imaging radar missions (SIR-C) in 1994. Each SIR-C mission was to consist of one week of daily observations for the watershed site. ESTAR and AirSAR collected data during portions of the campaign.
SGP97	Oklahoma	SGP97 was a broad multi-disciplinary experiment. One of its main objectives was to establish that the retrieval algorithms for surface soil moisture developed at higher spatial resolution using truck- and aircraft-based sensors can be extended to the coarser resolutions expected from satellite platforms. It included the L-band Electronically Scanned Thinned Array Radiometer (ESTAR) and a tower-based L and S-band system. The campaign spanned a longer time period (4 weeks) and covered a domain an order of magnitude larger than prior experiments.
SGP99	Oklahoma	SGP99 returned to the same study region as SGP97 with a new suite of aircraft-based sensors that included AMSR simulators and the recently developed L- and S-band PALS instrument. PALS was flown over the Little Washita Watershed on 5 days over a 6 day period.
SMEX02	Iowa	SMEX02 expanded previous aircraft-based experiments to higher biomass agricultural conditions (corn and soybeans). Both PALS (7 flights over two weeks) and AirSAR (5 flights over 9 days) data were collected.

SMEX03	Georgia, Alabama, Oklahoma	SMEX03 was designed in expand the diversity of land cover conditions that had been examined in previous campaigns. The experiment included the first application of the L-band 2D-STAR instrument and Airsar coverage at one site (Oklahoma).
SMEX04	Arizona, Mexico	SMEX04 continued the expansion of experimental sites conditions that had been examined in previous campaigns. The experiment included the first application of the L-band 2D-STAR instrument and Airsar coverage at one site (Oklahoma).
CLASIC07	Oklahoma	CLASIC included the first flights with new antenna for PALS. Eleven flights were conducted over four weeks for two watersheds.
SMAPVEX08	Maryland	SMAPVEX08First field campaigns dedicated to resolving SMAP algorithm issues. Agricultural sites and PALS were the focus. In addition, the campaign addressed questions related to RFI.
CanEx-SM10	Saskatoon, Canada	CanEx-SM10 was a collaboration between NASA and CSA over agricultural and forest sites. NASA flew the airborne UAVSAR instrument in conjunction the Canadian L-band airborne radiometer and ground sampling observation over one of the SMAP Core Validation Sites.
SMAPEx10-11	New South Wales, Australia	Collaboration led by the University of Melbourne and Monash University in Australia. Three week-long campaigns in 2010 and 2011 designed to specifically address SMAP soil moisture algorithm issues. Two post-launch campaigns will be conducted in 2015. The campaigns will include coincidental aircraft-based radiometer and radar measurements and ground observation over one of the SMAP Core Validation Sites
San Joaquin Valley Experiment	California	SJV involves the UAVSAR instrument deployed t on several days in 2010-2011. Sites are irrigated orchards and vineyards. The primary objective of the experiment is to develop Vegetation Water Content (VWC) retrieval from optical remote sensing instruments, supported by optical instruments. Soil moisture and backscatter relationships will be evaluated. A series of ten flights over 5 months is planned.
SMAPVEX12	Manitoba, Canada (MB)	SMAPVEX12 was conducted in summer 2012 to address the remaining algorithm issues before the launch. This experiment was a collaborative effort between NASA and CSA. The primary L-band observations were collected by the PALS instrument and UAVSAR. A large spatial domain (including agriculture and natural vegetation) over a six-week period was measured.
SMAPEx15 SMAPVEX15 SMAPVEX16	Australia Arizona IA, MB	Post-launch validation of SMAP.

7.1.3 Simulations Using the SMAP Algorithm Development Testbed

As mentioned in sections 4.5 and 5, the SMAP Algorithm Development Team developed Fortran codes at JPL that enable a set of closed-loop, end-to-end global simulation runs known as GloSim [45]. These simulations will serve several purposes, including providing a mechanism for intercomparison of the relative merits of the four candidate L2_SM_P retrieval algorithms. Additional simulations were run with GloSim to examine the performance of all candidate algorithms, and updated error budgets were

generated for each algorithm; these products were incorporated into the 2014 rehearsal campaign.

7.2 Validation

Postlaunch validation must provide the information necessary to address whether or not SMAP has achieved its mission requirement to produce an estimate of soil moisture in the 0-5 cm layer with an average ubRMSE of no more than 0.04 cm^3/cm^3 over areas where the vegetation water content ≤5 kg/m^2, excluding regions of frozen soil, permanent snow / ice, mountainous terrain, and open water at the footprint measurement scale (40 km for the L2_SM_P). It has been suggested by CEOS (http://lpvs.gsfc.nasa.gov/) that full validation of a satellite product can require a substantial effort in space and time data collection, and that a reasonable approach to the problem is to consider validation as consisting of several stages, which are summarized in Table 9.

Table 9. A Hierarchical Approach to Classifying Land Product Validation Stages as Adopted by CEOS through Consensus of the Land Product Validation Community in 2003 and Revised in 2009

Stage 1	• Product accuracy is assessed from a small (typically < 30) set of locations and time periods by comparison with in situ or other suitable reference data.
Stage 2	• Product accuracy is estimated over a significant set of locations and time periods by comparison with reference in situ or other suitable reference data. • Spatial and temporal consistency of the product and with similar products has been evaluated over globally representative locations and time periods. • Results are published in the peer-reviewed literature.
Stage 3	• Uncertainties in the product and its associated structure are well quantified from comparison with reference in situ or other suitable reference data. • Uncertainties are characterized in a statistically robust way over multiple locations and time periods representing global conditions. • Spatial and temporal consistency of the product and with similar products has been evaluated over globally representative locations and periods. • Results are published in the peer-reviewed literature.
Stage 4	• Validation results for stage 3 are systematically updated when new product versions are released and as the time-series expands.

Initial post-launch validation of the L2_SM_P product has been performed and is documented in the SMAP L2_SM_P beta, validated, and Version 4 release assessment reports [59, 60, 61] which are available through NSIDC; an L2_SM_P Data Release Version 5 assessment report [63] will be produced in June, 2018. Validation Stages 1 and 2 and beyond will be completed by the end of the official calibration/validation phase of

the SMAP mission in 2016 (12 months after the beginning of routine science operations on orbit (IOC)). All validation data and results will be provided through the NSIDC. Given that an initial journal article presenting an assessment of the L2_SM_P soil moisture product was published in August, 2016 [62], it is realistic that within two years after the end of IOC, Stages 1 through 3 will be complete, and work toward Stage 4 will be well underway.

The SMAP Cal/Val plan [46] describes five types of resources that will be utilized as sources of calibration/validation data. These types of data are listed in Table 10, which describes their perceived role and issues that are currently being addressed by the SMAP team. The NSPIRES DCL entry in the table refers to a Dear Colleague Letter request for information that was released by NASA to the science community to solicit members of the SMAP cal/val team and core validation and other validation sites globally. A NASA panel in consultation with the SMAP team selected ~27 investigator sites or supported instrument networks in Summer, 2011. Since then several new sites have been added. The assessment reports list the latest core validation sites used in performance evaluations.

Table 10. Overview of the SMAP Cal/Val Methodologies

Methodology	Role	Issues	Actions
Core Validation Sites	Accurate estimates of products at matching scales for a limited set of conditions	Calibration Up-scaling Limited number	*In Situ* Testbed Scaling methods NSPIRES DCL
Sparse Networks	One point in the grid cell for a wide range of conditions	Calibration Up-scaling Limited number	*In Situ* Testbed Scaling methods NSPIRES DCL
Satellite Products	Estimates over a very wide range of conditions at matching scales	Validation Comparability Continuity	Validation Studies CDF Matching
Model Products	Estimates over a very wide range of conditions at matching scales	Validation Comparability	Validation Studies
Field Experiments	Detailed estimates for a very limited set of conditions	Resources Schedule Conflicts	Simulators Partnerships

The baseline validation for the L2_SM_P soil moisture will be a comparison of retrievals at 36 km with ground-based observations that have been verified as providing a spatial average of soil moisture at the same scale, referred to as core validation sites (CVS) in the SMAP Calibration / Validation Plan. This matches up closely with the Stage 1 validation described in Table 9. Data from core validation sites will be supplemented by field experiments. In order to achieve Stage 2 validation and include a wider range of

conditions as well as a synoptic/global assessment, some combination of data from sparse networks, other satellite products, and model-based estimates must be utilized. Each of these data types has caveats associated with it that are described in Table 10. The following sections provide some additional details on how each of the resources listed in Table 11 will be utilized specifically for the L2_SM_P soil moisture product validation.

Table 11. SMAP Cal/Val Methodologies and Their Roles in the L2_SM_P Soil Moisture Product Validation

Methodology	Data Required	Importance	Metrics
Core Validation Sites	Grid Cell averages for each overpass	Primary	RMSE, ubRMSE, Bias, Correlation

Sparse Networks	Spatially scaled grid cell values for each overpass	Secondary: Pending results of scaling analyses	RMSE, ubRMSE, Bias, Correlation
Satellite Products	Orbit-based match-ups Key targets	Primary: Pending assessments and continued operation	RMSD, ubRMSD, Bias, Correlation
Model Products	Orbit-based match-ups Key targets	Secondary	RMSD, ubRMSD, Bias, Correlation
Field Experiments	Detailed estimates for a very limited set of conditions	Primary	RMSE, ubRMSE, Bias, Correlation

7.2.1 Core Validation Sites

As noted previously, the baseline validation (Stage 1) for the L2_SM_P soil moisture will be a comparison of retrievals at 36 km with ground-based observations that have been verified as providing a spatial average of soil moisture at the same scale, referred to as core validation sites (CVS) in the SMAP Calibration / Validation Plan. The CVS have been selected because they satisfied several criteria that included:

- A network of sensors with adequate replication
- For soil moisture, ideally, three nested levels of extent (3, 9, and 36 km)
- For soil moisture, verified against gravimetric samples for the 0-5 cm layer
- Minimal latency in providing data to the SMAP project
- Fully operational well before launch, with infrastructure to support the site through at least 2016 (and hopefully beyond)

NASA has established agreements with the CVS teams that require the teams to provide the ground-based data in a timely manner to the SMAP project (or the NASA-designated SMAP DAAC at NSIDC). There are expected to be ~15 of these CVS distributed over the globe, and these may increase in number over the next few years. Many of these sites have been used in AMSR-E and SMOS validation [47-50]. Multiple sample points at each site will be averaged or upscaled to estimate the footprint-scale soil moisture value that will be compared to the SMAP retrieval. The method of averaging will depend upon the amount of information provided by the CVS team. Some of these sites will also be the focus of intensive ground and aircraft field campaigns to further verify the accuracy of the collected data as well as improving scaling.

Having a global distribution of sites will be beneficial to SMAP validation. Based on the launch date of SMAP (January, 2015), the seasonal variations between the northern and

southern hemispheres may impact the usefulness of some regions in validation within the initial 12-month cal/val period. With a number of core sites in each hemisphere, this SMAP validation period is less affected by the seasonality of the launch date. The SMAP project is implementing a special product for validation that consists of L1C_TB data centered over the core validation sites to aid in SMAP validation. This is particularly important to the L2_SM_P product because it will allow the full exploitation of the *in situ* data.

7.2.2 Sparse Networks

The intensive network validation described above can be complemented by sparse networks as well as by new/emerging types of networks. Examples of sparse networks include the USDA Soil Climate Analysis Network (SCAN), the NOAA Climate Research Network (CRN), and the Oklahoma Mesonet. The defining feature of these networks is that the measurement density is low, usually resulting in one point per footprint. These observations cannot be used for validation without addressing two issues: verifying that they provide a reliable estimate of the 0-5 cm surface soil moisture layer and that the one measurement point is representative of the footprint. SMAP has been evaluating methodologies for upscaling data from these networks to SMAP footprint resolutions. A key element of the upscaling approach will be a method called Triple Co-location (Section 7.2.6) that combines the *in situ* data and SMAP product with another independent source of soil moisture, likely to be a model-based product.

Beyond these operational networks, there are new technologies being evaluated (COSMOS, GPS) that could provide distributed soil moisture information. SMAP is participating in the evaluation of these new technologies as part of its Marena, Oklahoma *In Situ* Sensor Testbed (MOISST) that is assessing both the verification of the relevant depth of measurement of these methods and scaling to SMAP footprints. The upscaling of these sparse networks remains an issue at present, and until this issue is resolved, the sparse networks will likely remain a secondary validation resource for the SMAP L2_SM_P soil moisture products.

7.2.3 Satellite Products

Depending upon mission timing and life, it is possible that SMOS, Aquarius, and JAXA's GCOM-W will be producing global soil moisture products at the same time as SMAP. SMOS and GCOM-W products are at the same nominal spatial resolution as the SMAP L2_SM_P soil moisture and are supported by validation programs, which should be mature by the time of the SMAP launch. As mentioned earlier, Aquarius soil moisture has a coarser resolution than these other satellites, but unfortunately failed in June, 2015.

In a previous section, the use of SMOS data prior to the launch of SMAP was described. Postlaunch soil moisture product comparisons with SMOS and GCOM-W are a very efficient means of validation over a wide range of conditions. If confidence in these products is high, they will provide an ideal resource for Stage 2 SMAP validation. The limitations of this type of comparison are the quality of the alternative product, differences

in overpass days, and accounting for system differences affecting the soil moisture product. In the case of GCOM-W, which collects data at 01:30 am and 01:30 pm, confusion factors would include both data acquisition at a different time of day from the SMOS/SMAP overpass time of 06:00 am and contributing depth issues associated with GCOM-W's C-band frequency. The SMAP team will actively participate in the validation of these alternative products during the SMAP prelaunch period, which will provide us with knowledge of the quality of both the SMOS and GCOM-W soil moisture.

Postlaunch validation will consist of comparisons between the SMAP / SMOS / GCOM-W / Aquarius soil moisture estimates that include:

- Core validation sites (CVS)
- Extended homogeneous regions
- Global maps

For the core validation sites and extended homogeneous regions, statistical comparisons will be conducted (Root Mean Square Difference, RMSD, will be used instead of RMSE because the alternative satellite products are not considered to be "ground truth"). The CVS will likely consist of approximately 15 sites distributed around the globe as described in the SMAP Cal/Val Plan [46]. Comparisons will be initiated as soon as SMAP soil moisture products become available; however, a sufficient period of record that includes multiple seasons will be necessary before any firm conclusions can be reached. It should also be noted that only dates when both satellites cover the same ground target at the same time will be useful. The overlap of the swaths will vary by satellite. The morning (and evening) orbits of SMAP and SMOS cross (the SMOS 6 am overpass is ascending while the SMAP 6 am overpass is descending). Obviously, coverage of a specific site by both satellites will be infrequent. Aquarius and SMAP have the same overpass times.

Although data collected over the CVS will be of the greatest value, additional sites with concurrent satellite observations are also useful, especially for regions that are relatively homogeneous in terms of land cover/vegetation and soils. One example would be the Sahara region.

Another role for the satellite products is in providing a synoptic perspective. Global image comparisons will be used to identify regions and/or time periods where the soil moisture products from the different satellites diverge.

Assessments will be conducted periodically throughout the SMAP postlaunch period to assess, monitor, and possibly correct bias offsets between SMAP products and SMOS/GCOM-W/Aquarius products. In order to fully exploit SMOS/GCOM-W/Aquarius soil moisture products for SMAP validation, it will be necessary for SMAP team members to participate in the assessment and validation of these products and to secure access to the data through ESA and JAXA.

7.2.4 Model-Based Products

In the simplest case, land surface models (either imbedded in a Numerical Weather Prediction (NWP) system or in off-line mode) can be used to generate soil moisture products at larger (basin-wide and continental) scales using land surface and meteorological forcing data sets that are independent of the SMAP remote sensing data. As in the case of satellite products, the resulting soil moisture fields can then be compared with the remotely sensed soil moisture product at validation sites (or synoptically) over diurnal and seasonal cycles. These model-derived soil moisture fields can also be used to extend comparisons to larger space and time domains than available from *in situ* observations, thus supporting Stage 2 validation. The L2_SM_P product matches the typical spatial resolution of currently available NWP products. An advantage of the model-based products is that they produce a synoptic global product every day, which means that more frequent comparisons to SMAP and ground-based observations are possible.

Several Numerical Weather Prediction (NWP) centers (including ECMWF, NCEP, and NASA/GMAO) routinely produce operational or quasi-operational soil moisture fields at a scale comparable to the SMAP radiometer product that could be used in SMAP validation. [This is distinct from the GMAO generation of the SMAP L4_SM surface and root zone soil moisture product which uses an ensemble Kalman filter (EnKF) to merge SMAP observations with soil moisture estimates from the NASA Catchment land surface model.] The NWP-derived data products rely on the assimilation of a vast number of atmospheric observations (and select land surface observations) into General Circulation Models (GCMs). Although there are many caveats that need to be considered in using these data, they are readily available and they are consistent with the atmospheric forcings (precipitation and radiation) and land use information that determine the spatial and temporal patterns in soil moisture fields.

There is significant inherent uncertainty in any model-based soil moisture product since this is not one of the NWP primary variables. In addition, the models typically simulate a thicker surface soil layer than the layer that dominates the satellite measurement. Little effort has been put so far into validating the soil moisture products of these models. Therefore, while these model products are useful, they must be used very carefully. As a result, they are considered to be a secondary resource for validating L2_SM_P soil moisture.

7.2.5 Field Experiments

Post-launch field experiments will play an important role in a robust validation of the L2_SM_P data product. These experiments provide critical information that can be used to independently assess the contributions of radiometer calibration, algorithm structure and parameterization, and scaling on performance. Field experiments require numerous elements that include ground and aircraft resources, which involve many participants and associated financial support. However, they provide moderate-term intensive measurements of soil moisture and other surface characteristics at SMAP footprint scales.

While it is desirable to acquire such information as soon as possible after launch, the uncertainties of the actual launch date, the relationship of the launch date to the season, and the logistics of allocation of fiscal year resources require that such commitments be conservative. Therefore, the field experiments should be scheduled for some time post-launch and used as part of the more robust validation of the SMAP products. Based on a January, 2015 launch, field campaigns are scheduled in 2015 in Australia and Arizona. Additionally, one major extended post-launch field campaign, which will include one or more core validation sites (such as Manitoba, Canada and the U.S. Midwest/Iowa), is scheduled for Summer 2016.

7.2.6 Combining Techniques

Recent work has extended the application of the "Triple Co-location" (TC) approach to soil moisture validation activities [51, 52]. These approaches are based on cross-averaging three independently-acquired estimates of soil moisture to estimate the magnitude of random error in each product. One viable product-triplet is the use of passive-based remote sensing, active-based remote sensing and a model-based soil moisture product [51, 53]. If successfully applied, TC can correct model versus SMAP soil moisture comparisons for the impact of uncertainty in the model product. However, TC cannot provide viable bias information and, therefore, only assesses the random error contribution to total RMSE. Note that TC can also be applied to reduce the impact of sampling error when upscaling sparse *in situ* measurements during validation against ground-based soil moisture observations.

8. MODIFICATIONS TO ATBD

This ATBD will continue to be modified under configuration control as new information becomes available and as the SMAP team refines its decisions regarding algorithm configuration, ancillary data selection, and the setting of flag thresholds.

The following updates are relevant to L2_SM_P Data Release Version 4 and L2_SM_P_E Version 1 in December, 2016 [61]:

8.1 Soil Moisture Retrievals at 6 PM

From the start of routine SMAP science operations on March 31, 2015, the soil moisture retrievals in the standard L2_SM_P product were generated using 6 am brightness temperatures as described in Section 2.4. Starting with SMAP's L2_SM_P Data Release Version 4 in December, 2016, 6 pm soil moistures were also produced by applying the baseline 6 am retrieval algorithm to T_B data from the 6 pm ascending passes. It was anticipated that the accuracy of the 6 pm soil moisture values would be somewhat worse than the 6 am soil moistures since some of the assumptions underlying the L2_SM_P

retrieval algorithm at 6 am (low Faraday rotation, hydraulic and thermal equilibrium between the upper soil layers and the overlying air/vegetation layer, etc.) are more likely to be violated at 6 pm. However, some early results from the SMOS mission suggested that the additional error associated with 6 pm retrievals may not be as large as expected [48], and in fact SMAP 6 pm soil moisture retrievals are only slightly worse than the 6 am retrievals [61, 63]. Although the 6 pm soil moisture retrieval performance will not be included in the evaluation of whether the L2_SM_P product meets the SMAP mission Level 1 requirements, the 6 pm retrievals have been compared against *in situ* observations of soil moisture to assess their accuracy as is done with the 6 am soil moisture values. The latest comparisons for End-of-Prime-Mission will be reported in the Data Release Version 5 assessment report available from NSIDC [63].

8.2 Soil Moisture Retrievals using the Enhanced L1C_TB_E Product

After the demise of the SMAP radar in July, 2015, the SMAP Project focused its attention on generating a new brightness temperature data set by using a Backus-Gilbert interpolation approach to take advantage of the SMAP radiometer oversampling on orbit. The resulting brightness temperatures are posted on a 9 km EASE2 grid. Details of this new algorithm approach can be found in the SMAP Algorithm Theoretical Basis Document: Enhanced L1B_TB_E Radiometer Brightness Temperature Data Product, SMAP Project, JPL D-56287, Jet Propulsion Laboratory, Pasadena, CA. The new L1B_TB_E brightness temperatures are used to produce a L1C_TB_E gridded product which is the starting point of the L2_SM_P_E soil moisture retrievals. These retrievals use the same algorithm as the standard L2_SM_P soil moisture retrievals, but have an aggregation domain of 33 km compared to 36 km for the standard product, and are posted at 9 km. The accuracy of the L2_SM_P_E soil moistures are compared to soil moisture observations in the L2_SM_P_E Data Release Version 1 and 2 assessment reports [61, 63], which also includes a more complete description of the L2_SM_P_E product. The L2_SM_P_E product includes both 6 am and 6 pm retrieved soil moisture posted on a 9 km grid. A journal article published late in 2017 indicates that the accuracy of the L2_SM_P_E retrievals is similar to the accuracy of L2_SM_P retrievals [64].

9. REFERENCES

1. National Research Council, "Earth Science and Applications from Space: National Imperatives for the Next Decade and Beyond," pp. 400, 2007.

2. Entekhabi, D., E, Njoku, P. O'Neill, K. Kellogg, plus 19 others, "The Soil Moisture Active Passive (SMAP) Mission," *Proceedings of the IEEE*, Vol. 98, No. 5, May, 2010.

3. Y. Kerr and J.-P. Wigneron, "Vegetation models and observations –A review," in: *Passive Microwave Remote Sensing of Land-Atmosphere Interactions (B. Choudhury, Y. Kerr, E. Njoku, P. Pampaloni, Eds.),* VSP, Utrecht, 1995.

4. Jackson, T. J., "Measuring surface soil moisture using passive microwave remote sensing," *Hydrol. Process.*, vol. 7, pp. 139-152, 1993.

5. Jackson, T. J., D. E. LeVine, C. T. Swift, T. J. Schmugge, and F. R. Schiebe, "Large area mapping of soil moisture using the ESTAR passive microwave radiometer in Washita'92," *Remote Sens. Environ*, 53:27-37, 1995.

6. Jackson, T. J. and D. E. LeVine, "Mapping surface soil moisture using an aircraft-based passive microwave instrument: Algorithm and example," *J. Hydrol*., 184:85-99, 1996.

7. Crow, W., T. Chan, D. Entekhabi, P. Houser, T. Jackson, E. Njoku, P. O'Neill, JC Shi, and X. Zhan, "An observing system simulation experiment for SMAP radiometer soil moisture products," *IEEE Trans. Geosci. Rem. Sens.,* 43(6), pp. 1289-1303, 2005.

8. Kerr, Y., P. Waldteufel, J.-P. Wigneron, J.-M. Martinuzzi, J. Font, and M. Berger, "Soil moisture retrieval from space: the Soil Moisture and Ocean Salinity (SMOS) mission," *IEEE Trans. Geosci. Rem. Sens.,* 39(8), pp. 1729-1735, 2001.

9. Wigneron, J.-P., Y. Kerr, P. Waldteufel, K. Saleh, M.-J. Escorihuela, P. Richaume, P. Ferrazoli, P. de Rosnay, R. Gurney, J.-C. Calvet, J. Grant, M. Guglielmettih, B. Hornbuckle, C. Matzler, T. Pellarin, and M. Schwank, "L-band microwave emission of the biosphere (L-MEB) model: description and calibration against experimental data sets over crop fields," *Remote Sens. Environ*, 107(4), pp. 639-655, 2007.

10. Saleh, K., J.-P. Wigneron, P. Waldteufel, P. de Rosnay, M. Schwank, J.-C. Calvet, and Y. Kerr, "estimates of surface soil moisture under grass covers using L-band radiometry," *Remote Sens. Environ*, 109(1), pp. 42-53, 2007.

11. Wigneron, J.-P., M. Parde, P. Waldteufel, A. Chanzy, Y. Kerr, S. Schmidl, and N. Skou, "Characterizing the Dependence of Vegetation Model Parameters on Crop Structure, Incidence Angle, and Polarization at L-Band, " *IEEE Trans. Geosci. Rem. Sens.,* 42(2), pp. 416-425, 2004.

12. Kerr, Y., P. Waldteufel, P. Richaume, I. Davenport, P. Ferrazoli, and J.-P. Wigneron, *SMOS Level 2 Processor Soil Moisture Algorithm Theoretical Basis Document (ATBD)*, Toulouse, France, CESBIO, SM-ESL (CBSA), vol. SO-TN-ESL-SM-GS-0001, v5.a, 2006.

13. Basharinov, A. and A. Shutko, "Simulation studies of the SHF radiation characteristics of soils under moist conditions," *NASA Tech. Transl.,* TT F-16, 1975.

14. Ulaby, F., R. Moore, and A. Fung, *Microwave Remote Sensing: Vols. I, II, and III*, Addison-Wesley, Reading, MA, 1982.

15. Jackson, T. J. and T. J. Schmugge, "Vegetation effects on the microwave emission from soils," *Rem. Sens. Environ.,* vol. 36, pp. 203-212, 1991.

16. Choudhury, B. J., T. J. Schmugge, A. Chang, and R. W. Newton, "Effect of surface roughness on the microwave emission from soil," *J. Geophys. Res,* 84(C9): 5699-5706, 1979.

17. Wang, J. R., "Passive microwave sensing of soil moisture content: the effects of soil bulk density and surface roughness," *Remote Sens. Environ.*, vol. 13, pp. 329-344, 1983.

18. Wang, J and B. J. Choudhury, "Passive Microwave Radiation From Soil: Examples of Emission Models and Observations," in Choudhury, B., Y. Kerr, E. Njoku, and P. Pampaloni, *Passive Microwave Remote Sensing of Land-Atmosphere Interactions,* VSP, Utrecht, 1995.

19. Mironov, V. L., L. G. Kosolapova, and S. V. Fomin, "Physically and mineralogically based spectroscopic dielectric model for moist soils," *IEEE Trans. Geosci. Remote Sens.*, 47(7), pp. 2059–2070, 2009.

20. Dobson, M. C., F. T. Ulaby, M. T. Hallikainen, and M. A. El-Rayes, "Microwave dielectric behavior of wet soil – Part II: Dielectric mixing models," *IEEE Trans. Geosci. Rem. Sens.,* vol. GE-23, pp. 35-46, 1985.

21. Wang, J. R and T. J. Schmugge, "An empirical model for the complex dielectric permittivity of soils as a function of water content," *IEEE Trans. Geosci. Rem. Sens.*, 18, pp. 288-295, 1980.

22. Ulaby, F., P. Dubois, and J. van Zyl, "Radar mapping of surface soil moisture," *Journal of Hydrology,* 184(1-2), pp. 57-84, 1996.

23. Njoku, E. G. and J. A. Kong (1977): Theory for passive microwave remote sensing of near-surface soil moisture, *J. Geophys. Res., 82*, 3108-3118.

24. Fagerlund, E., B. Kleman, L. Sellin, and H. Svensson, "Physical Studies of Nature by Thermal Mapping," *Earth-Science Reviews*, 6, pp. 169-180, 1970.

25. Jackson, T. and J. Kimball, "SMAP Mission Science Issues Associated with Overpass Time," SMAP Science Document No. 003, JPL, March 31, 2009.

26. NSIDC, "EASE-Grid Data," [Online] Available: http://nsidc.org/data/ease/index.html [Accessed: Jun 14, 2010].

27. NSIDC, "EASE-Grid Data: Data Summaries," [Online] Available: http://nsidc.org/data/ease/data_summaries.html [Accessed: Jun 14, 2010].

28. SMAP Level 2 Science Requirements (JPL D-45955), Feb 11, 2009. Available online: https://pdms.jpl.nasa.gov.

29. Klein, L. A. and C. T. Swift, "An Improved Model for the Dielectric Constant of Sea Water at Microwave Frequencies," *IEEE Journal of Oceanic Engineering*, vol. 2, no. 1, January, 1977.

30. Ryu, D., T. Jackson, R. Bindlish, D. LeVine, and M. Haken, "Soil Moisture Retrieval using Two-Dimenional L-Band Synthetic Aperture Radiometer in a Semi-Arid Environment," *IEEE Trans. Geosci. Remote Sens.*, 48 (12), pp. 4273-4284, 2010.

31. O'Neill, P., M. Owe, B. Gouweleeuw, E. Njoku, J. Shi, and E. Wood, "Hydros Soil Moisture Retrieval Algorithms: Status and Relevance to Future Missions," *Proc. 2006 IEEE International Geoscience and Remote Sensing Symposium (IGARSS 2006)*, Denver, Colorado, July 31-August 4, 2006.

32. Zhan, X., W. Crow, T. J. Jackson, P. O'Neill, "Improving Spaceborne Radiometer Soil Moisture Retrievals With Alternative Aggregation Rules for Ancillary Parameters in Highly Heterogeneous Vegetated Areas," *IEEE Trans. Geosci. Rem. Sens.*, 5(2), pp. 261-265, 2008.

33. Njoku, E. and L. Li, "Retrieval of Land Surface Parameters Using Passive Microwave Measurements at 6-18 GHz," *IEEE Trans. Geosci. Rem. Sens*., vol. 37, pp. 79–93, 1999.

34. Yueh, S., S. Dinardo, S. K. Chan, E. Njoku, T. Jackson, R. Bindlish, "Passive and Active L-Band System and Observations During the 2007 CLASIC Campaign," *Proc. 2008 IEEE International Geoscience and Remote Sensing Symposium (IGARSS 2008)*, Boston, Massachusetts, July 6-11, 2008.

35. Owe, M., R. De Jeu, and J. Walker, "A methodology for surface soil moisture and vegetation optical depth retrieval using the microwave polarization difference index," *IEEE Trans. Geosci. Rem. Sens.*, 39, pp. 1643-1654, 2001.

36. de Jeu, R., T. Holmes, R. Panciera, and J. Walker, "Parameterization of the Land Parameter Retrieval Model for L-Band Observations Using the NAFE'05 Data Set," *IEEE Geoscience and Remote Sensing Letters*, 6 (4), pp. 630-634, October, 2009.

37. Mo, T., B. J. Choudhury, T. J. Schmugge, J. R. Wang, and T. J. Jackson, "A model for microwave emission from vegetation-covered fields," *J. Geophys. Res.*, 87(13), pp. 11229-11237, 1982.

38. Meesters, G. C., R. de Jeu, R. and M. Owe, "Analytical derivation of the vegetation optical depth from the microwave polarization difference index," *IEEE Geosci. and Remote Sensing Letters*, 2, pp. 121-123, 2005.

39. Holmes, T., T. Jackson, R. Reichle, and J. Basara, An Assessment of Surface Soil Temperature Products from Numerical Weather Prediction Models using Ground-based Measurements," *Water Resources Research,* in review, 2011.

40. Chan, S, R. Hunt, R. Bindlish, E. Njoku, J. Kimball, and T. Jackson, "Ancillary Data Report for Vegetation Water Content," *SMAP Project Document* # D-53061, JPL, July, 2011.

41. Jackson, T., R. Bindlish, and T. Zhao, "Justification Memo for Vegetation Index Climatology," *SMAP Science Documents*, JPL, February, 2011.

42. Das, N., "Evaluation of Urban/Rural Datasets for the SMAP Mission," *SMAP Science Document* #D-53060, 1.0, JPL, March, 2011.

43. Kerr, Y. H. , Waldteufel, P., Wigneron, J., Delwart, S., Cabot, F., Boutin, J., Escorihuela, M., Font, J., Reul, N., Gruhier, C., Juglea, S. E., Drinkwater, M. R., Hahne, A., Martín-Neira, M.,and Mecklenburg, S., "The SMOS mission: New tool for monitoring key elements of the global water cycle," *Proceedings of the IEEE*, 98(5), pp. 666- 687, 2010.

44. Le Vine, D. M., Lagerloef, G. S., and Torrusio, S. E., "Aquarius and remote sensing of sea surface salinity from space," *Proceedings of the IEEE*, 98(5), pp. 688-703, 2010.

45. SMAP SDS Web, "GloSim 2003," Available online: http://smap-sds-web.jpl.nasa.gov/confluence/display/algorithm/GloSim+2003.

46. SMAP SDS Web, "SMAP Science Data Calibration and Validation Plan," Available online: http://smap-sds-web.jpl.nasa.gov/confluence/display .

47. Jackson, T. J., Cosh, M. H., Bindlish, R., Starks, P. J., Bosch, D. D., Seyfried, M. S., Goodrich, D. C., and Moran, M. S., "Validation of Advanced Microwave Scanning Radiometer soil moisture products," *IEEE Trans. Geosci. Rem. Sens.*, 48, pp. 4256-4272, 2010.

48. Jackson, T. J., Bindlish, R., Cosh, M. H., Zhao, T., Starks, P. J., Bosch, D. D., Seyfried, M. S., Moran, M. S., Kerr, Y., and Leroux, D., "Validation of Soil Moisture and Ocean Salinity (SMOS) soil moisture over watershed networks in the U.S.," *IEEE Trans. Geosci. Rem. Sens.,* 2012, pp: 1530 - 1543.

49. Draper, C. S., Walker, J. P., Steinle, P. J., de Jeu, R. A, and Holmes, T. R., "An evaluation of AMSR-E derived soil moisture over Australia," *Remote Sens. Environ*, 113(4), pp. 703-710, 2009.

50. Gruhier, C., de Rosnay, P., Hasenauer, S., Holmes, T., de Jeu, R., Kerr, Y., Mougin, E., Njoku, E., Timouk, F., Wagner, W., and Zribi, M., "Soil moisture active and passive microwave products: intercomparison and evaluation over a Sahelian site," *Hydrol. Earth Syst. Sci. Discuss.*, 6, pp. 5303-5339, 2009.

51. Scipal, K., Holmes, T., de Jeu, R., Naeimi, V., and Wagner, W., "A possible solution for the problem of estimating the error structure of global soil moisture data set", *Geophys. Res. Let.*, 35, 2008.

52. Miralles, D. G., Crow, W. T., and Cosh, M. H., "A technique for estimating spatial sampling errors in coarse-scale soil moisture estimates derived from point-scale observations," *Journal of Hydrometeorology*, 11(6), pp. 1404-1410, 2010.

53. Dorigo, W. A., Scipal, K., Parinussa, R. M., Liu, Y. Y., Wagner, W., de Jeu, R. A. M., and Naeimi, V., "Error characterisation of global active and passive microwave soil moisture datasets," *Hydrol. Earth Syst. Sci*., 14, pp. 2605-2616, doi:10.5194/hess-14-2605-2010, 2010.

54. Das, N. and P. O'Neill, "Selection of Soil Attributes Datasets for the SMAP Mission," SMAP Science Document #D-53058, 1.1, JPL, Dec., 2010.

55. Calvo-Alvarado, J., N. McDowell, and R. Waring, "aalometric Relationships Predicting Foliar Biomass and Leaf Area/Sapwood Area Ratio from Tree Height in Five Costa Rican Rain Forest Species," *Tree Physiology*, 28, pp. 1601-1608, 2008.

56. O'Neill, P., T. Jackson, D. Entekhabi, and E. Njoku, "Survey of Tower and Airborne L-Band Sensor Systems Relevant to Soil Moisture Space Missions," *Geoscience & Remote Sensing Newsletter*, IEEE, 151, June, 2009, pp. 13-16.

57. Bindlish, R., T. Jackson, M. Cosh, T. Zhao, and P. O'Neill, "Global Soil Moisture from the Aquarius Satellite: Description and Initial Assessment," IEEE Geoscience and Remote Sensing Letters, 2014, in press, doi 10.1109/LGRS.2014.2364151.

58. Choudhury, B., Schmugge, T., and Mo, T, "A Parameterization of Effective Soil Temperature for Microwave Emission," J. Geophys. Res., 87: 1301-1304, 1982.

59. Jackson, T., P. O'Neill, E. Njoku, S. Chan, and R. Bindlish, "SMAP Project Calibration and Validation for the L2/3_SM_P Beta-Release Data Products," JPL D-93981, jet Propulsion Laboratory, Pasadena, CA, September, 2015.

60. Jackson, T., P. O'Neill, E. Njoku, S, Chan, R. Bindlish, A. Colliander, F. Chen, M. Burgin, S. Dunbar, J. Piepmeier, M. Cosh, T. Caldwell, J. Walker, X. Wu, A. Berg, T. Rowlandson, A. Pacheco, H. McNairn, M. Thibeault, J. Martínez-Fernández, Á. González-Zamora, M. Seyfried, D. Bosch, P. Starks, D. Goodrich, J. Prueger, Z. Su, R. van der Velde, J. Asanuma, M. Palecki, E. Small, M. Zreda, J. Calvet, W. Crow, Y. Kerr, S. Yueh, and D. Entekhabi, April 30, 2016. *Calibration and Validation for the L2/3_SM_P Version 3 Data Products*, SMAP Project, JPL D-93720, Jet Propulsion Laboratory, Pasadena, CA.

61. Jackson, T., P. O'Neill, S, Chan, R. Bindlish, A. Colliander, F. Chen, M. Burgin, S. Dunbar, J. Piepmeier, M. Cosh, T. Caldwell, J. Walker, X. Wu, A. Berg, T. Rowlandson, A. Pacheco, H. McNairn, M. Thibeault, J. Martínez-Fernández, Á. González-Zamora, E. Lopez-Baeza, F. Udall, M. Seyfried, D. Bosch, P. Starks, C. Holifield, J. Prueger, Z. Su, R. van der Velde, J. Asanuma, M. Palecki, E. Small, M. Zreda, J. Calvet, W. Crow, Y. Kerr, S. Yueh, and D. Entekhabi, December 15, 2016. *Calibration and Validation for the L2/3_SM_P Version 4 and L2/3_SM_P_E Version 1 Data Products*, SMAP Project, JPL D-56297, Jet Propulsion Laboratory, Pasadena, CA.

62. Chan, S., R. Bindlish, P. O'Neill, E. Njoku, T. Jackson, A. Colliander, F. Chen, M. Burgin, S. Dunbar, J. Piepmeier, S. Yueh, D. Entekhabi, M. Cosh, T. Caldwell, J. Walker, X. Wu, A. Berg, T. Rowlandson, A. Pacheco, H. McNairn, M. Thibeault, J. Martínez-Fernández, Á. González-Zamora, M. Seyfried, D. Bosch, P. Starks, D. Goodrich, J. Prueger, M. Palecki, E. Small, J. Calvet, W. Crow, and Y. Kerr, "Assessment of the SMAP Level 2 Passive Soil Moisture Product," *IEEE Trans. on Geoscience and Remote Sensing*, vol. 54, no. 8, August 2016, pp. 4994-5007, doi: 10.1109/TGRS.2016.2561938.

63. Jackson, T., P. O'Neill, S, Chan, R. Bindlish, A. Colliander, F. Chen, M. Burgin, S. Dunbar, J. Piepmeier, M. Cosh, T. Caldwell, J. Walker, X. Wu, A. Berg, T. Rowlandson, A. Pacheco, H. McNairn, M. Thibeault, J. Martínez-Fernández, Á. González-Zamora, E. Lopez-Baeza, F. Udall, M. Seyfried, D. Bosch, P. Starks, C. Holifield, J. Prueger, Z. Su, R. van der Velde, J. Asanuma, M. Palecki, E. Small, M. Zreda, J. Calvet, W. Crow, Y. Kerr, S. Yueh, and D. Entekhabi, June 6, 2018. *Calibration and Validation for the L2/3_SM_P Version 5 and L2/3_SM_P_E Version 2 Data Products*, SMAP Project, JPL D-56297, Jet Propulsion Laboratory, Pasadena, CA.

64. Chan, S., R. Bindlish, P. O'Neill, T. Jackson, E. Njoku, S. Dunbar, J. Chaubell, J. Piepmeier, S. Yueh, D. Entekhabi, A. Colliander, F. Chen, M. Cosh, T. Caldwell, J. Walker, A. Berg, H. McNairn, M. Thibeault, J. Martínez-Fernández, F. Uldall, M. Seyfried, D. Bosch, P. Starks, C. Holifield Collins, J. Prueger, R. van der Velde, J. Asanuma, M. Palecki, E. Small, M. Zreda, J-C. Calvet, W. Crow, and Y. Kerr, "Development and Assessment of the SMAP Enhanced Passive Soil Moisture Product," *Remote Sensing of Environment*, vol. 204, pp. 931-941, January 2018, online October 13, 2017, 10.1016/j.rse.2017.08.025.

65. Lawrence, H., Wigneron, J. -P., Demontoux, F., Mialon, A., and Kerr, Y., "Evaluating the Semiempirical H-Q Model Used to Calculate the L-Band Emissivity of a Rough Bare Soil," *IEEE Transactions on Geoscience and Remote Sensing*, 51(7), pp. 4075–4084, 2013.

66. Konings, A. G., M. Piles, N. Das, and D. Entekhabi, “L-band vegetation optical depth and effective scattering albedo estimation from SMAP,” Remote Sensing of Environment, Vol. 198, pp. 460-470, 2017.

67. Fernandez-Moran, R, A. Al-Yaari, A. Mialon, A. Mahmoodi, A. Al Bitar, G. De Lannoy, N. Rodriguez-Fernandez, E. Lopez-Baeza, Y. Kerr, and J-P Wigneron, “SMOS-IC: An Alternative SMOS Soil Moisture and Vegetation Optical Depth Product,” *Remote Sensing*, 9(5):457, 2017.

68. O’Neill, P., S. Chan, R. Bindlish, M. Chaubell, A. Colliander, F. Chen, S. Dunbar, T. Jackson, J. Piepmeier, S. Misra, M. Cosh, T. Caldwell, J. Walker, X. Wu, A. Berg, T. Rowlandson, A. Pacheco, H. McNairn, M. Thibeault, J. Martínez-Fernández, Á. González-Zamora, E. Lopez-Baeza, F. Udall, M. Seyfried, D. Bosch, P. Starks, C. Holifield, J. Prueger, Z. Su, R. van der Velde, J. Asanuma, M. Palecki, E. Small, M. Zreda, J. Calvet, W. Crow, Y. Kerr, S. Yueh, and D. Entekhabi, August 15, 2019. *Calibration and Validation for the L2/3_SM_P Version 6 and L2/3_SM_P_E Version 3 Data Products*, SMAP Project, JPL D-56297, Jet Propulsion Laboratory, Pasadena, CA.

69. Chaubell, J., et al., "Improving Brightness Temperature Measurements Near Coastal Areas for SMAP," in IEEE Journal of Selected Topics in Applied Earth Observations and Remote Sensing, vol. 12, no. 11, pp. 4578-4588, Nov. 2019, doi: 10.1109/JSTARS.2019.2951323.

70. Hengl, T., J. de Jesus, G. Heuvelink, M. Gonzalez, M. Kilibarda, A. Blagotić, W. Shangguan, M.Wright, X. Geng, B. Bauer-Marschallinger, and M. Guevara, *SoilGrids250m: Global gridded soil information based on machine learning*, PLoS one, 12(2), 2017, p.e0169748. https://doi.org/10.1371/journal.pone.0169748.

71. Dai, Y., W. Shangguan, N. Wei, Q. Xin, H. Yuan, S. Zhang, L. Shupeng, L. Shaofeng, L. Xingjie, W. Dagang, and Y. Fapeng, “A review of the global soil property maps for Earth system models” SOIL 5, 2019, pp. 137-158, 10.5194/soil-5-137-2019.

APPENDIX 1: L2_SM_P Output Product Data Fields

The specific details of all of the fields in the L2_SM_P and L3_SM_P output products can be found in the L2/3_SM_P Data Product Specification Document available from the NSIDC DAAC. A summary is given in the table below. Data fields in **boldface** indicate fields that are new in the current release; data fields marked with an asterisk are available only in L2_SM_P but not in L3_SM_P. **Note that the 'roughness coefficient' and 'albedo' fields are associated with SCA-V in L2_SM_P but DCA in L3_SM_P as of the R18 data release in October, 2021. Additional information can be found in the pointer tables in Appendix 6.**

Data Fields	Description
tb_time_seconds	Average TB sample acquisition time in a grid cell
tb_time_utc	Average TB sample acquisition time in a grid cell
EASE_row_index	Global 36-km EASE2 Grid 0-based row index
EASE_column_index	Global 36-km EASE2 Grid 0-based column index
grid_surface_status	Land (0) or water (1) based on footprint boresight
latitude	L1C_TB center latitude
longitude	L1C_TB center longitude
latitude_centroid	L1C_TB centroid latitude
longitude_centroid	L1C_TB centroid longitude
boresight_incidence	L1C_TB incidence angle
tb_h_corrected	H-polarized TB with water correction
tb_v_corrected	V-polarized TB with water correction
tb_h_uncorrected	L1C_TB uncorrected H-polarized TB
tb_v_uncorrected	L1C_TB uncorrected V-polarized TB
surface_water_fraction_mb_h	H-polarized antenna-gain-weighted water fraction
surface_water_fraction_mb_v	V-polarized antenna-gain-weighted water fraction
tb_3_corrected	L1C_TB uncorrected 3rd Stokes parameter
tb_4_corrected	L1C_TB uncorrected 4th Stokes parameter
tb_qual_flag_h	Quality flag of L1C_TB H-polarized TB
tb_qual_flag_v	Quality flag of L1C_TB V-polarized TB
tb_qual_flag_3	Quality flag of L1C_TB 3rd Stokes parameter
tb_qual_flag_4	Quality flag of L1C_TB 4th Stokes parameter
static_water_body_fraction	Areal fraction of static water
radar_water_body_fraction	Set to static_water_body_fraction
freeze_thaw_fraction	Areal fraction of freeze/thaw state
soil_moisture	Retrieved soil moisture using the DCA algorithm
soil_moisture_option1 *	Retrieved soil moisture using the SCA-H algorithm
soil_moisture_option2 *	Retrieved soil moisture using the SCA-V algorithm
soil_moisture_option3 *	Retrieved soil moisture using the DCA algorithm
vegetation_opacity	Retrieved 'tau' parameter derived from DCA
vegetation_opacity_option1 *	Retrieved 'tau' parameter derived from NDVI

vegetation_opacity_option2 *	Retrieved 'tau' parameter derived from NDVI
vegetation_opacity_option3 *	Retrieved 'tau' parameter derived from DCA
retrieval_qual_flag	Quality flag of retrieved soil moisture using DCA
retrieval_qual_flag_option1 *	Quality flag of retrieved soil moisture using SCA-H
retrieval_qual_flag_option2 *	Quality flag of retrieved soil moisture using SCA-V
retrieval_qual_flag_option3 *	Quality flag of retrieved soil moisture using DCA
soil_moisture_error	Error of retrieved soil moisture
surface_flag	Surface conditions that indicate retrievability
vegetation_water_content	Vegetation water content derived from NDVI
surface_temperature	Effective soil temperature
albedo	Single-scattering albedo used in SCA-V and SCA-H
albedo_option3	Single-scattering albedo used in DCA
roughness_coefficient	'h' parameter used in SCA-V and SCA-H
roughness_coefficient_option3	'h' parameter from ancillary file used in DCA
landcover_class	Top three dominant IGBP land cover classes
landcover_class_fraction	Top three dominant land cover class fractions
organic_content	**The aggregated organic content within the 36 km grid cell**
sand_fraction	**The aggregated sand fraction within the 36 km grid cell**
clay_fraction	The aggregated clay fraction within the 36 km grid cell
bulk_density	The aggregated bulk density within the 36 km grid cell

APPENDIX 2: L2_SM_P_E Output Product Data Fields

The specific details of all of the fields in the L2_SM_P_E and L3_SM_P_E output products can be found in the L2/3_SM_P_E Data Product Specification Document available from the NSIDC DAAC. A summary is given in the table below. As of the R18 data release in October, 2021, L2_SM_P_E data fields on global and polar grids are organized in two separate HDF5 data groups called 'Soil_Moisture_Retrieval_Data' and 'Soil_Moisture_Retrieval_Data_Polar', respectively, in the same granule. Each group contains the same data fields and their associated definitions. Data fields in **boldface** indicate fields that are new in the current release; data fields marked with an asterisk are available only in L2_SM_P_E but not in L3_SM_P_E. **Note that the 'roughness coefficient' and 'albedo' fields are associated with SCA-V in L2_SM_P_E but DCA in L3_SM_P_E as of the R18 data release in October, 2021. Additional information can be found in the pointer tables in Appendix 6.**

Data Fields	Description
tb_time_seconds	Average TB sample acquisition time in a grid cell
tb_time_utc	Average TB sample acquisition time in a grid cell
EASE_row_index	Global 9-km EASE2 Grid 0-based row index
EASE_column_index	Global 9-km EASE2 Grid 0-based column index
grid_surface_status	Land (0) or water (1) based on footprint boresight
latitude	L1C_TB_E center latitude
longitude	L1C_TB_E center longitude
latitude_centroid	L1C_TB_E centroid latitude
longitude_centroid	L1C_TB_E centroid longitude
boresight_incidence	L1C_TB_E incidence angle
tb_h_corrected	H-polarized TB with water correction
tb_v_corrected	V-polarized TB with water correction
tb_h_uncorrected	L1C_TB_E uncorrected H-polarized TB
tb_v_uncorrected	L1C_TB_E uncorrected V-polarized TB
surface_water_fraction_mb_h	H-polarized antenna-gain-weighted water fraction
surface_water_fraction_mb_v	V-polarized antenna-gain-weighted water fraction
tb_3_corrected	L1C_TB_E uncorrected 3rd Stokes parameter
tb_4_corrected	L1C_TB_E uncorrected 4th Stokes parameter
tb_qual_flag_h	Quality flag of L1C_TB_E H-polarized TB
tb_qual_flag_v	Quality flag of L1C_TB_E V-polarized TB
tb_qual_flag_3	Quality flag of L1C_TB_E 3rd Stokes parameter
tb_qual_flag_4	Quality flag of L1C_TB_E 4th Stokes parameter
static_water_body_fraction	Areal fraction of static water
radar_water_body_fraction	Set to static_water_body_fraction
freeze_thaw_fraction	Areal fraction of freeze/thaw state
soil_moisture	Retrieved soil moisture using the DCA algorithm
soil_moisture_option1 *	Retrieved soil moisture using the SCA-H algorithm

soil_moisture_option2 *	Retrieved soil moisture using the SCA-V algorithm
soil_moisture_option3 *	Retrieved soil moisture using the DCA algorithm
vegetation_opacity	Retrieved 'tau' parameter derived from DCA
vegetation_opacity_option1 *	Retrieved 'tau' parameter derived from NDVI
vegetation_opacity_option2 *	Retrieved 'tau' parameter derived from NDVI
vegetation_opacity_option3 *	Retrieved 'tau' parameter derived from DCA
retrieval_qual_flag	Quality flag of retrieved soil moisture using DCA
retrieval_qual_flag_option1 *	Quality flag of retrieved soil moisture using SCA-H
retrieval_qual_flag_option2 *	Quality flag of retrieved soil moisture using SCA-V
retrieval_qual_flag_option3 *	Quality flag of retrieved soil moisture using DCA
soil_moisture_error	Error of retrieved soil moisture
surface_flag	Surface conditions that indicate retrievability
vegetation_water_content	Vegetation water content derived from NDVI
surface_temperature	Effective soil temperature
albedo	Single-scattering albedo used in SCA-V and SCA-H
albedo_option3	Single-scattering albedo used in DCA
roughness_coefficient	'h' parameter used in SCA-V and SCA-H
roughness_coefficient_option3	'h' parameter from ancillary file used in DCA
landcover_class	Most dominant IGBP land cover classes
organic_content	**The aggregated organic content within the 9 km grid cell**
sand_fraction	**The aggregated sand fraction within the 9 km grid cell**
clay_fraction	The aggregated clay fraction within the 9 km grid cell
bulk_density	The aggregated bulk density within the 9 km grid cell

APPENDIX 3: Parameterization of Effective Soil Temperature (T_{eff})

Accurate soil moisture retrievals from SMAP 1.4 GHz brightness temperature data require an estimate of the soil effective temperature (T_{eff}). The Choudhury two-layer approach for T_{eff} [Choudhury et al., 1982] has been used in all previous SMAP data releases and by other missions with good success. This approach combines estimates of a "surface" temperature and a "deep" temperature using a proportional coefficient dependent on the microwave wavelength. In the SMAP 2018 data release, the Choudhury approach was modified by an additional parameter K to address an observed bias between ancillary modeled soil temperatures and measured *in situ* temperatures at core validation sites and sparse network stations. In January, 2020 NASA GMAO modified atmospheric and land modules in the GEOS-FP modeling system, resulting in a change to the soil temperature ancillary data used in SMAP processing and a change in the definition of soil layer depths [Koster et al., 2020]. As a result, the SMAP project conducted a number of different analyses to determine the most appropriate parameterization of the Choudhury effective temperature. This appendix contains two summaries of these efforts. As of the R17 release in August, 2020, the approach outlined in section A3.2 was adopted as the baseline approach for T_{eff} formulation.

A3.1. Rationale for a Two-Layer Effective Soil Temperature Model for SMAP Passive Soil Moisture Products

(Lead Investigator: Steven Chan, JPL)

Experimental and theoretical literature (Choudhury 1982 and Lv 2014, 2016) have long established the physics that at L-band frequencies, microwave emission from land primarily comes from the deep soil layer ($\boldsymbol{T_{deep}}$), and to a lesser extent, the shallower soil layer ($\boldsymbol{T_{top}}$). The combined use of $\boldsymbol{T_{deep}}$ and $\boldsymbol{T_{top}}$ in effective soil temperature ($\boldsymbol{T_{eff}}$) modeling has in the past enabled great science advances for L-band satellite missions including SMOS (2009-present) and SMAP (2015-present) as well as enabling other research reported in refereed literature.

The upcoming SMAP R17 release consists of upgrades in/changes to radiometer calibration, GMAO ancillary soil temperatures, GMAO soil layer depths, and the global soil texture database used. As such, the pre-R17 two-layer $\boldsymbol{T_{eff}}$ model was examined to see if parameter retuning was required. Since the impacts of $\boldsymbol{T_{eff}}$ are most directly felt in soil moisture retrieval accuracy, sensitivity analysis was applied to the *in situ* soil moisture observations from core validation sites to determine the new parameters (*C, K*) for the R17 two-layer $\boldsymbol{T_{eff}}$ model. To ensure validation with minimal partiality in product assessment, observations from only a random half of all CVS stations were used at a time in the sensitivity analysis.

The parameters determined in this way also independently confirmed three outcomes: (1) a larger $\boldsymbol{T_{top}}$ contribution in R17 that is in line with theoretical prediction (e.g., Lv, 2014) and the new GEOS-FP soil depth layer definitions, (2) the validity of a two-layer model to describe $\boldsymbol{T_{eff}}$ for SMAP 6:00 AM data, and (3) the validity of using C=1 to

describe $\boldsymbol{T_{eff}}$ for SMAP 6:00 PM data. The resulting retrieval performance metrics and spatial/temporal variability continue to be consistent with those derived before R17, giving additional confidence in SMAP's continued ability to produce high-quality soil moisture data products.

The analysis started with the objective to determine if (a) SMAP $\boldsymbol{T_B}$ observations and (b) footprint-scaled CVS soil moisture observations support a two-layer $\boldsymbol{T_{eff}}$ model or a one-layer $\boldsymbol{T_{eff}}$ model. Baseline soil moisture retrieval time series were obtained at all CVS one (C, K) pair at a time using the following two-layer $\boldsymbol{T_{eff}}$ formulation, which reduces to a one-layer $\boldsymbol{T_{eff}}$ model when $C = 1$.

$$\boldsymbol{T_{eff} = K \times [\, T_{SOIL1} \times C + T_{SOIL2} \times (1 - C)]}$$

where K is a factor that modifies the original Choudhury formulation to address an observed bias between ancillary modeled soil temperature and measured *in situ* temperature at core validation sites and sparse network stations. T_{soil1} refers to the average soil temperature for the first soil layer (5-15 cm) and T_{soil2} refers to the average soil temperature for the second soil layer (15-35 cm) of the GMAO GEOS-FP land surface model. Assuming direct correspondence between (a) and (b) above, favorable metrics are expected along $C = 1$ for the validity of a one-layer $\boldsymbol{T_{eff}}$ model, or along $C \neq 1$ for the validity of a two-layer $\boldsymbol{T_{eff}}$ model. In this sensitivity analysis setup, no implicit *a priori* assumption was made on what (C, K) values should take to dictate the metric pattern one way or the other.

The SMAP CVS data are comprised of *in situ* soil moisture observation time series from 15 stations. To minimize partiality upon assessing the data product with the same dataset, 8 stations were randomly selected (~50% of all available stations) at a time, and their time series were used to determine one realization of (C, K). This process was repeated until all ${}_{15}C_8 = 15! / (7! \times 8!) = 6{,}435$ possible combinations were exhausted. All realizations of (C, K) were then averaged to provide their mean values and standard deviations:

$$(C, K) = (0.43 \pm 0.14, 1.0106 \pm 0.0042)$$

which approach their theoretical limits (C, K) = (0.46,1.0103) had all CVS been used in the first place. However, this random-selection sensitivity analysis approach is not without drawbacks: for example, even though only half of them were used in sensitivity analysis for any given realization, all of them were eventually involved, though not all at the same time. In view of the inherent difficulty in $\boldsymbol{T_{eff}}$'s direct observability other than in soil moisture retrievals, however, this lack of rigor in analysis design appears to be a temporary but reasonable compromise in subsequent validation in order to help answer the following pressing question that initiated this investigation:

> Do SMAP $\boldsymbol{T_B}$ observations and CVS soil moisture observations indicate a two-layer $\boldsymbol{T_{eff}}$ model or a one-layer $\boldsymbol{T_{eff}}$ model?

As an illustration, Figure A3-1 shows the 6:00 AM and 6:00 PM performance metrics over the (C, K) space for the 4-year T16540 OASIS run. Two observations follow from this figure. First, favorable 6:00 PM metrics – defined as low ubRMSE, small bias

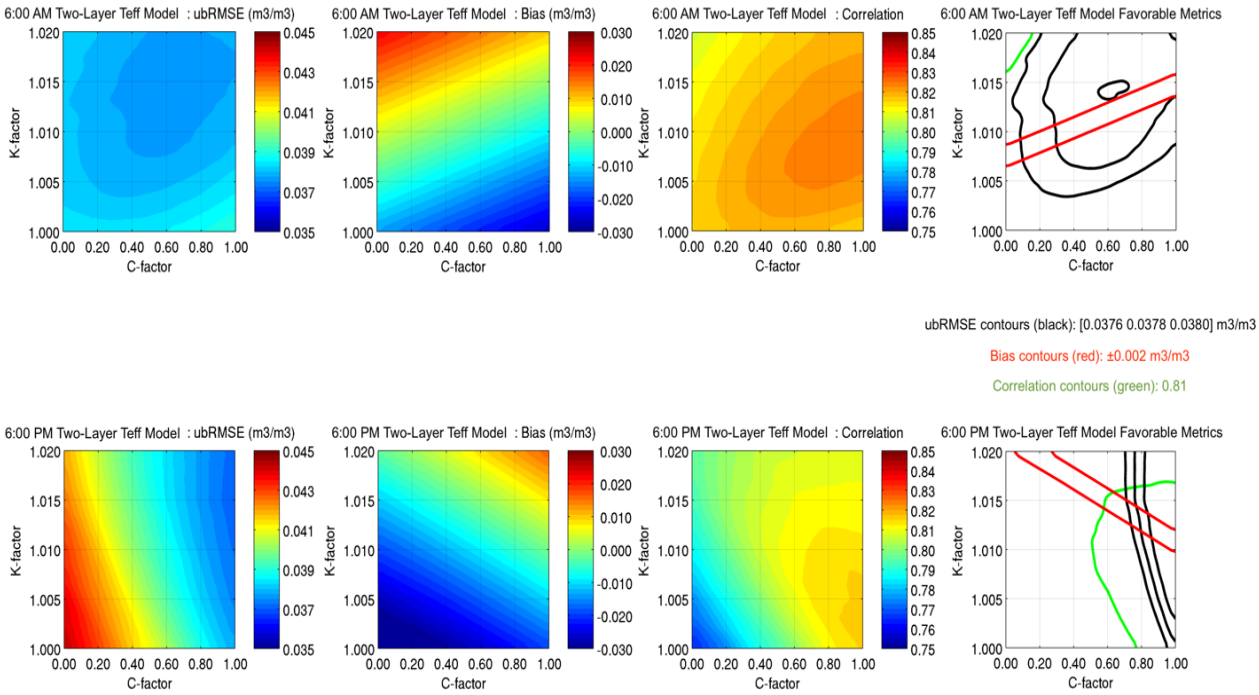

Figure A3-1. 6:00 AM and 6:00 PM performance metrics as a function of *C* and *K* observed over CVS

magnitude, *and* high correlation – all occur simultaneously near the $C = 1$ line. The corresponding K varies within a narrow band of values around 1.01. The fact that $C = 1$ implies that the one-layer model provides the best analytical form for $\boldsymbol{T_{eff}}$ at 6:00 PM. This result independently affirms the choice made by the team in 2017 to simply use $C = 1$ for the SMAP 6:00 PM data. Under this formulation, the effect of $\boldsymbol{T_{SOIL2}}$ is negated and only $\boldsymbol{T_{SOIL1}}$ is used for $\boldsymbol{T_{eff}}$ modeling in Level 2 soil moisture geophysical inversion for 6:00 PM data.

On the other hand, the favorable 6:00 AM metrics (low ubRMSE, small bias magnitude, *and* high correlation) convey a different structure. Unlike their 6:00 PM counterparts, they do not align well with the $C = 1$ line, implying that the two-layer model is necessary to provide the best analytical form for $\boldsymbol{T_{eff}}$ for the SMAP 6:00 AM data. Since $C \neq 1$ to obtain the best results at 6:00 AM, both $\boldsymbol{T_{SOIL1}}$ and $\boldsymbol{T_{SOIL2}}$ are needed simultaneously to explain the correspondence between the SMAP $\boldsymbol{T_B}$ observations and CVS soil moisture observations for 6:00 AM data.

Although the two-layer model can be reduced to the one-layer model by setting $C = 1$ (as for the 6:00 PM data), the converse is not possible – the one-layer model cannot be modified easily to predict and absorb the contribution of $\boldsymbol{T_{SOIL2}}$ implicitly in the simple analytical form: $\boldsymbol{T_{eff}} = \mathbf{K} \times \boldsymbol{T_{SOIL1}}$. For this reason, the two-layer $\boldsymbol{T_{eff}}$ model is recognized to be the better candidate for its flexibility to take into account the need to use $\boldsymbol{T_{SOIL1}}$ and $\boldsymbol{T_{SOIL2}}$ for the 6:00 AM data and $\boldsymbol{T_{SOIL1}}$ only for the 6:00 PM data.

Note also that the colocation of the favorable 6:00 AM metric patterns in Fig. A3-1 occurs around $C \sim 0.40$. This value of C is higher than the traditional Choudhury value ($C = 0.246$) used in previous data releases. In other words, based on the results shown in Figure A3-1, $\boldsymbol{T_{SOIL1}}$ should now assume a 40% weight in $\boldsymbol{T_{eff}}$. This increase is consistent with (1) a change in soil depth definitions in the GEOS-FP ancillary soil temperatures as well as (2) theoretical predictions outlined in Lv, 2014 (Figure A3-2). Because the CVS soil temperatures in the sensitivity analysis do not stay constant everywhere at 20 ºC as assumed in Lv's calculations, a perfect match is not expected between our C and Lv's C, but they are nonetheless in close agreement.

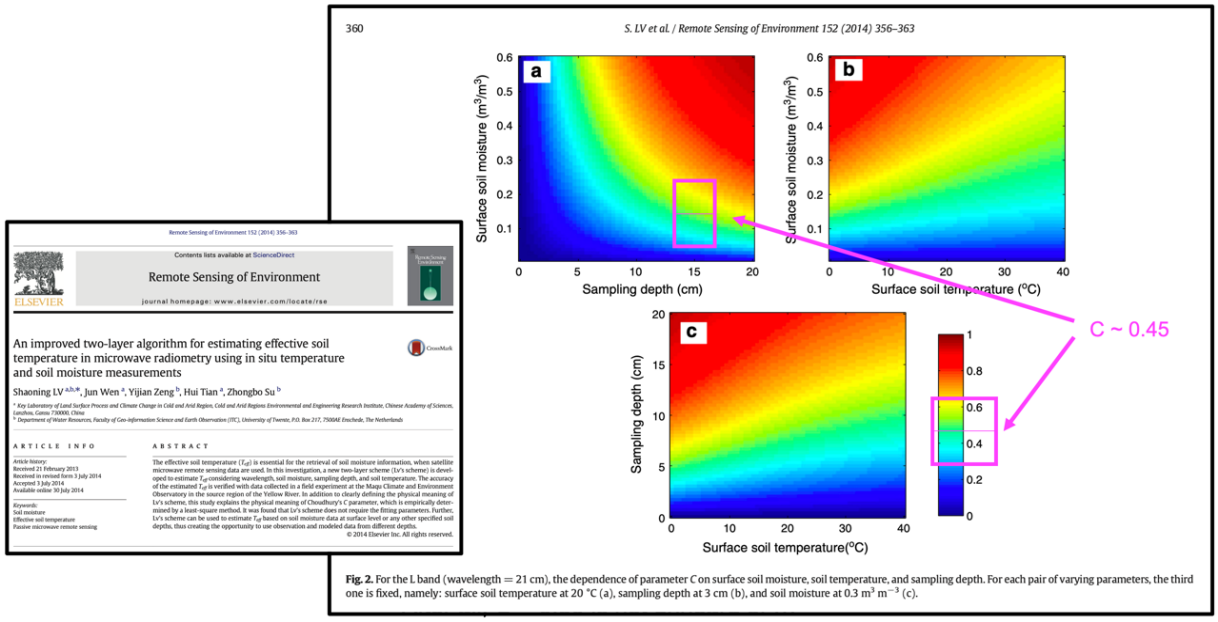

Figure A3-2. Theoretical prediction of $C \sim 0.45$ for the typical dynamic range of soil moisture observations at CVS and the sampling depth of $\boldsymbol{T_{SOIL1}}$ according to the new GMAO GEOS-FP soil depth layer definition.

CONCLUSION

Using the sensitivity analysis outlined above, the two-layer $\boldsymbol{T_{eff}}$ model was determined to provide the best explanation for the correspondence between the SMAP $\boldsymbol{T_B}$ observations and CVS soil moisture observations, with $C = 0.435$ for the SMAP 6:00 AM data and $C = 1$ for the SMAP 6:00 PM data ($K = 1.01$ in both cases) over biomes where SMAP soil moisture retrieval is expected to meet or exceed the mission target accuracy of 0.040 m^3/m^3 (1-sigma).

ADDENDUM

No account for justifying the two-layer $\boldsymbol{T_{eff}}$ model is considered complete without a critical examination into why the other alternative – the one-layer $\boldsymbol{T_{eff}}$ model – is considered a less preferred candidate. From a modeling perspective, the one-layer $\boldsymbol{T_{eff}}$ model is

conceptually simple and elegant; it adheres well to a minimalist's approach, requiring no "knobs" to account for the contribution from the deeper soil layers.

It turns out the lack of "knobs" in the one-layer T_{eff} model is also one of its major limitations – there is simply no robust way to account for diverse land surface conditions where the contribution from the deeper soil layers is significant, unless additional corrections are developed on top of this formulation to model the impacts of heat diffusion, soil texture, and soil moisture from the deeper soil layers. None of these are trivial to implement in Level 2 soil moisture geophysical inversion. As a rule of thumb in using and understanding remote sensing data, effective corrections should be applied as close to the first source(s) as possible. Since T_{SOIL2} is already available in the SMAP operational data stream, there is strong incentive to use it to provide correction sooner at T_{eff} rather than later. Furthermore, there is a large body of theoretical and experimental research which indicates that at L-band frequencies, there is significant contribution to the observed T_B from the deeper soil layers. This is especially true in areas where there is not an excessive amount of vegetation and/or soil moisture. Globally, these areas represent a significant portion of the original "SMAP Retrieval Mask" where mission target accuracy is expected to be satisfied.

For the one-layer T_{eff} model to be able to "ignore" contributions to the emission temperature from T_{SOIL2}, it is necessary that the isothermal condition be met. The isothermal condition is a rather stringent condition because it goes beyond requiring the vertical thermal gradient in the soil to be small or minimum (e.g. at dawn hours) – it actually requires $T_{SOIL1} = T_{SOIL2}$ so that their difference is zero (mathematically, as long as T_{SOIL2} is a constant multiple of T_{SOIL1}, the two-layer T_{eff} model can still be reduced to the one-layer T_{eff} model but nature is not likely to act like this everywhere all the time!). To examine the validity of this isothermal condition, both T_{SOIL1} and T_{SOIL2} were extracted and global local solar time correction was performed using all available hourly files from the GEOS-FP soil temperatures. Figure A3-3 shows the global T_{SOIL1} - T_{SOIL2} differences at local solar time 6:00 AM everywhere.

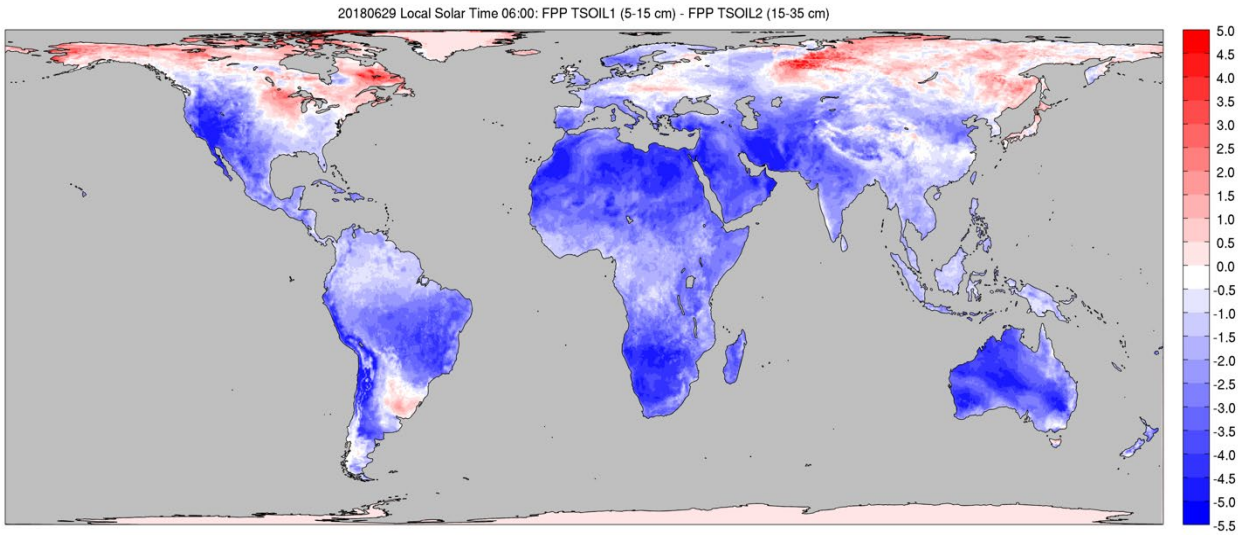

Figure A3-3. Global T_{SOIL1} - T_{SOIL2} difference at local solar time 6:00 AM

White areas indicate where $T_{SOIL1} = T_{SOIL2}$, whereas blue areas indicate where $T_{SOIL1} < T_{SOIL2}$ by about 3-5 K. Clearly, there are non-zero thermal gradients over many places even at dawn hours, thus undermining the validity of the one-layer T_{eff} model. Note that Figure A3-3 refers to only the difference between the 5-15 cm soil layer and the 15-35 cm soil layer as given by the GEOS-FP model. If soil temperature for the 0-5 cm soil layer were available, its gradient from the 5-15 cm soil layer would be even greater (see Fig. 1 in Choudhury et al., 1982). This would further challenge the isothermal condition required by the one-layer T_{eff} model.

A3.2. Emission Temperature and Its Inference from Dynamic Ancillary Data

(Lead Investigator: Dara Entekhabi, MIT)

I. The Effects of Temperature and Moisture Profiles and Their Parameterization

The microwave emission brightness temperature of soils T depends on the soil temperature profile $T_g(z)$ and the attenuation coefficient $\alpha(z)$ profile:

$$T = \int_0^\infty T_g(z) \cdot \alpha(z)\, exp\left[-\int_0^z \alpha(z')\, dz'\right] dz$$

where

$$\alpha(z) = \frac{4\pi}{\lambda} \frac{\epsilon''(z)}{2\sqrt{\epsilon'(z)}}$$

$\epsilon = \epsilon' + i\,\epsilon''$ is the complex dielectric constant that is dependent on the soil volumetric water content, and λ is the wavelength.

In order to produce estimates of surface soil moisture from brightness temperature observations, the soil temperature T_g has to be treated as a dynamic ancillary data input which can be inferred from atmospheric forecast models that include land surface parameterizations (surface energy balance and heat diffusion into discretized soil media). NASA GMAO's Goddard Earth Observing System-Forward Processing **(**GEOS-FP) modeling system is the source of these soil temperature forecasts for the SMAP project.

Atmospheric modeling systems discretize the soil column into a finite set of nodes for solving the heat diffusion and advection in the soil vertical profile. The number of nodes is usually limited (typically in the two to five range). Therefore, the emission temperature has to be parameterized in terms of a finite number of soil layers. The Choudhury et al. (1982) model is applicable to estimating an emission temperature based on finite soil temperature estimates within the profile. An emission temperature is defined based on two soil temperature values – one near the surface T_{surf} and another deep in the soil T_{deep} – such that:

$$T = T_{deep} + C \cdot (T_{surf} - T_{deep})$$

The factor C primarily depends on wavelength λ but can also be influenced by soil texture, time-of-day, and soil moisture and temperature profile shapes. Choudhury et al. (1982) used the coherent radiative transfer model of Wilheit (1978) in conjunction with observed soil moisture temperature and moisture profiles at a site in Phoenix, Arizona in order to estimate the value of factor C. The soil temperature and moisture observations are at multiple depths, allowing definition of a vertical profile. The site in Arizona experienced large variations in diurnal soil temperature profiles. Since the site is in an arid region and was sporadically irrigated, the soil moisture profile conditions also spanned a large range. Based on the coherent radiative transfer model and the soil profile observations, Choudhury et al. (1982) reported that at L-band $\lambda = 21\ [cm]$, $C = 0.246 \pm 0.009$. SMAP has adopted this value for estimating an emission temperature T based on T_{surf} and T_{deep} ancillary data inputs (current baseline SMAP L2/L3 products have all used $C = 0.246$ for the descending 6 AM overpass time since the start of SMAP science data acquisition). The SMAP Level 1 science requirements for the accuracy of retrieved surface soil moisture products are defined only for descending overpass times (about 6 AM local time). At this time the soil and overlying vegetation temperatures are least divergent compared to the rest of the day (near isothermal condition) which allows simplification of the radiative transfer model at the core of the retrieval algorithm. The ~6 PM ascending overpass data are similarly used to produce estimates of surface soil moisture for 6 PM, but these retrievals are not strictly required to meet the same level of accuracy as the 6 AM retrievals. Not having an accuracy requirement also means that 6 PM soil moisture retrievals are not a driver of algorithm design and independent ground truth science product assessment and validation.

II. Source of Dynamic Soil Temperature Ancillary Data

For SMAP the source of ancillary soil temperature data is the GMAO GEOS-FP system. In January 2020 the GEOS-FP system upgraded to a new land surface model that redefined the surface and soil temperature layer depths as shown below (Koster et al., 2020):

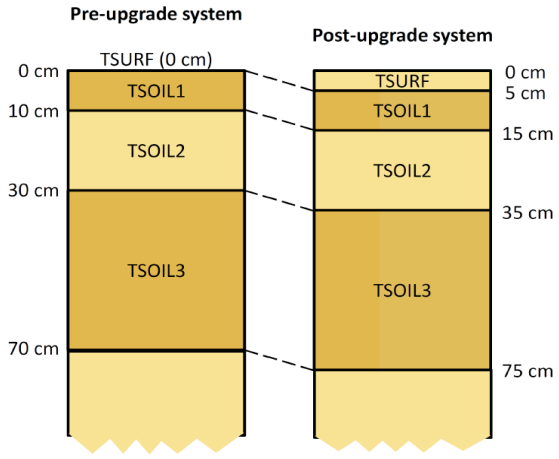

In the upgraded GEOS system, $Tsurf$ is a temperature prognostic that is formed based on bare soil, vegetation, and snowpack temperatures in proportion to their prevalence across the pixel area. This temperature is a flux temperature which is used in the gradient-driven exchanges of heat between the surface and the atmospheric boundary layer. $TSOIL1$ and $TSOIL2$ are consistently soil media temperature prognostic variables that are characterized by these extensive attributes:

	Depth Range	Node Center Position
$TSOIL1$	-5 to -15 [cm]	-10 [cm]
$TSOIL2$	-15 to -35 [cm]	-25 [cm]

These GEOS temperature variables ($TSOIL1$ and $TSOIL2$) need to be linked to the Choudhury et al. (1982) model variables (T_{surf} and T_{deep}).

III. Offset and Scaling Biases in Model Prognostics

Atmospheric and land surface model forecasts of soil temperatures may be biased (model structural biases) and may need corrections to represent soil temperatures T_{surf} and T_{deep}. Such structural biases are inevitable given the fact that they are parameterized and the result of numerical models as well as because the model grids (in the horizontal) are often tens of kilometers which span large heterogeneities in landscape conditions like slope, aspect, land use, and soil texture.

The model variables can be biased (offset) or they can be modulated (scaled). The offset and scaling may be seasonally variable and depend on land use and soil physical characteristics. Identification of the required scaling (modulation of the seasonal and diurnal amplitude) and its dependence on landscape characteristics is complicated and beyond the immediate priorities of the SMAP Project. The offset, however, is identifiable with the use of *in situ* soil temperature measurements.

To start this analysis, the $TSOIL1$ variable at the time of the descending overpass was compared with the most common measurement of soil temperature at *in situ* stations, i.e., $T_g(z = -5\ [cm])$. The offset between the two variables may be captured by an additive factor or a multiplicative factor. The figure below over the range of typical non-frozen soil temperatures shows that when the temperatures are given in units of [Kelvin], the additive and multiplicative characterization of the offset factor is comparable.

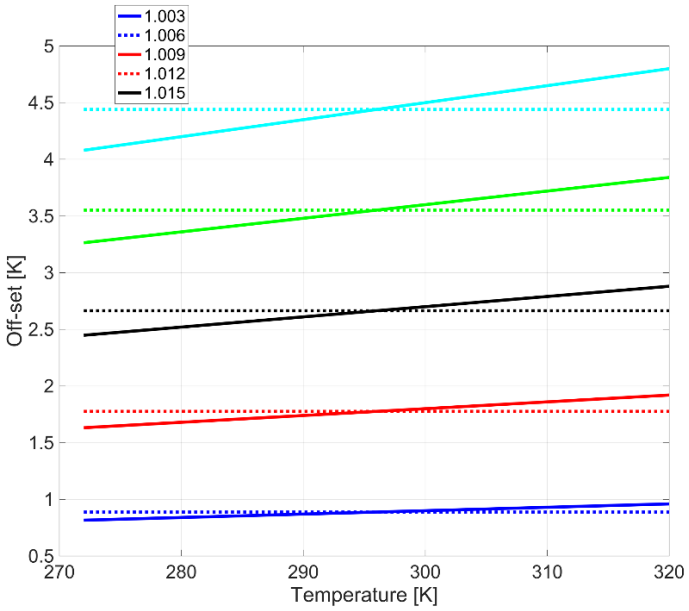

Based on the above figure, the decision was made to proceed with a multiplicative model for the offset so that:

$$T_{surf} = K_{surf} \cdot TSOIL1$$

IV. Descending Overpass Time

Based on ground-based observations of soil temperature $T_g(z = -5\ [cm])$ and GMAO GEOS-FP $TSOIL1$, the values of K_{surf} across CVS and sparse network ground stations are:

Descending Overpasses (~6:00 am Local Time)		
	K_{surf}	Number of Stations
CVS (Chaubell, 2020, personal communication)	1.006 +/- 0.005	15
USCRN (Colliander, 2020, personal communication)	1.0068 +/- 0.0051	299

Colliander (2020) and Chaubell (2020) show that K_{surf} has a distinct seasonal cycle at some stations (peak in the summer) and that drier soil climates have higher K_{surf} values. Examples at the TxSON and REMEDHUS stations (in red) are shown below (Chaubell, 2020):

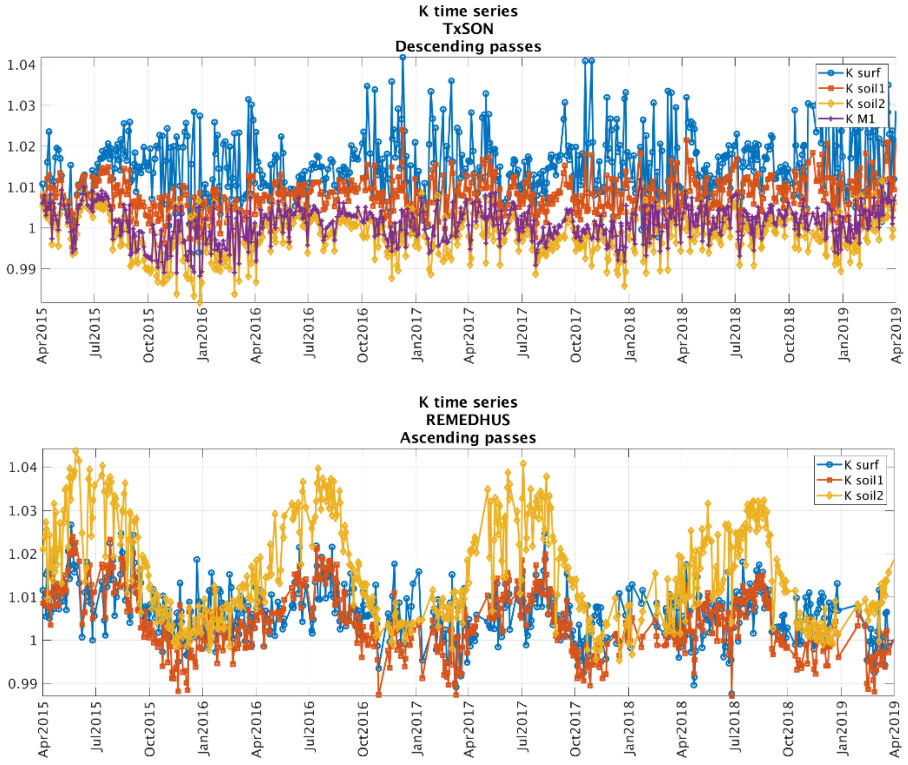

Repeat of the same offset identification but for the deep soil temperature, i.e.

$$T_{deep} = K_{deep} \cdot TSOIL2$$

has more options to consider. The first option is to estimate K_{deep} in the same manner as for the surface soil but using deeper ground-based observations of soil temperature such as $T_g(z = -20\ [cm])$. The availability of ground-based soil temperature at this depth is more limited. But a more serious consideration is the potential hazard of disturbing the soil temperature gradient provided by the GMAO GEOS-FP system if separate multiplicative offset factors are applied.

As a solution, offsets are applied to the GMAO GEOS-FP soil temperature prognostics that preserve the gradient but shift the profile so that they match the surface ground-based soil temperature measurements. This implies $K_{deep} = K_{surf} = K$. With this approach the GMAO GEOS soil temperature gradient is not disturbed and the shift is a translation on the temperature scale.

Based on the table above, $K = 1.007$ is selected together with the Choudhury et al. (1982) $C = 0.246$ for the 6 AM descending passes according to the combined model:

$$T = K \cdot [C \cdot TSOIL1 + (1 - C) \cdot TSOIL2]$$

V. Ascending Overpass Time

There are no SMAP project requirements on the accuracy of soil moisture retrievals using ascending pass 6 PM data. Nevertheless, the project makes every effort to provide accurate soil moisture retrievals from the 6 PM SMAP observations as well as from 6 AM to essentially double the soil moisture estimates available to the science and applications community. There are known challenges to applying the retrieval algorithm to ascending data since isothermal conditions between the soil and the overlying vegetation canopy is one of the major requirements of the soil moisture retrieval algorithm as it is formulated now, and this condition is more likely to be violated at 6 PM.

The SMAP project has identified two major use-cases for the ascending soil moisture retrievals: 1) those that are interested in the diurnal cycle of soil moisture (in response to daytime drying and nighttime re-moistening by hydraulic lift of soil water from below to the drier surface) during non-precipitating days, and 2) those who seek to double their data count for more robust time-series analyses. These two use-cases lead to conflicting design criteria: the first use-case requires detection of the subtle small changes associated with the diurnal cycle of soil moisture, while the second use-case requires much consistency between ascending and descending estimates, i.e., no saw-tooth patterns.

Meeting the requirements of the first use-case is very challenging since characterization of the temperature gradient between the soil and the canopy – to the accuracy required to detect subtle diurnal soil moisture changes – is not readily feasible. This use-case community is encouraged to access the SMAP Level 1 brightness temperature data and design their own retrieval algorithms that might better suit their particular application (including the use of alternative ancillary data sources).

The second use-case can be enabled by ensuring an ascending (6 PM) data product that best meets two criteria: 1) best possible performance in terms of matching *in situ* soil moisture at the time of the evening overpass, and 2) as much as possible tracking the descending soil moisture product except for when precipitation events occur in between the two measurements.

The offset factor for the ascending overpass time (6 PM) may be approached in the same manner as for the descending (6 AM) overpasses described above. The results of this estimation process are listed in the table below.

Ascending Overpasses (~6 PM Local Time)		
	K_{surf}	Number of Stations
CVS (Chaubell, 2020, personal communication)	1.002 +/- 0.007	15
USCRN (Colliander, 2020, personal communication)	1.0024 +/- 0.0071	299

Since the ascending overpass time is not part of the SMAP Science Requirements, there is greater latitude in selecting the K and C parameters, with the possibility that the nominal values from the current analysis will be revisited in the future.

For the parameter C for the 6 PM ascending overpasses, the project plans to continue to use $C = 1$, which is the same as the value used to produce the baseline surface soil moisture science data product publicly available now. This value was selected based on the understanding of the evolution of canopy and soil profile temperatures during the course of the solar day. It should be revisited with more evidence based on radiative transfer modeling and *in situ* observations of canopy and multi-layer soil temperatures.

For the parameter K, a lower value than the descending pass estimated value is warranted. At this time it was decided to use the same K during the ascending time as the descending time, i.e., $K = 1.007$, until the fidelity of the forecasts of the diurnal cycle amplitude in the GMAO GEOS-FP system is better understood. This diurnal cycle amplitude is certainly related to the vegetation cover, soil moisture level, season, and available energy and other environmental factors. It is prudent to not assign a different offset to the ascending overpass time model temperatures until there is greater understanding of the role of the amplitude of the diurnal cycle.

	K	C
Descending	1.007	0.246
Ascending	1.007	1.000

VI. Assessments

In the analysis described here, the soil emission temperature parameter estimation has only used *in situ* soil temperatures and model temperature prognostics. This leaves CVS and sparse network soil moisture information intact for use invalidation of the SMAP retrieved soil moisture values. The table below shows the assessment of the SMAP surface soil moisture product at CVS using Plan 2.2 of the L1 brightness temperature calibration

as well as the new OpenLandMap soil texture database. The results of the independent assessment are:

	ubRMSE (m3 m-3)	Bias (m3 m-3)	RMSE (m3 m-3)	Correlation
Descending Orbits	0.037	-0.006	0.048	0.816
Ascending Orbits	0.037	-0.008	0.048	0.811

The random errors (ubRMSE) and correlation are unaffected by the updated parameters of the soil emission model and updated GMAO GEOS-FP soil temperature dynamic soil temperature ancillary data inputs. Although slightly larger than before the updates, the bias is small and within the bounds of uncertainty (~0.01) in determining grid-average values based on finite point samples (Chen et al., 2019).

Two major use-cases were identified for the combined descending and ascending surface soil moisture products. Besides product performance based on 6 AM/6 PM local time *in situ* soil moisture ground truth, efforts were made to minimize spurious 'saw-tooth' variations beyond normal differences in the two overpass soil moisture estimates. This saw-tooth pattern would manifest itself in the mean bias between the ascending and descending soil moisture as well as in other statistics. With the current selection of soil emission parameters, the bias between the descending and ascending surface soil moisture estimates averaged over all CVS is small (around -0.002 m^3 m^{-3}).

REFERENCES

A1. Chen, F. et al., "Uncertainty of Reference Pixel Soil Moisture Averages Sampled at SMAP Core Validation Sites," *J. Hydrometeorology*, 20, 2019.

A2. Choudhury, B., T. J. Schmugge and T. Mo, "A Parameterization of Effective Soil Temperature for Microwave Emission," *Journal of Geophysical Research*, 87(C2): 1301-1304, 1982.

A3. Koster, R. et al., "Land-Focused Changes in the Updated GEOS-FP System (Version 5.25)," *GMAO Research Brief*, 11 pgs, 2020.

A4. Lv, S. et al., "An Improved Two-Layer Algorithm for Estimating Effective Soil Temperature in Microwave Radiometry using *In Situ* Temperature and Soil Moisture Measurements," *Remote Sensing of Environment*, vol. 152, pp. 356-363, 2014.

A5. Lv, S. et al., "A Reappraisal of Global Soil Effective Temperature Schemes," *Remote Sensing of Environment*, vol. 183, pp. 144-153, 2016.

A6. Wilheit, T., "Radiative Transfer in a Plane Stratified Dielectric," *IEEE Transactions on Geoscience Electronics*, 16(2), 1978.

APPENDIX 4: Unmixing of Surface-Corrected Brightness Temperatures in the SMAP Level 1C Gridded Brightness Temperature Product

A4.1. INTRODUCTION

Surface-based radiometric correction was a key update introduced in Version 4 of the SMAP Level 1B Time-Ordered Brightness Temperature Product ("SPL1BTB") in 2018. This correction procedure was intended to mitigate the impacts of contaminating radiometric sources on SMAP brightness temperature (T_B) observations. Specifically, it dealt with (1) T_B correction over land by removing emission contribution of nearby water and (2) T_B correction over water by removing emission contribution of nearby land. Around coastal areas and areas surrounding inland open water bodies (e.g. lakes, rivers, etc.), this correction procedure is expected to improve the retrieval accuracy of soil moisture over land and ocean salinity over water.

Which type of correction is to be performed within the SPL1BTB processor is determined by the boresight location of a particular time-ordered T_B field-of-view (FOV) sample. When the boresight falls onto a location considered as land according to a high-resolution static land/water mask, T_B correction over land for water contamination will be performed as long as the water fraction within the FOV is below 0.90, and when the boresight falls onto a location considered as water as determined by the same static mask, T_B correction over water for land contamination will be performed as long as the land fraction within the FOV is below 0.90. The resulting water-corrected T_B and land-corrected T_B data fields are available in SPL1BTB, in addition to the original uncorrected T_B. **Table A4.1** summarizes the types, triggers, and correction sources considered by these correction schemes as of Version 4 of SPL1BTB:

Table A4.1: Surface-based radiometric correction implemented in SPL1BTB.

Correction Type	Retrieval	Boresight	Trigger	Correction Source
T_B correction over land to remove water contamination	Soil Moisture	Land (surface_status = 0)	FOV water fraction ≤ 0.9	Nearby 3° × 3° area-averaged SMAP T_B over water
T_B correction over water to remove land contamination	Salinity	Water (surface_status = 1)	FOV land fraction ≤ 0.9	Nearby 1° × 1° area-averaged SMAP T_B over land

A more detailed description of this surface-based radiometric correction procedure can be found in:

Chaubell, M.J., S.H. Yueh, R.S. Dunbar, S.K. Chan, F. Chen, J. Piepmeier, R. Bindlish, D. Entekhabi, P.E. O'Neill, "Improving Brightness Temperature

Measurements Near Coastal Areas for SMAP," *IEEE Journal of Selected Topics in Applied Earth Observations and Remote Sensing*, pp. 4578—4588, 12(11), 2019.

The SMAP Level 1C Gridded Brightness Temperature Product ("SPL1CTB") processor ingests the time-ordered data fields from SPL1BTB and grids them on the EASE Grid 2.0 global (M), north polar (N), and south polar (S) projections. The following discussion applies to how SPL1BTB data fields were and are binned by the SPL1CTB processor under all three projections.

Between Versions 4 (2018) and 5 (2020), the SPL1CTB processor binned water-corrected $\boldsymbol{T_B}$ and land-corrected $\boldsymbol{T_B}$ from SPL1BTB together when they fall into the same EASE Grid 2.0 grid cell. This mixing is undesirable because the resulting gridded $\boldsymbol{T_B}$ would undo the intended purpose of $\boldsymbol{T_B}$ correction over land for water contamination and $\boldsymbol{T_B}$ correction over water for land contamination implemented in the SPL1BTB processor. Nonetheless, this indiscriminate binning was decided and implemented out of necessity, given the constraints of processing infrastructure available at that time. Note that this indiscriminate binning affected only the SPL1CTB product; its enhanced counterpart ("SPL1CTB_E") was not affected. The rest of this memo deals with our attempt to undo this mixing of water-corrected $\boldsymbol{T_B}$ and land-corrected $\boldsymbol{T_B}$ within the SPL1CTB processor.

A4.2. REMEDY

The SPL1CTB processor has recently gone through a major code overhaul to implement an algorithm-based workaround to circumvent the limitations of the previous indiscriminate binning. The fix involved creation of extra "containers" during the binning process to separate the binning of water-corrected $\boldsymbol{T_B}$ from the binning of land-corrected $\boldsymbol{T_B}$. The binned data fields from these "containers" remain available until the end of processing where the SPL1CTB processor will decide if a given grid cell is considered land or water based on the value of the nearest-neighbor SPL1BTB's surface_status field. If the nearest-neighbor surface_status field is 0 (**Table A4.1**, 2nd row), the processor will retrieve the "container" for water-corrected $\boldsymbol{T_B}$ and drop the corresponding binned result in the final output field. Conversely, if the nearest-neighbor surface_status field is 1 (**Table A4.1**, 3rd row), SPL1CTB will retrieve the "container" for land-corrected $\boldsymbol{T_B}$ and drop the corresponding binned result in the final output field. In other words, the nearest-neighbor surface_status field of SPL1BTB was used as a transfer platform to enable the SPL1CTB processor to copy the input high-resolution static land/water mask available only to the SPL1BTB processor.

This code overhaul was implemented entirely internally inside the SPL1CTB processor and thus did not require any sophisticated external processing configurations. **Figure A4.1** describes how the indiscriminate binning in SPL1CTB since Version 4 was revised for the next data release of the product.

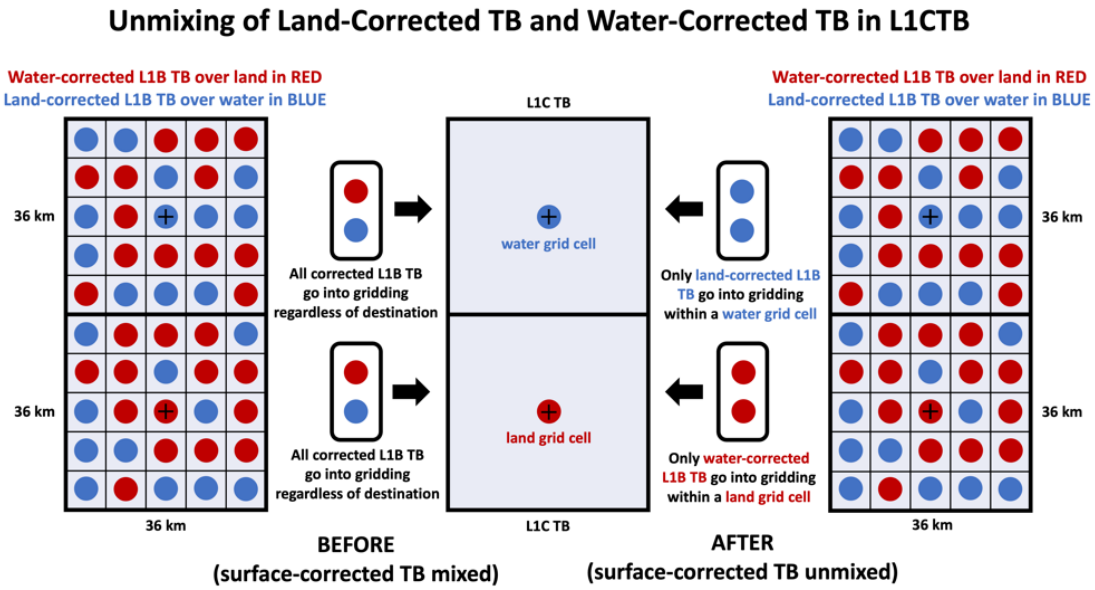

Figure A4.1: Separate binning of water- and land-corrected T_B (right) for the next data release of SPL1CTB. After unmixing, only water-corrected T_B samples go to land grid cells (red) and only land-corrected T_B samples go to water grid cells (blue).

It is evident that the revised binning scheme would preserve the water-corrected T_B and land-corrected T_B from SPL1BTB with a higher fidelity. Given the triggers (**Table A4.1**, 4th column) for this surface correction procedure, the improvements will be most visible along boundaries that separate land from water. In general, they correspond to coastal areas and areas surrounding inland open water bodies.

A few observations on the accuracy of the water-corrected T_B from SPL1BTB follow. From **Table A4.1**, the correction source for T_B correction over land is the average SMAP T_B over water within a 3° × 3° latitude/longitude search box. This coverage is about 9 times greater than what is covered by the main beam (2.5 × HPBW ~ 108 km) of the SMAP antenna. As such, the corresponding correction may involve T_B observations not directly contributing to a single time-ordered T_B field-of-view (FOV) sample, potentially leading to correction errors that translate to subsequent soil moisture retrieval bias. One example of this processing artifact can be seen over Finland in **Figure A4.4b**, where a 3° × 3° latitude/longitude search box at this high latitude would introduce SMAP T_B dominated by the cold water T_B in the vertical dimension. The resulting water-corrected T_B over land after water T_B subtraction may become over-corrected (i.e. higher than reality), leading to very dry soil moisture retrieval. The limitations of this latitude/longitude search approach can be mitigated by a search domain that coincides with the actual FOV footprint projected on the land surface.

A4.3. IMPACTS ON SOIL MOISTURE RETRIEVAL

The SMAP Level 2 Radiometer-only Soil Moisture Product ("SPL2SMP") uses the water-corrected T_B over land from SPL1CTB for soil moisture retrieval. The revised binning described in Section 2 is expected to more thoroughly remove the contribution by water to SMAP T_B, resulting in higher T_B for soil moisture retrieval. A comparison in soil moisture retrieval before and after this unmixing is expected to reveal (1) lower soil moisture around coastal areas and areas surrounding inland open water bodies and (2) little change in retrieval elsewhere where the triggers in **Table A4.1** are not set. **Figures A4.2 and A4.3** confirm these expectations. By and large, **Figure A4.2a** and **A4.2b** are visually identical. Their difference (**Figure A4.3)**, however, reveals dry bias in retrieval around coastal areas and areas surrounding inland open water bodies.

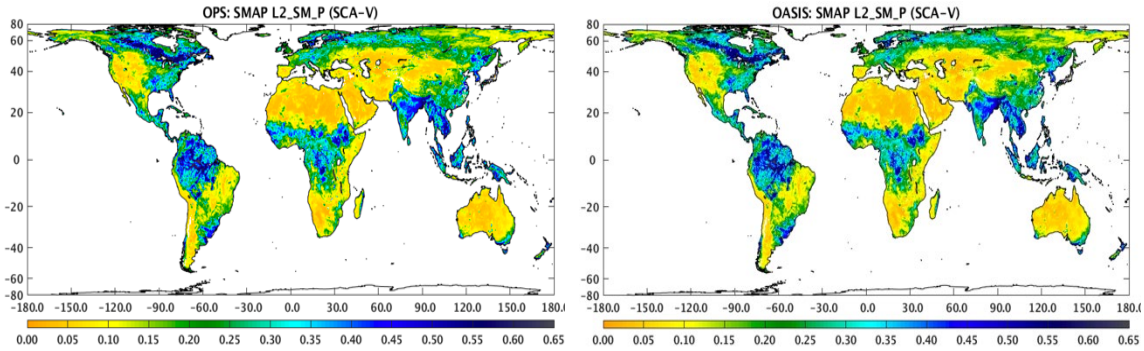

(a) (b)

Figure A4.2: 6:00 am SPL2SMP between June 1-5, 2020 using SPL1CTB gridded vertically polarized T_B (a) before the unmixing of surface-corrected T_B and (b) after unmixing of surface-corrected T_B.

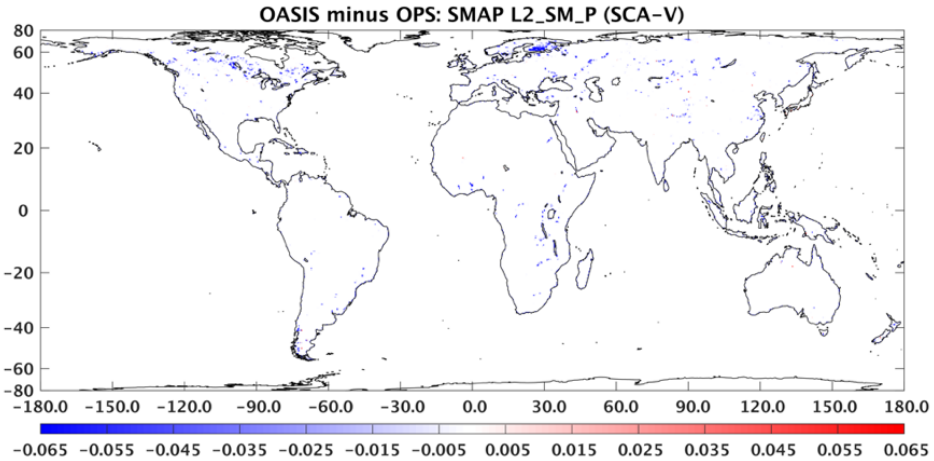

Figure A4.3: Difference in SPL2SMP soil moisture retrieval before and after the unmixing of surface-corrected T_B.

Figure A4.3 can be further cropped over different geographical regions for a better visualization of the regional retrieval difference before and after unmixing. This is shown in **Figure A4.4**.

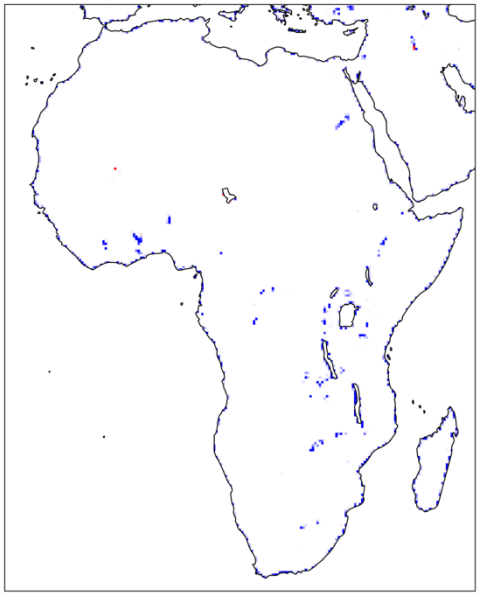

(a)

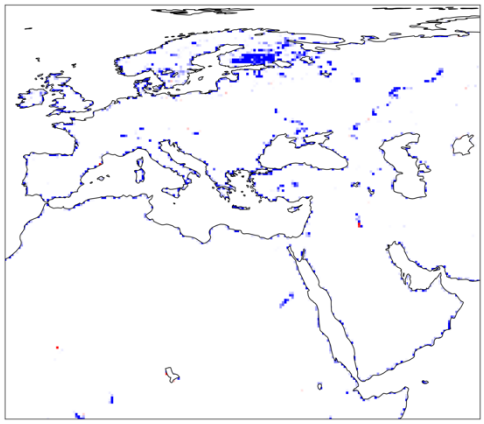

(b)

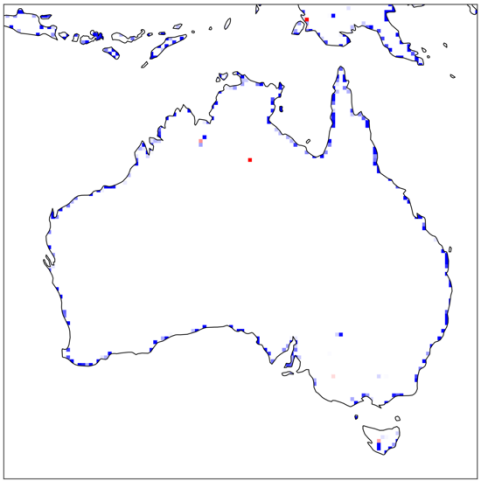

(c)

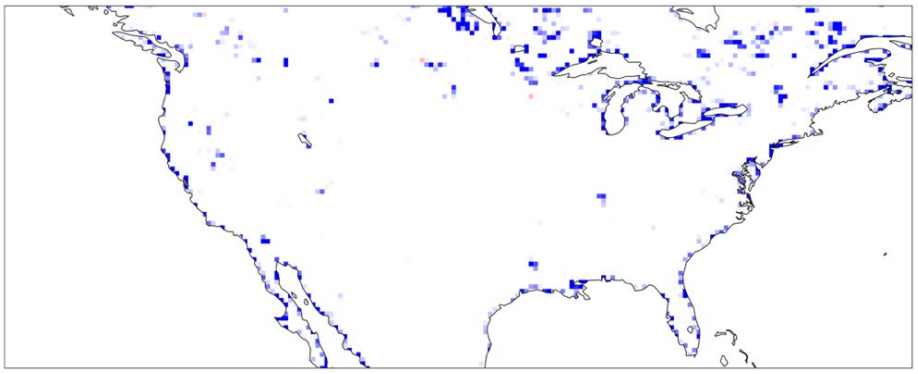

(d)

Figure A4.4: Difference in SPL2SMP soil moisture retrieval before and after the unmixing of surface-corrected T_B over (a) Africa, (b) Europe, (c) Australia, and (d) CONUS.

Figure A4.3 also indicates the very small percentage of land pixels that see a change in soil moisture retrieval before and after the unmixing of surface-corrected T_B. The histogram in **Figure A4.5** shows the distribution of retrieval difference in percentage upon a consideration of all global land pixels.

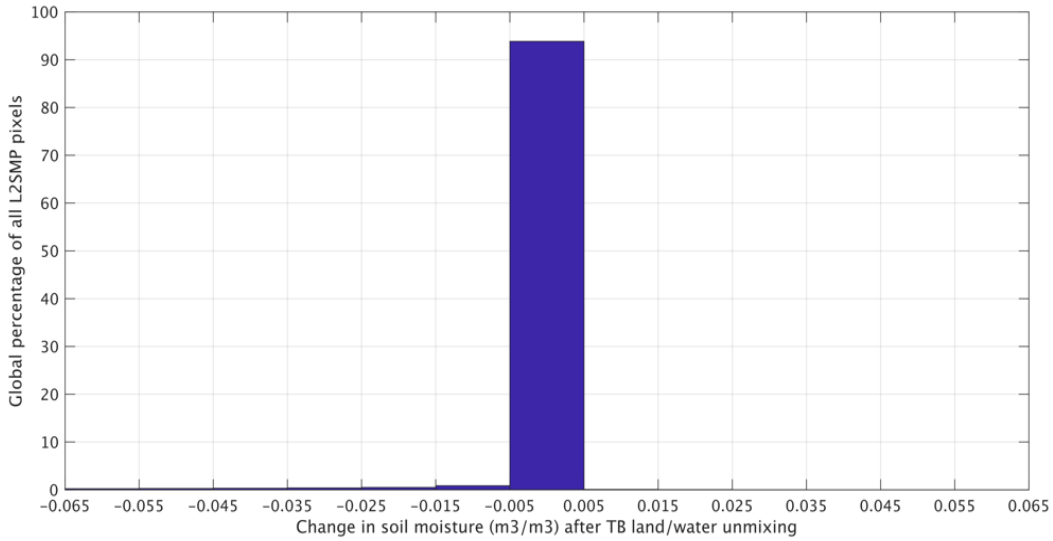

Figure A4.5: Histogram of retrieval difference before and after the unmixing of surface-corrected T_B.

It is clear from **Figure A4.5** that the histogram exhibits a tail that mostly extends to the negative half of the x-axis, implying the lower soil moisture retrieval after the unmixing of surface-corrected T_B, which is consistent with the discussion earlier in this section. Most global land pixels, on the other hand, do not see any change in soil moisture retrieval, as

indicated by the overwhelmingly high percentage in the middle of the histogram. **Table A4.2** presents a numerical breakdown of **Figure A4.5**. Further calculations indicated that 92.9% of all global land pixels show a retrieval difference of less than ±0.001 m^3/m^3.

Table A4.2: Numerical breakdown of soil moisture retrieval difference in Figure A4.5.

Soil Moisture Range (m^3/m^3)		Percent (%)
−0.065	−0.055	0.23
−0.055	−0.045	0.28
−0.045	−0.035	0.33
−0.035	−0.025	0.40
−0.025	−0.015	0.50
−0.015	−0.005	0.87
−0.005	+0.005	93.84
+0.005	+0.015	0.08
+0.015	+0.025	0.04
+0.025	+0.035	0.02
+0.035	+0.045	0.01
+0.045	+0.055	0.01
+0.055	+0.065	0.00

A4.4. CONCLUSION

The unmixing of surface-corrected $\boldsymbol{T_B}$ described in this memo provides an improved mechanism to preserve water-corrected $\boldsymbol{T_B}$ and land-corrected $\boldsymbol{T_B}$ with a higher fidelity. The resulting surface-corrected $\boldsymbol{T_B}$ fields will be available beginning in Version 6 of SPL1CTB and Version 8 of SPL2SMP in the upcoming R18 data release expected in 2021. The impacts of unmixing are observable mostly around coastal areas and areas surrounding inland open water bodies. 92.9% of all global land pixels show a retrieval difference of less than ±0.001 m^3/m^3 after unmixing, confirming the limited scope of this procedure on the majority of global land pixels and thus ensuring the continuing consistency of the upcoming SPL2SMP baseline soil moisture retrieval.

APPENDIX 5: North Polar EASE2 Projection

Starting with SMAP data release R18 in October 2021, the L2/3_SM_P_E Version 5 Soil Moisture Data Product is also provided on the North Polar 9-km EASE2 grid projection in addition to the original Global 9-km EASE2 grid projection. A feature of the global grid is that its grid cells become significantly distorted (from the nominal square shape) at higher latitudes. The polar grid projection offers a more uniform spatial sampling at high latitudes, which will facilitate studies with soil moisture in the boreal and arctic regions. Better spatial representation of the grid with respect to the SMAP radiometer footprint will also help in the improvement of the retrieval algorithms to account for the unique soil and vegetation conditions of the boreal and arctic landscapes.

The algorithms used to generate soil moisture on the polar grid (SCA-H, SCA-V and DCA) are exactly the same as the ones used to generate soil moisture on the global grid. However, the algorithms use the polar grid TB from the L1C_TB_E product (which has always been available in the L1C_TB products) instead of the TB on the global grid (see reference for L1C_TB, Revision B ATBD on p.6). The ancillary data sources are the same as those used by the global grid soil moisture, but the ancillary data are gridded on the polar grid instead of the global grid before being input to the soil moisture retrieval algorithms for soil moisture on the polar grid. The approach to assign quality and surface flags and the threshold values used in the flag assignments are exactly the same as the ones used for the global grid soil moisture. Any difference between the soil moisture values found on the global grid and on the polar grid for a similar location is, therefore, due to the differences in the gridding. The differences are likely to be more significant at higher latitudes compared to lower latitudes because of the larger distortion of the global grid at the higher latitudes.

APPENDIX 6: Algorithm Variable Pointer Tables for L2/L3 Product Output Fields

These tables are provided as a quick reference guide for users of these soil moisture products to associate the correct variable output fields with the correct retrieval algorithm, and to associate the pointer elements to the correct variable.

For the L2_SM_P/P_E soil moisture products:

List of Variables Associated with Each Soil Moisture Algorithm Option		
DCA	**SCA-V**	**SCA-H**
soil_moisture_option3^	soil_moisture_option2	soil_moisture_option1
vegetation_opacity_option3^	vegetation_opacity_option2	vegetation_opacity_option1
retrieval_quality_flag_option3^	retrieval_quality_flag_option2	retrieval_quality_flag_option1
roughness_coefficient_option3	roughness_coefficient*	roughness_coefficient*
albedo_option3	albedo*	albedo*
* the SCA-H and SCA-V algorithms share the same roughness_coefficient and albedo variables		
^ these variables also correspond to the pointer elements listed in the table below		

List of Pointer Elements and Their Corresponding Variables	
Pointer Element	**Variable**
soil_moisture	soil_moisture_option3
vegetation_opacity	vegetation_opacity_option3
retrieval_quality_flag	retrieval_quality_flag_option3

For the L3_SM_P/P_E soil moisture products:

List of Variables Associated with Each Soil Moisture Algorithm Option		
DCA	**SCA-V**	**SCA-H**
soil_moisture_dca^	soil_moisture_scav	soil_moisture_scah
vegetation_opacity_dca^	vegetation_opacity_scav	vegetation_opacity_scah
retrieval_quality_flag_dca^	retrieval_quality_flag_scav	retrieval_quality_flag_scah
roughness_coefficient_dca^	roughness_coefficient_scav	roughness_coefficient_scah
albedo_dca^	albedo_scav	albedo_scah
^ these variables also correspond to the pointer elements listed in the table below		
NOTE: The variable names in the Soil_Moisture_Retrieval_Data_PM data group have the suffix "_pm" attached.		

List of Pointer Elements and Their Corresponding Variables	
Pointer Element	**Variable**
soil_moisture[_pm]	soil_moisture_dca[_pm]
vegetation_opacity[_pm]	vegetation_opacity_dca[_pm]
retrieval_quality_flag[_pm]	retrieval_quality_flag_dca[_pm]
roughness_coefficient[_pm]	roughness_coefficient_dca[_pm]
albedo[_pm]	albedo_dca[_pm]